NASA/TM—2000-210020

Effects of Melt Convection and Solid Transport on Macrosegregation and Grain Structure in Equiaxed Al-Cu Alloys

Rodney S. Rerko
The University of Iowa, Iowa City, Iowa

Henry C. de Groh, III
Glenn Research Center, Cleveland, Ohio

Christoph Beckermann
The University of Iowa, Iowa City, Iowa

May 2000

The NASA STI Program Office . . . in Profile

Since its founding, NASA has been dedicated to the advancement of aeronautics and space science. The NASA Scientific and Technical Information (STI) Program Office plays a key part in helping NASA maintain this important role.

The NASA STI Program Office is operated by Langley Research Center, the Lead Center for NASA's scientific and technical information. The NASA STI Program Office provides access to the NASA STI Database, the largest collection of aeronautical and space science STI in the world. The Program Office is also NASA's institutional mechanism for disseminating the results of its research and development activities. These results are published by NASA in the NASA STI Report Series, which includes the following report types:

- TECHNICAL PUBLICATION. Reports of completed research or a major significant phase of research that present the results of NASA programs and include extensive data or theoretical analysis. Includes compilations of significant scientific and technical data and information deemed to be of continuing reference value. NASA's counterpart of peer-reviewed formal professional papers but has less stringent limitations on manuscript length and extent of graphic presentations.

- TECHNICAL MEMORANDUM. Scientific and technical findings that are preliminary or of specialized interest, e.g., quick release reports, working papers, and bibliographies that contain minimal annotation. Does not contain extensive analysis.

- CONTRACTOR REPORT. Scientific and technical findings by NASA-sponsored contractors and grantees.

- CONFERENCE PUBLICATION. Collected papers from scientific and technical conferences, symposia, seminars, or other meetings sponsored or cosponsored by NASA.

- SPECIAL PUBLICATION. Scientific, technical, or historical information from NASA programs, projects, and missions, often concerned with subjects having substantial public interest.

- TECHNICAL TRANSLATION. English-language translations of foreign scientific and technical material pertinent to NASA's mission.

Specialized services that complement the STI Program Office's diverse offerings include creating custom thesauri, building customized data bases, organizing and publishing research results . . . even providing videos.

For more information about the NASA STI Program Office, see the following:

- Access the NASA STI Program Home Page at ***http://www.sti.nasa.gov***

- E-mail your question via the Internet to help@sti.nasa.gov

- Fax your question to the NASA Access Help Desk at (301) 621-0134

- Telephone the NASA Access Help Desk at (301) 621-0390

- Write to:
  NASA Access Help Desk
  NASA Center for AeroSpace Information
  7121 Standard Drive
  Hanover, MD 21076

NASA/TM—2000-210020

Effects of Melt Convection and Solid Transport on Macrosegregation and Grain Structure in Equiaxed Al-Cu Alloys

Rodney S. Rerko
The University of Iowa, Iowa City, Iowa

Henry C. de Groh, III
Glenn Research Center, Cleveland, Ohio

Christoph Beckermann
The University of Iowa, Iowa City, Iowa

National Aeronautics and
Space Administration

Glenn Research Center

May 2000

Acknowledgments

The authors would like to take this opportunity to thank Professors L.D. Chen, and T.F. Smith for reviewing this work; Bob Feller who worked on the software and hardware for the Bulk Undercooling Furnace; our colleagues in the solidification laboratory, Richard Hardin, Xinglin Tong, and Venkatesh Raghavendra for their willingness to share knowledge; and Jeff Blank and Nicola Mawer for helping in the editing of the thesis this document is based upon. The financial support for this work, by NASA's Microgravity Materials Science program, under cooperative agreements and grants "Transport Phenomena During Equiaxed Solidification of Alloys" and "Equiaxed Dendritic Solidification Experiment," is gratefully acknowledged.

Available from

NASA Center for Aerospace Information
7121 Standard Drive
Hanover, MD 21076
Price Code: A06

National Technical Information Service
5285 Port Royal Road
Springfield, VA 22100
Price Code: A06

TABLE OF CONTENTS

LIST OF NOMENCLATURE

A	area
CI	confidence interval
C_l	liquid concentration
C_o	initial composition
c_p	specific heat
d	grain diameter
D	spatial diameter
F_o	Fourier number
k	thermal conductivity
h	heat transfer coefficient
L	length
m	slope
M	magnification
N_A	grains per unit area
N_L	lineal density of grains
N_V	grains per unit volume
RA	relative accuracy
S_v	grain boundary surface area per unit volume
t	time
T	temperature
T_{liq}	liquidus temperature
T_m	melting temperature
V	volume
x	position

Greek symbols

α	thermal diffusivity
Δh	latent heat
ε_s	solid fraction
ε_l	liquid fraction
κ	segregation coefficient
ρ	density
λ	lineal intercept length of a grain

Subscripts

c	cooling
eu	eutectic
g	generation
i	current control volume
l	liquid
liq	liquidus
m	melt
o	initial
s	solid
st	storage

Superscripts

p	present time

EXECUTIVE SUMMARY

Macrosegregation in metal casting can be caused by thermal and solutal melt convection, and the transport of unattached solid crystals. These free grains can be a result of, for example, nucleation in the bulk liquid or dendrite fragmentation. In an effort to develop a comprehensive numerical model for the casting of alloys, an experimental study has been conducted to generate benchmark data with which such a solidification model could be tested. It was our goal to examine equiaxed solidification in situations where sinking of gains are (and are not) expected. The objectives were: 1) experimentally study the effects of solid transport and thermosolutal convection on macrosegregation and grain size distribution patterns; and 2) provide a complete set of controlled thermal boundary conditions, temperature data, segregation data, and grain size data, to validate numerical models such as Beckermann and Wang's (1995).

It is expected that modeling efforts will use the thermocouple measurements in the walls of the crucible and perhaps the top thermocouple in the sample as input boundary conditions and that the code will solve for the temperatures in the sample. These numerically determined sample temperatures will then be compared to the measurements made in the sample interior. Through the control of end cooling and side wall heating, radial temperature gradients in the sample and furnace were minimized. Thus a simplifying assumption that the vertical crucible wall is adiabatic can be made; in which case the thermocouple measurements in the side wall may not be needed. Regardless of the details of any numerical effort, the locations of the thermocouples and sample domain are needed to setup the simulation and compare results. The thermocouple locations and crucible/sample dimensions are given in Figures 2.2, 2.3, 2.4. The length of the sample varies during different stages of the experiment due to thermal expansion and expansion upon melting. The volume of the samples at room temperature was 24 cm^3, the volume displaced by the immersion of the thermocouples in the sample was about 1.3 cm^3, thus making the total volume of the sample 25.3 cm^3. The length of the samples at room temperature, with thermocouples inserted, was 95 mm, and when fully liquid the sample length was about 100 mm. The thermophysical properties for the alloys are given in Table 6. Also provided in this section, page 75, are details and references needed for the inclusion of the settling and advection characteristics of equiaxed dendrites, such as the experimentally found drag coefficient of a equiaxed dendrite.

The alloys used were Al-1 wt. pct. Cu, and Al-10 wt. pct. Cu; the starting point for the solidification of these samples can be considered to be: isothermal at 710 °C and 685 °C respectively. To induce an equiaxed structure (and the opportunity for grain movement) various amounts of the grain refiner TiB_2 were added. Samples were either cooled from the top, or the bottom. The composition, direction solidified, and amount of grain refiner in the nine ingots processed are summarized in Table 4, page 22.

Several trends in the data stand out. In attempting to model these experiments, concentrating on experiments which show clear trends or differences may be beneficial.

Comparing Experiments 2 and 7: Experiments 2 (E2) and 7 (E7) had the same Al-10wt. pct. Cu alloy concentration and about the same initial cooling rates (16 and 12

K/min respectively) and additions of TiB_2 grain refiner (0.045 and 0.067wt. pct. respectively). At this alloy concentration, 10wt. pct. Cu, the primary Al grains have nearly the same density as the melt. Experiment 2 was cooled from the bottom, solidifying upward, with the longitudinal temperature and concentration gradients being stable. Experiment 7 was cooled from the top, thus solidifying downward, with longitudinal temperature and solutal gradients being unstable. The temperature measurements for E2 and E7 are shown in Figures 4.3, 4.4, 4.13 and 4.14 and the numerical values are provided in Appendix C, Tables C2 and C7. As shown in Figures 5.12 and 5.17, the grain size in E7 was about 3 times larger than in E2. We believe grains nucleated in the upper portion of the E7 ingot were carried by convection to lower and hotter areas in the ingot where some melted; thus resulting in fewer nucleated grains surviving and the larger grain size. In E2 convection and grain advection is expected to be less extensive, resulting in less grain annihilation and a smaller grain size. We hope in future work to examine segregation in E2 and E7.

Comparison of Experiments 3, 4, and 5 to Experiments 8 and 9: Experiment 3, E4, E5, E8 and E9 had the same starting composition of Al-1wt. pct. Cu. Experiment 3, E4 and E5 were cooled from the bottom and resulted in completely columnar structures. Experiment 8 and E9 were cooled from the top and resulted in completely equiaxed structures. The initial cooling rate imposed during E3, E4, and E5 was about 20 K/min., and about 12 K/min. in E8 and E9. Figures 4.5 through 4.10 and 4.15 through 4.18 show the thermal data, with the numerical data provided in Appendix C, Tables C3, C4, C5, C8 and C9. At this initial composition, 1 wt. pct. Cu, the primary solid Al grains are heavier than the surrounding liquid. In E3, E4, and E5, thermal and solutal gradients are stable, and if there is any settling of Al grains - it is expected to be down - not up into the far field liquid. In E8 and E9 thermal and solutal gradients are unstable and free Al grains and dendrite fragments are expected to settle down - into the far field liquid. The center line composition measurements of E8 show nearly no segregation, see Figures 6.10 through 6.13 and Table 5 of Section 6.2. The columnar structures of E3, E4, and E5 may have been caused by the higher cooling rate, though we believe the development of equiaxed growth in E8 and E9 was assisted by the relatively strong convection expected, perhaps causing some dendrite fragmentation, and that the flat composition profile is caused by settling and advection of solid Al grains.

Comparison of Experiments 6 and 8: Experiment 6 and E8 were both cooled from the top, thus solidified from the top down. But the composition and initial cooling rate used during E6 were Al-10wt. pct. Cu and 5.3 K/min. and the composition and cooling during E8 were Al-1wt. pct. Cu and 12 K/min.; thermal measurements are provided in Figures 4.11, 4.12, 4.15, and 4.16, and in Tables C6 and C8. Figures 5.12 and 5.22 show the grain size in E6 and E8 to be about 2.8 mm, and 5.6 mm respectively; these grain size differences are expected to be dominated by differences in solute concentration, and perhaps cooling rate. Table 5, Figures 6.7 and 6.10 show the Cu concentration of E6 going from about 7wt. pct. at the top of the ingot to about 14wt. pct. at the bottom, and negligible longitudinal segregation in E8. This large difference in amounts of segregation are believed to be due to more extensive settling and pooling of Cu rich liquid in E6, and more extensive settling of Al rich solid grains in E8.

CHAPTER 1

INTRODUCTION

1.1 Background and Motivation

Solidification of metal alloys is characterized by the presence of microscopically complex interfacial structures that can exist on different physical scales. The most common structure for a solid crystal or grain is the dendrite which can exist in either columnar or equiaxed form, as shown schematically in Figure 1.1. The dendrite is characterized by a tree-like structure and is illustrated with the electron microscope image shown in Figure 1.2. Equiaxed dendrites in an alloy nucleate and grow in a temperature and concentration region referred to as the solid+liquid region, or mushy zone, of the equilibrium phase diagram. A typical binary alloy phase diagram can be seen in Figure 1.3. The growth, shape, and composition of equiaxed dendrites are strongly influenced by their movement as will be discussed in the literature review. Movement of equiaxed grains is a result of gravity induced forces in the casting. This includes movement due to sedimentation or floating of the solid and movement due to convection patterns in the melt. Sedimentation or floating of grains is a result of density differences between the grains and the bulk liquid that arise from the rejection or incorporation of solute during the solidification process, and solidification shrinkage. Convection in the melt is due to a combination of density differences resulting from temperature and composition variations in the liquid, typically referred to as thermosolutal convection.

Depending on how cooling is applied to the system and the concentration and density of the constituents, the thermal and solutal buoyancy forces may oppose or add to one another leading to various complex convection patterns (Muller et al., 1984; de Groh III and Lindstrom, 1994). The buoyancy induced melt flow and transport of solid that occurs during solidification generates compositional and structural nonuniformities at the macroscopic level (de Groh III, 1994; Song et al., 1996). It is the goal of current numerical simulation work to predict such compositional and structural nonuniformities in an attempt to minimize their negative affect on the final macrostructure. One numerical model of particular interest was developed by Beckermann and Wang (1995). This model uses a multi-phase/multi-scale approach that allows for the movement of both the solid and the liquid phases during solidification. Beckermann and Wang undertook the first attempt toward predicting equiaxed dendritic microstructures in the presence of melt convection and solid movement. The microstructures of specific interest include the grain size and macrosegregation patterns as a result of combined melt convection and solid movement. They performed limited experimental validation of the model using a NH_4Cl-H_2O transparent model alloy. In addition they demonstrated a numerical application of the model to equiaxed dendritic solidification of Al-Cu alloy in a rectangular cavity. Further validation of the model is needed but a complete set of experimental data is required. It is one of the aims of this research to provide a sufficient set of quantitative data for further validation of their model.

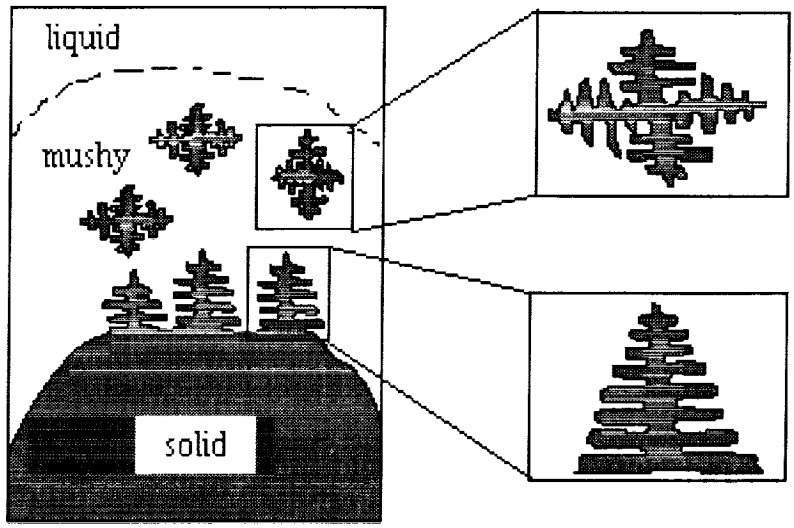

Figure 1.1 Schematic illustrations of the macroscopic regions consisting of solid, liquid, and mushy zones and columnar (bottom right) and equiaxed (top right) dendrites.

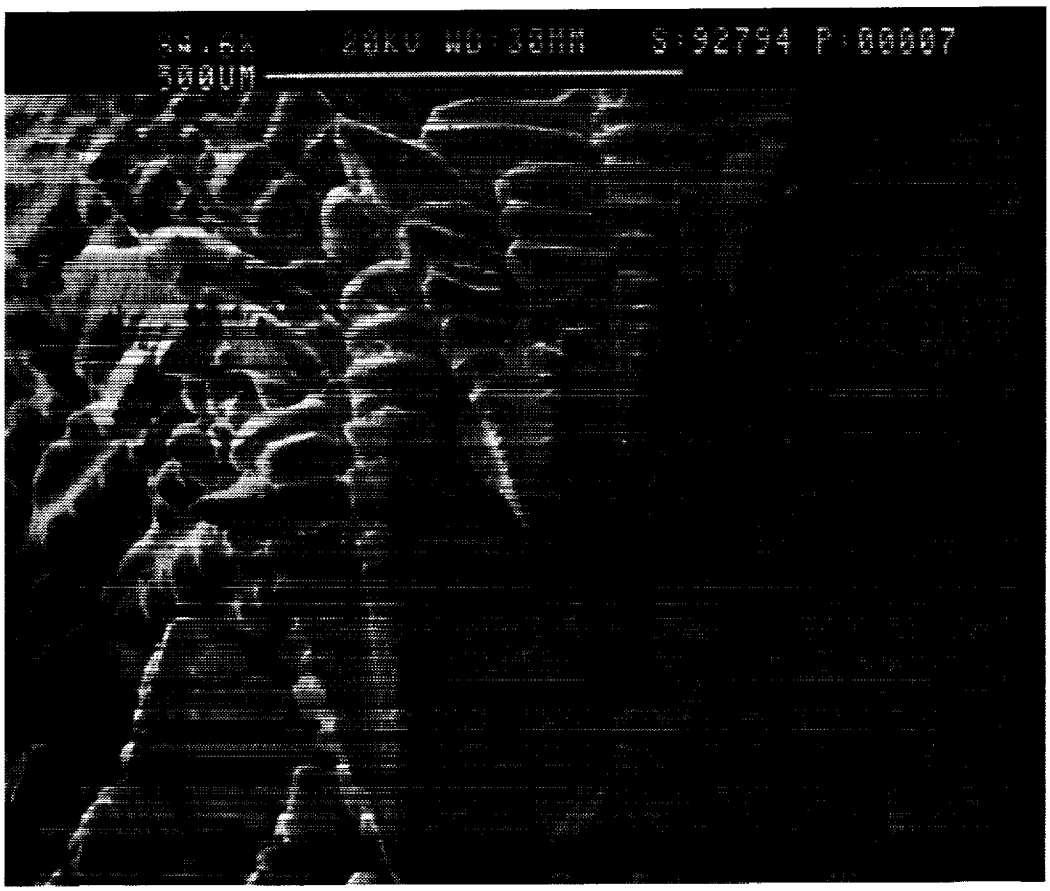

Figure 1.2 Electron microscope image of a lead dendrite on the surface of an ingot. The image illustrates the tree-like structure of a dendrite. (de Groh III, 1998)

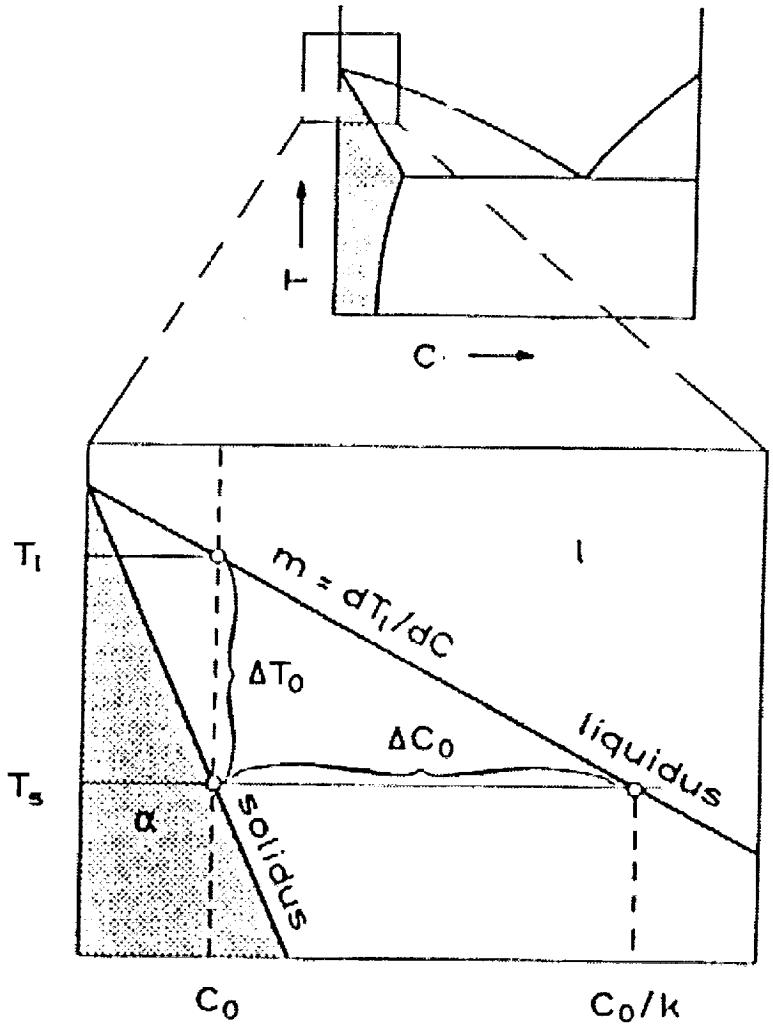

Figure 1.3 Typical phase equilibrium diagram for a binary alloy. The region between the solidus and liquidus lines is commonly referred to as the mushy zone. (Kurz and Fisher, 1986)

1.2 Literature Review

Numerous studies have been done which illustrate the effects of solid transport on the final structure of an alloy. The following section provides a brief overview of a select few of these studies along with an overview of a couple of studies that heavily influenced the setup of the experiments for this thesis.

A fine equiaxed grain structure is often preferred over a columnar structure for reasons such as uniform mechanical properties and better overall strength and resistance to fatigue. In many castings a mixed columnar/equiaxed grain structure exists. Much research has been done to determine the major factors that influence the columnar-to-equiaxed transition (CET) (Griffiths et al., 1996; McCartney and Ahmady, 1994; Ziv and Weinberg, 1989; Sato and Sato, 1982; Doherty et al., 1977). One such study was the unidirectionally solidified casting experiments of Al-3 wt. pct. Cu alloy by Ziv and Weinberg (1989). In these experiments the configuration was thermally and solutally stable, hence minimizing the effect of thermosolutal convection. Figure 1.4 shows a sequence of grain structures where the heat transfer coefficient at the bottom was varied. It can be seen from these experiments that the length of the columnar region increases with stronger cooling. The increased columnar region can be attributed to the stronger thermal gradient in the mushy zone which inhibits the development of free-floating equiaxed crystals which can impinge upon the advancing solidification front and force the CET. Attention is drawn to this result due to its relevance to the solidification experiments performed in the current study. Another important result from this study was the effect of the addition of a grain refiner. In the second set of experiments, the cooling rate and all other conditions were identical except for the addition of minute amounts of grain refiner (TiB_2). With increasing amounts of grain refiner, the structure changes from a coarse-grained mixed structure to one of fine equiaxed grains. Figure 1.5 shows the sequence of experiments from left to right with increasing grain refiner. The grain refiner reduces the size of the grains by effectively increasing the number of nucleation sites and therefore increasing the number of nucleated grains which compete in the mushy zone.

Movement of equiaxed grains can cause particularly severe macrosegregation due to sedimentation as observed in solidification of undercooled Pb-Sn eutectic alloys (de Groh III, 1988; de Groh III and Laxmanan, 1988). In these experiments the eutectic melt was substantially undercooled before solidification. The undercooling caused the primary Pb phase to nucleate first. Since the Pb dendrite is more dense than the bulk liquid, the Pb-rich dendrites tend to sink leaving behind a Sn-rich melt. As illustrated in Figure 1.6, the settling effect of grains can be seen with the insertion of a stainless steel screen near the center of the ingot. The plot shown to the left in Figure 1.6 illustrates the corresponding macrosegregation profile. The solid movement due to the density differences between the bulk liquid and the solute-poor grains results in the strong increase in Pb concentration toward the screen and the sample bottom, with an approximate 20 wt. pct. jump at the location of the screen. Similar experiments were performed with an Al-Cu alloy (Ohno, 1987). Figure 1.7 illustrates the resulting macrostructure of an aluminum ingot after inserting a stainless steel filter into the melt.

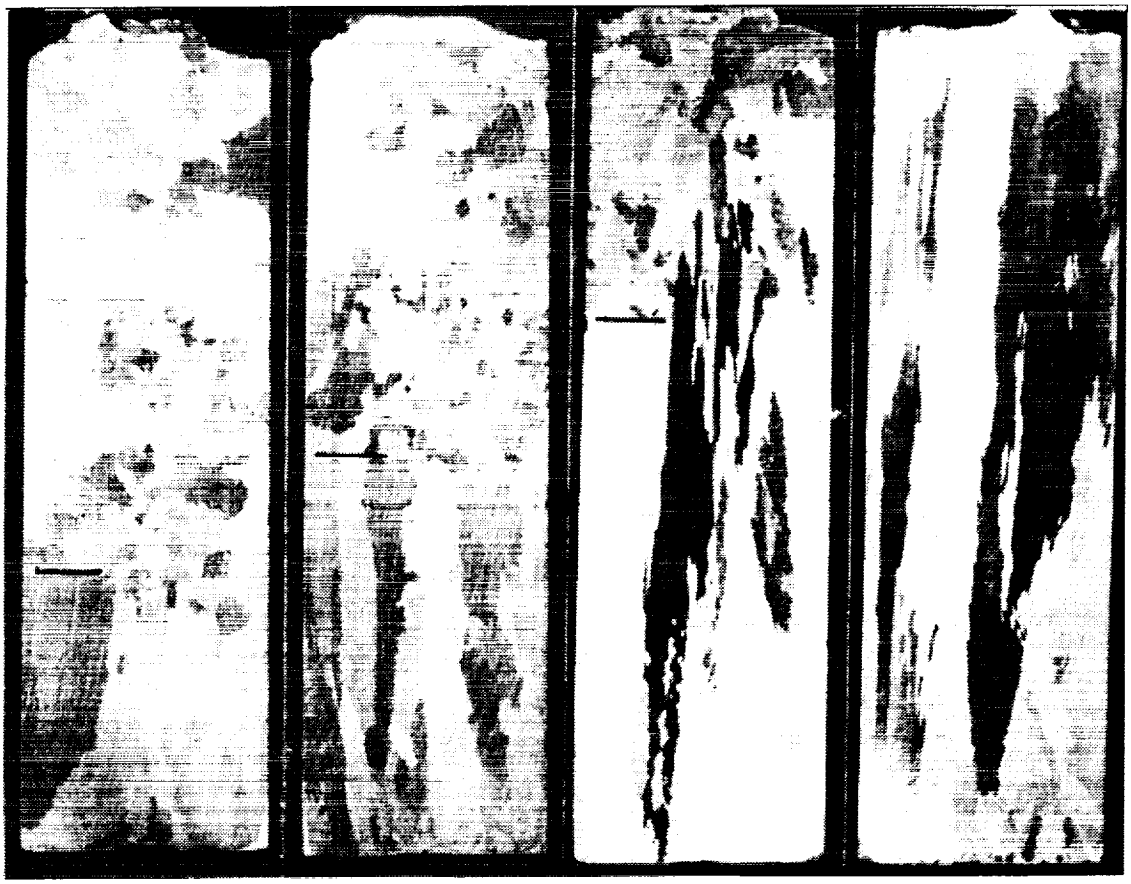

Figure 1.4 Grain structure of a vertically solidified Al-3 wt. pct. Cu alloy showing the columnar-to-equiaxed transition. (Ziv and Weingerg, 1989)

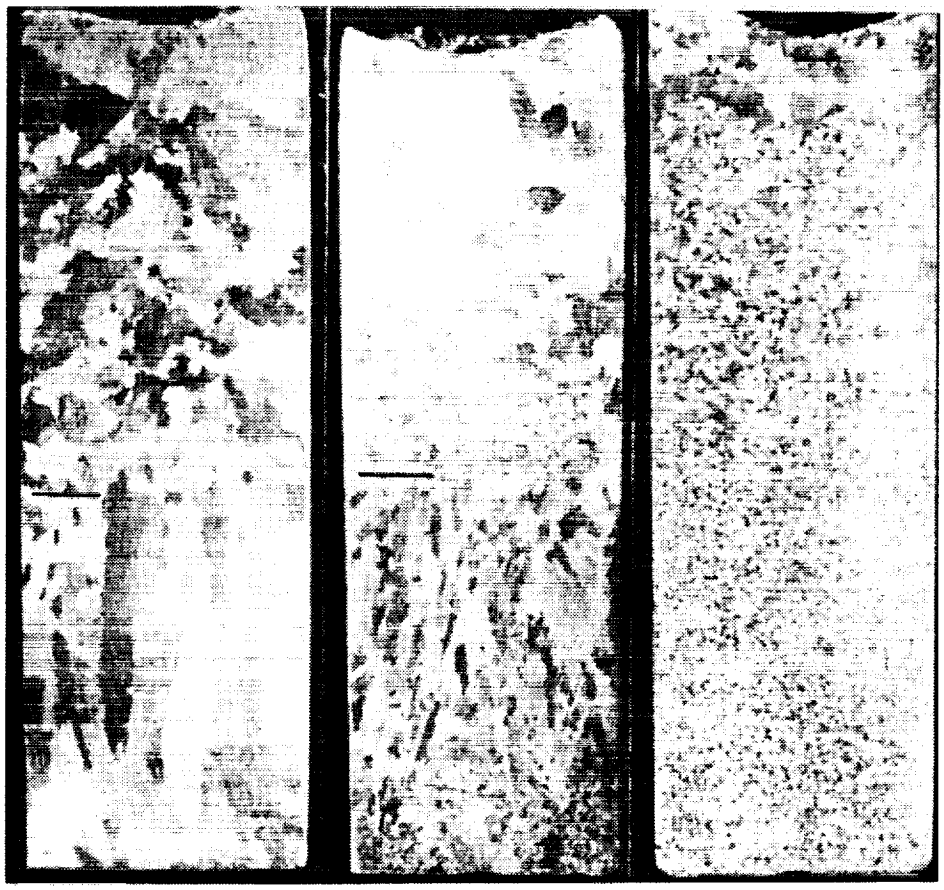

Figure 1.5 Grain structure of a vertically solidified Al-3 wt. pct. Cu alloy showing the effect of increasing grain refiner (TiB_2) concentration (from left to right). (Ziv and Weinberg, 1989)

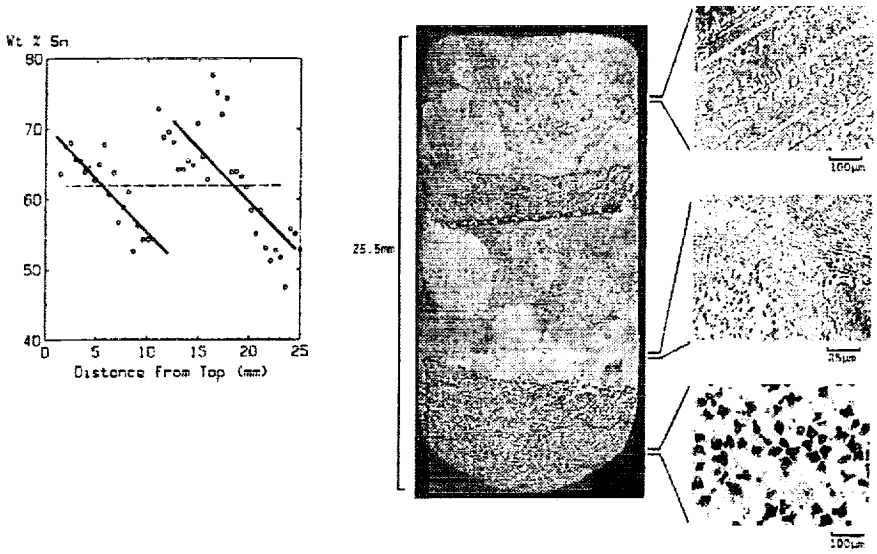

Figure 1.6 Effects of settling of equiaxed grains on solidification of an undercooled Pb-Sn eutectic alloy with a stainless steel screen near the center. (left) Microprobe composition measurements. (center and right) Micrographs of longitudinal cross-sections. (de Groh III and Laxmanan, 1988)

Figure 1.7 Resulting macrostructure of an aluminum ingot after inserting a stainless steel filter into the melt prior to quenching. (Ohno, 1987)

In these experiments (Fig. 1.7) the solute-poor grains were heavier than the bulk liquid, as with the Pb-Sn experiments (Fig. 1.6), resulting in the similar effect of settled grains on top of the inserted stainless steel screen. The rate and manner by which free equiaxed grains settle influence the amount and distribution of segregation. An understanding of this settling behavior is necessary for the understanding and possible control of the solidification process. The basic settling characteristics of manufactured dendritic shapes and natural dendrites in clear metal analogs have been examined by Zakhem et al., 1993; Ahuja, 1992; Ahuja et al., 1992; de Groh III et al., 1993; and Wang et al., 1995, and has resulted in the solution of the interfacial drag between equiaxed dendrites and their surroundings over a wide range of solid volume fractions thereby enabling the determination of grain movement in numerical modeling.

As mentioned in the introduction, gravity induced forces not only result in sedimentation and floating of solid grains, but also cause convection in the melt. One such study that illustrates this was done on an aqueous solution of NH_4Cl (Hellawell et al., 1993). In this study channel plume flow was observed directly in the transparent aqueous solution and evidence of plume flow was found in fully solidified alloys. Figure 1.8 shows plumes that have develop in the mushy zone and erupted into the liquid. These plumes can transport solid fragments and cause segregation on the system scale. The permeability of the mushy zone has a large effect on the development of these plumes. Another study showing the influence of fluid flow on macrostructure was done by Griffiths and McCartney (1993). In this study, hypoeutectic alloys of Al-Cu and Al-Si were solidified downwards to promote thermosolutal convection in the melt. Fragmentation processes versus heterogeneous nucleation were investigated for their affect on the CET. There was no evidence found from Griffiths and McCartney's investigation that fragments of the solidification front were responsible for the CET, but rather it was suggested that the main contributor to the equiaxed zones was the heterogeneous nucleation ahead of the solidification front. Lastly, essential principles of thermosolutal convection are outlined in a paper by Hansen et al. (1996). The paper discusses some consequences of thermosolutal convection on the grain structure of castings. A discussion of the two contributors to buoyancy within a fluid, thermal and solutal contributions, is thoroughly discussed.

While the studies reviewed showed the effects of solid movement and thermosolutal convection on macrosegregation and grain size distribution, none of them presented all of the data required for a thorough validation of a numerical model. That is, none of the previous studies carefully controlled and presented thermal boundary conditions, temperature data, segregation data, and grain size data all at the same time. As mentioned earlier, a complete set of experimental data is required for validation of the numerical model of interest. For this reason, there is a need for carefully controlled solidification experiments.

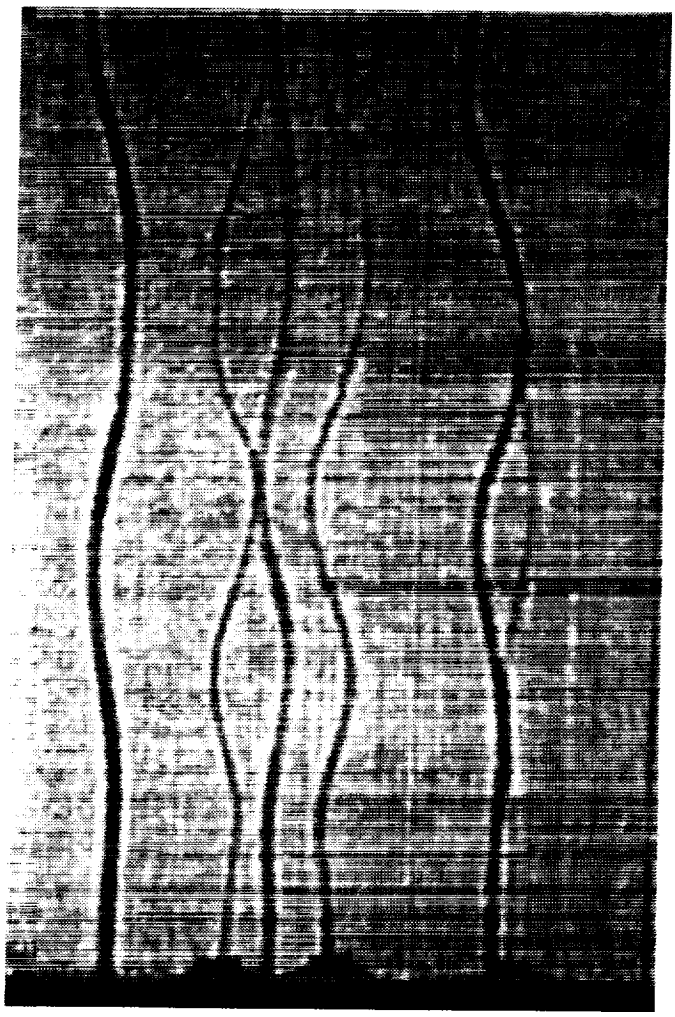

Figure 1.8 Plume convection patterns above an aqueous NH_4Cl growth front. (Hellawell, Sarazin, and Steube, 1993)

1.3 Objectives of Current Study

The objectives of this research are as follows:

1) Experimentally study the effects of solid transport and thermosolutal convection on macrosegregation and grain size distribution patterns.

2) Provide a complete set of experimental data: controlled thermal boundary conditions, temperature data, segregation data, and grain size data, to validate numerical models such as the one developed by Beckermann and Wang (1995).

In the next chapter, the experimental setup and procedures for the solidification of the Al-Cu alloy ingots are presented. Chapter 3 describes procedures required for obtaining the grain size and segregation data from the fully solidified samples. Chapter 4 discusses the results of the solidification experiments and presents the measured cooling curves and thermal boundary conditions. In Chapter 5 the grain size measurements are set forth with illustrations and discussion. Pictures of the overall grain structure are presented along with various calculated quantities required to evaluate the grain size. Chapter 6 discusses the result of the segregation measurements. Chapter 7 provides preliminary numerical work by applying the experimental boundary conditions to a one-dimensional model of solidification. The final chapter summarizes the major conclusions from this study as well as recommendations for future research.

CHAPTER 2

EXPERIMENTAL SETUP AND PROCEDURES

2.1 Introduction

The primary objective of the solidification experiments is to determine how convection in the liquid and settling of free grains, interrelate and result in segregation in castings. A secondary objective is to provide quantitative data on the Al-Cu alloy system to allow a critical test of the numerical model developed by Beckermann and Wang (1995).

Experiments were conducted with a detailed consideration of the theoretical model with concentration on equiaxed solidification of bulk ingots. The Glove Box Casting Facility (GBCF) and the Bulk Undercooling Furnace (BUF) in the Microgravity Materials Science Laboratory at the NASA Glenn Research Center in Cleveland, Ohio were used to perform the experiments. The GBCF was used to prepare the necessary constituents for the experiments while the BUF was used to provide computer control over the thermal gradients and boundary conditions of the experiments.

Internal temperatures of the ingot were measured during solidification through the use of strategically placed thermocouples. After solidification, the ingots were sectioned and etched to determine structural and compositional variation. Variations were

determined through the use of light microscopy techniques to measure grain size variation and microprobe analysis to measure macrosegregation.

2.2 Experimental Setup

2.2.1 Experimental Materials and Conditions

In order to see transport phenomena such as solid sedimentation and fragmentation, two different Al-Cu alloys were selected. Al-1 wt. pct. Cu was chosen because the dendrites that grow will be denser than the bulk liquid and tend to sink (See Appendix A for calculations). The second alloy chosen was Al-10 wt. pct. Cu; this selection was based on the nearly equal buoyancy of the liquid and solid states at the start of solidification.

Since a fully equiaxed microstructure is desired for the experiments, factors on the Columnar to Equiaxed Transition (CET) are taken into consideration. Determination of melt superheat is based on previous work by Suri et al. (1997), finding that the extent of the columnar region increases with superheat. In adherence with this finding, a temperature of 50°C above the liquidus temperature was selected for the experiments. A nucleating agent or grain refiner was also used in some experiments to promote the CET by providing more locations for heterogeneous nucleation. The refiner chosen for the experiments was TiB_2 (11 μm average particle size).

The grain refined samples of Al-1 wt. pct. Cu and Al-10 wt. pct. Cu consisted of 0.45 and 0.045 wt. pct. TiB_2, respectively. The amount of TiB_2 added is based on the study by McCartney and Ahmady (1994) according to the parameter β (See Appendix B). Later, additional experiments were performed with additional refiner, 0.67 wt. pct. for the 1 wt. pct. Cu alloy and 0.067 wt. pct. for the 10 wt. pct. aluminum alloy. The additional refiner was needed to further reduce the grain size in the resulting casting.

2.2.2 Description of Equipment

Two separate facilities were used to conduct the experiments. One facility was used to prepare the Al-1 wt. pct. and Al-10 wt. pct. Cu samples and the other facility was used to perform the controlled cooling experiments. The first facility used, The Glove Box Casting Facility (GBCF), is a stainless steel glove box that is kept at a positive pressure of argon. The GBCF has an operating temperature range of 25 to 950°C. The inert atmosphere and the high temperature capability of the furnace were the primary reasons why the GBCF was selected to prepare the samples of aluminum and copper.

Once the samples are prepared the experiments are conducted in an apparatus referred to as the Bulk Undercooling Furnace (BUF) shown in Figure 2.1. The BUF is a three-zone furnace with water and gas cooling systems at the top and bottom ends. The BUF is designed to study the effects of undercooling in metal alloys, however, it can be used to directionally solidify materials upward or downward. The operating temperature range of the BUF is from 25 to 800°C. Thermal gradients can be achieved between the range of 0 to 70°C/cm for the bottom cooler and 0 to 10°C/cm for the top cooler.

For the current experiments, the BUF houses a cylindrical Boron Nitride crucible that contains the Al-Cu sample. The specifications of the Boron Nitride crucible are shown in Figure 2.2. Nine thermocouples are located within the furnace and crucible to control the heat ramp up, the constant temperature soak, and the adiabatic quench of the alloys. Figures 2.2, 2.3, and 2.4 detail the thermocouple locations.

An IBM Compatible PC and HP 3497A data acquisition unit were used to control heat input to the system as well as record the thermal history of the experiments. The software incorporated into the PC implemented a proportional-integral control algorithm for the power supplies and provided a data scan rate of 1 Hz for thermocouple outputs. The software controlled the top and bottom heating zones only; therefore, of the three heating zones available only the top and bottom zones were used in these experiments.

Of the nine thermocouples, two different types are used in the experiments. The three thermocouples that are placed in the sample are a K-type Transition Junction style thermocouple with a grounded junction while the remaining thermocouples are a K-type Nextel covered flexible thermocouple with a welded bead, exposed junction. The specifications of the two K-type thermocouples are presented in Table 1.

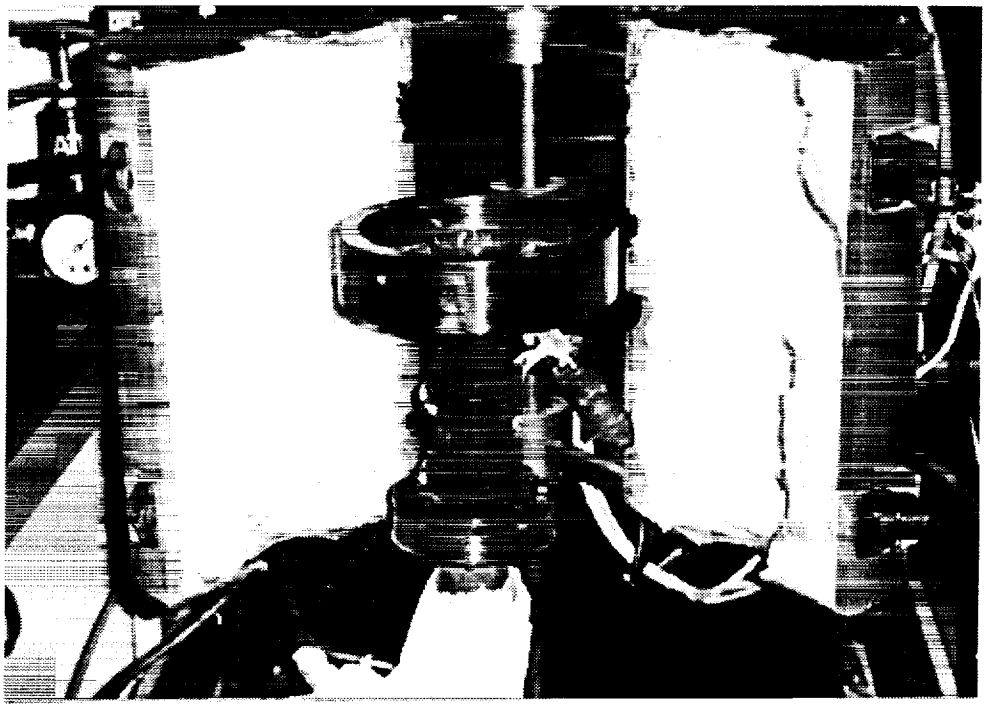

Figure 2.1 Illustration of Bulk Undercooling Furnace at the NASA Glenn Research Center. The Bulk Undercooling Furnace was used to perform the directional solidification experiments.

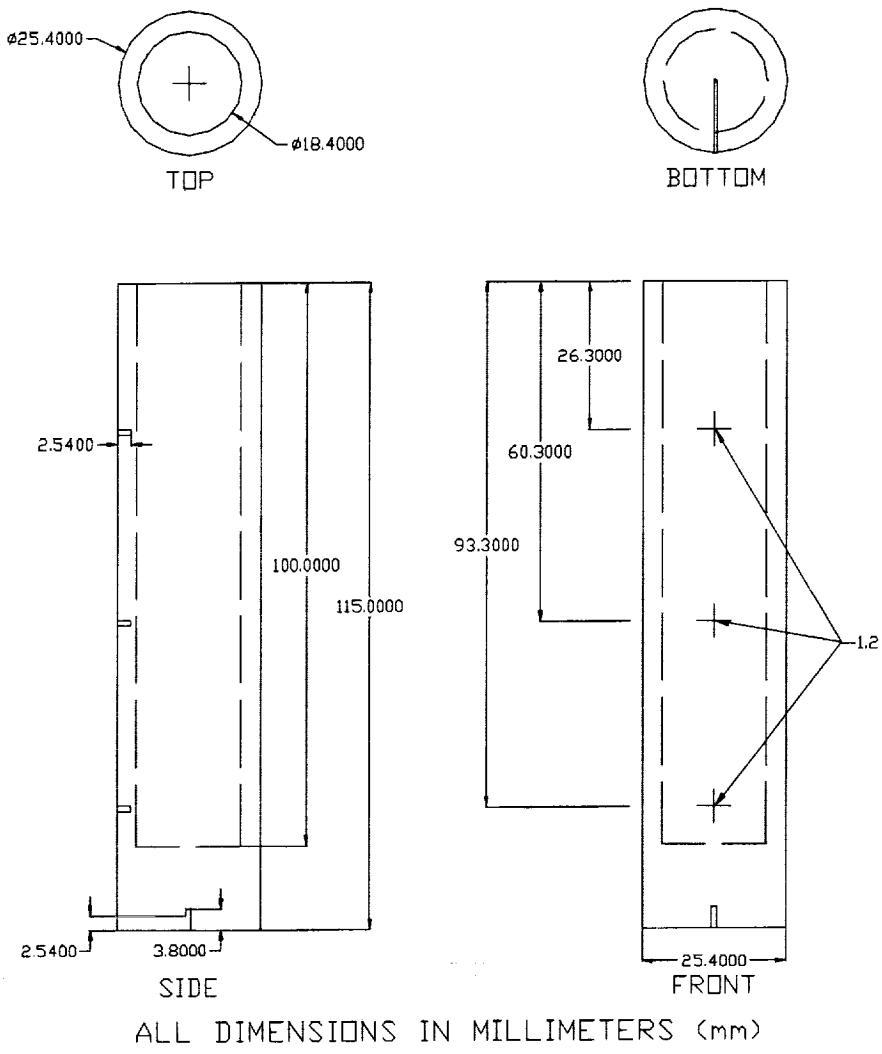

Figure 2.2 Boron Nitride crucible dimension specifications. The schematic above also shows the location of the holes for the four thermocouples that were attached to the crucible.

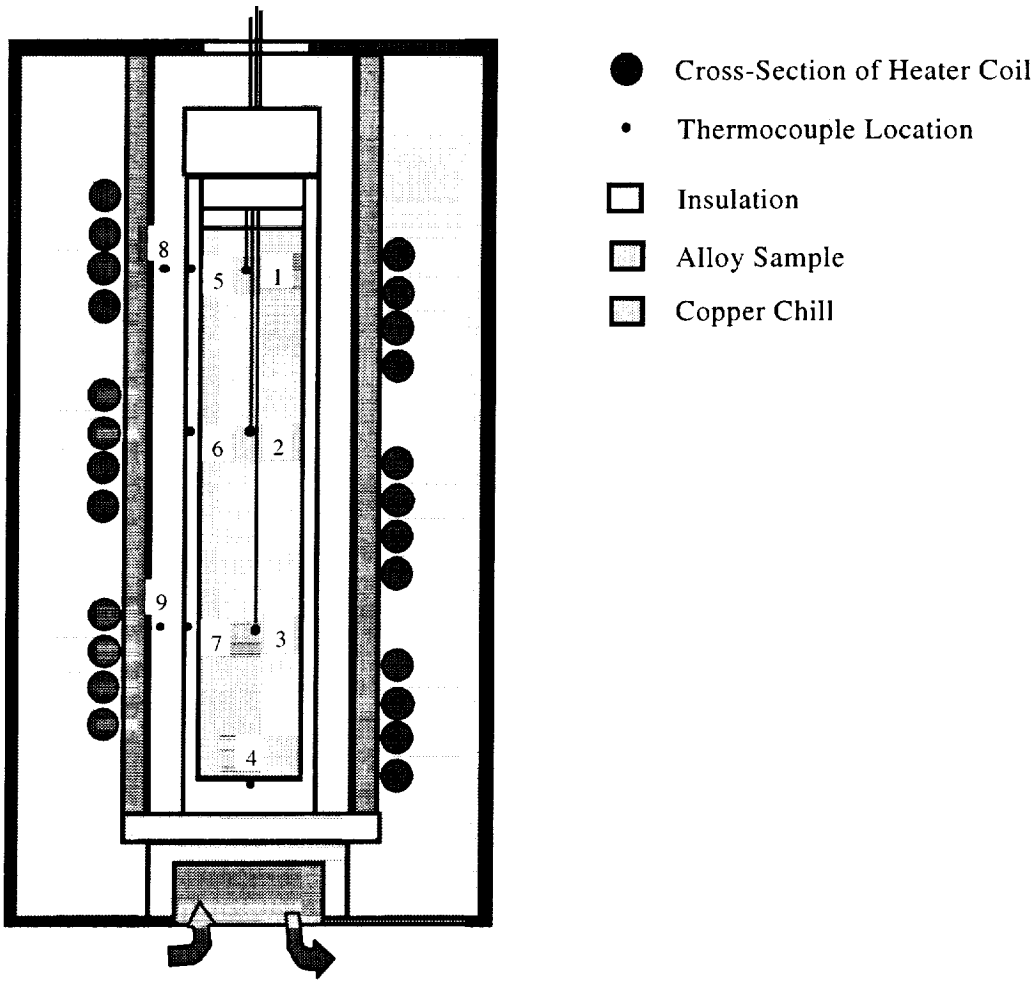

Figure 2.3 Cross-sectional View of Bulk Undercooling Furnace.

As shown in Figure 2.3, the BUF contains a total of nine thermocouples as follows:

- Three sample thermocouples (No.1-3) with a 1.62 mm diameter boron nitride coated sheathing; see Fig. 2.4 for longitudinal locations.
- One thermocouple (No.4) located at the bottom interior wall of the crucible
- Three thermocouples (No.5-7) located along the crucible wall adjacent to their respective sample thermocouples (No.1-3)
- Two furnace thermocouples (No.8, No.9) located within the insulation that surrounds the crucible and at the same height location along the ingot as thermocouples No.5 and No.7.

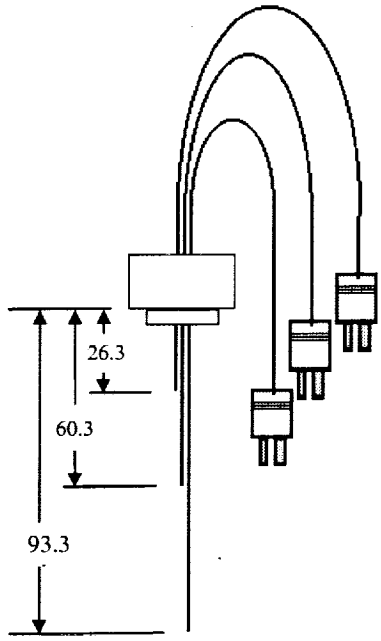

Figure 2.4 Thermocouple and Boron Nitride cap assembly. All dimensions in millimeters.

Table 1. Thermocouple Specifications

Configuration	Metal-Sheathed, Molded Transition Junction Probes	Nextel Insulated Exposed Junction
Calibration	K Chromega®/Alomega® (Ni-Cr/Ni-Al)	K Chromega®/Alomega® (Ni-Cr/Ni-Al)
Temperature Range	probe to 982°C	insulation to 1200°C thermocouple to rated limits
Insulation/Sheathing	MgO insulation with 304 or 321 stainless steel sheathing	high temperature Nextel ceramic
Size	1.5 mm diameter and 450 mm length	0.813 mm and 600 mm length

2.3 Experimental Procedures

2.3.1 Preparation of Samples

Before the experiments could be performed several steps were taken to prepare the alloys. For each experiment, 24.0 cm^3 samples were prepared by heating the necessary constituents (see Table 2) in a Boron Nitride crucible inside the GBCF. Properties used to determine the amount of each constituent are shown in Table 3. A portion of the commercial grade aluminum was first melted in the crucible and the remaining constituents incrementally added and allowed to dissolve in the liquid aluminum. The furnace was allowed to reach a set point temperature of 780°C to ensure adequate superheat for the pure aluminum, which has a liquidus temperature of 660.37°C.

The sample was left to soak for approximately two hours stirring the mixture repeatedly with a boron nitride coated stirring rod. Sample thermocouples positioned at the appropriate locations within a boron nitride cap are next inserted into the crucible (see Figure 2.4) and the crucible is removed from the furnace, the sample then cools and solidifies. Once cooled the sample is then ready to be transferred to the BUF.

2.3.2 Procedures for Directional Solidification

Throughout each experiment, argon gas is allowed to trickle down into the BUF to help reduce oxidation of the samples. Samples processed in the BUF are put through controlled heating, soak, and quench stages with temperature measurements taken every thirty seconds. Each heating stage consists of a constant heat ramp up of 10°C/min., which is followed by a one hour soak at a fixed temperature 50°C above the liquidus temperature, 685°C for Al-10 wt. pct. Cu and 710°C for Al-1 wt. pct. Cu. The melting temperature of the alloys and the superheat are shown graphically on the phase diagram for Al-Cu, Figure 2.5. The quench stage consists of either bottom quenching, which is achieved though the use of a water (25 mm gauge flow) cooled copper chill plate located at the bottom surface of the crucible, or top quenching, in which argon gas (30 psi inlet pressure and 2.5 mm gauge flow) is injected directly onto the top surface of the sample. The individual stages of the experiment are computer controlled through the use of the

bottom and top heater coils, quenching fluids, and seven of the nine thermocouples contained within the BUF. The end result of the samples processed in the BUF is a directionally solidified sample from either the top or bottom.

The cooling rate near the end being cooled for each experiment is given in Table 4. For experiments cooled from the top, Table 4 gives the cooling rate measured by thermocouple 1. For experiments cooled from the bottom, Table 4 provides the cooling rate measured by thermocouple 3. Cooling rates were taken just before T_o was reached. The variations in cooling rate are believed to be due to the different cooling capabilities of the two quench techniques, variation in cooling fluid flow rate and temperature, and contact resistances.

Referring back to Figure 2.4, the top (No.1) and bottom (No.3) sample thermocouples are used to control the heat ramp up and soak stages while thermocouples No.5 and No.8, and No.7 and No.9 are used to enforce adiabatic conditions on the crucible wall during the quench stage. The adiabatic boundary condition is achieved by minimizing radial thermal gradients in the quench stage through a proportional-integral control algorithm that minimizes the difference in temperatures between thermocouple's 5 and 8 and between thermocouple's 7 and 9. The furnace thermocouples 8 and 9 are kept slightly hotter than the wall thermocouples 5 and 7 through heat addition to the system, thereby preventing radial heat loss.

The procedure discussed was used to perform nine experiments in the BUF; the sample concentration, amount of grain refinement, and solidification direction of all experiments are summarized in Table 4. Before the results of these experiments are presented and discussed, experimental procedures are set forth. While it was not necessary to completely analyze each experiment before moving onto the next it was critical to determine the overall grain structure. By reviewing the grain structure it was possible to determine if the experiment showed promise for being a critical test of the numerical model being developed.

Table 2. Properties for Determining Constituents

Volume of Sample	24 cm^3
Density of Solid Al, room temp.	2.6989 g/cm^3
Density of Liquid Al, T_m	2.38 g/cm^3
Density of Solid Cu, room temp.	8.96 g/cm^3
Density of Liquid Cu, T_m	7.99 g/cm^3

Table 3. Masses of Constituents

Al-1 wt. pct. Cu	Mass (grams)
Copper	0.652
Aluminum	64.577
Total Mass	65.229
Al-10 weight pct. Cu	
Copper	6.964
Aluminum	62.676
Total Mass	69.640

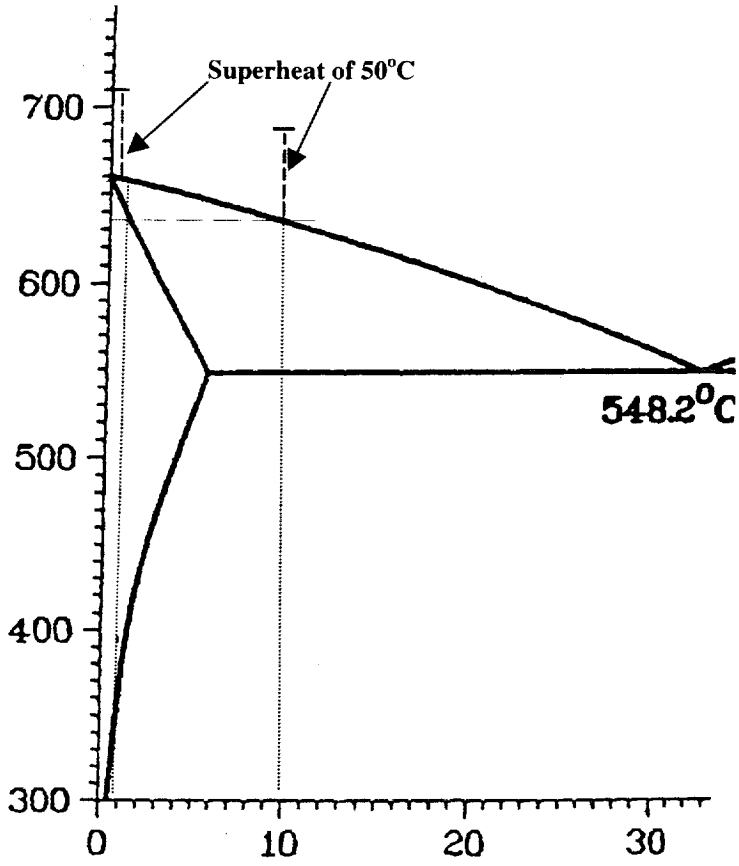

Figure 2.5 A portion of the Al-Cu alloy phase diagram. The points of intersection between the liquidus line and the vertical lines at the alloy compositions of interest are shown schematically above. These points correspond to the point where solidification begins. The amount of superheat used in the experiments is also shown.

Table 4. Summary of Experiments Conducted in the Bulk Undercooling Furnace. Cooling rate just before T_o (about 635 and 660 °C) is reached, measured from T1 for top cooled experiments and T3 when bottom quenched.

Experiment	Alloy Composition	Refiner Added (TiB_2)	Direction Solidified	Cooling Rate
E1	Al-10 wt. pct. Cu	No Refiner Added	Bottom to Top	12.4 °C/min.
E2	Al-10 wt. pct. Cu	0.045 wt. pct.	Bottom to Top	16
E3	Al-1 wt. pct. Cu	0.450 wt. pct.	Bottom to Top	18
E4	Al-1 wt. pct. Cu	No Refiner Added	Bottom to Top	19
E5	Al-1 wt. pct. Cu	0.670 wt. pct.	Bottom to Top	24
E6	Al-10 wt. pct. Cu	0.045 wt. pct.	Top to Bottom	5.3
E7	Al-10 wt. pct. Cu	0.067 wt. pct.	Top to Bottom	11.9
E8	Al-1 wt. pct. Cu	0.450 wt. pct.	Top to Bottom	12
E9	Al-1 wt. pct. Cu	0.670 wt. pct.	Top to Bottom	11.3

CHAPTER 3

GRAIN SIZE AND SEGREGATION MEASUREMENT PROCEDURES

3.1 Introduction

The following section presents sample preparation for grain size and segregation measurements. Once the samples had been prepared appropriately, the procedures set out in Section 3.3 and 3.4 were used to measure the grain size and segregation.

3.2 Preparation Procedures

3.2.1 Cutting Procedures

In order to determine the grain size and measure segregation several procedures needed to be performed on each ingot. After each experiment the ingot was cut for polishing purposes and some form of etching was performed to bring out the grain structure.

At the conclusion of each experiment, the solidified samples were removed from the crucible and cut with a band saw longitudinally down the centerline (see Figure 3.1). One half of the sample was then cut transversely into four sections, each section being mounted in metallographic epoxy and polished.

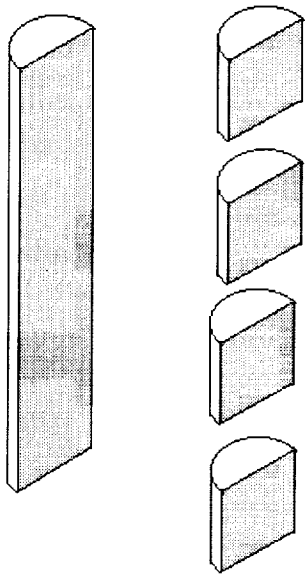

Figure 3.1 Cut sections of sample, one half is cut into four sections for auto-polishing and microprobe analysis while the other half is hand polished and used for grain size measurements.

3.2.2 Polishing Procedures

The four transversely cut sections that were mounted in metallographic epoxy were submitted to the metallurgy lab at the NASA Glenn Research Center where an automatic polishing procedure was performed. The uncut half of the sample was large enough to be hand held for subsequent grinding and polishing. Grinding was performed in successive steps using silicon carbide abrasive papers of 180, 400, and 600 grit. Polishing was done in successive steps using diamond-polishing pastes of 6, 3, and 1 μm on a DAC polishing cloth. A final polish was done with an OP Chem cloth and a slightly acidic silica solution.

3.2.3 Etching Procedures

An etchant called Modified Keller's Reagent, Equation 3.1, was used to prepare the uncut half of the ingot for photography.

$$15 \text{ ml HF} + 4.5 \text{ ml } HNO_3 + 9.0 \text{ ml HCl} + 271.5 \text{ ml } H_2O \qquad (3.1)$$

The etchant was applied to the sample by submerging the sample for 15-30 seconds. A second etchant, equation 3.2, was then used to help highlight the grain boundaries.

$$0.5 \text{ g NaOH} + 1 \text{ g } KMnO_4 + 250 \text{ ml distilled water} \qquad (3.2)$$

Between etchants the samples were washed with water and alcohol, then with phosphoric acid and distilled water and allowed to air dry. Finally, the samples were submersed three times for 20 to 40 seconds each in the second etchant.

3.3 Grain Size Measurements

One of the important quantitative measurements is the measurement of the microstructure grain size. The procedures used for the grain size measurements are intended for a fully equiaxed microstructure. Non-equiaxed grain structures require measurements on three principal planes i.e., the longitudinal, planar, and traverse planes. Due to the additional information required, it would be beyond the scope of this study to determine the grain size for those experiments having a non-equiaxed microstructure. Samples that were not equiaxed were not analyzed further.

The grain size was determined using the procedures outlined in ASTM E112 for measurement of equiaxed grains by the intercept method. The intercept method consists of a template of three concentric circles with a total line length of 500 mm. The template is placed over the grain structure without bias, and the number of intercepts, N_i, is counted. For each experiment, an appropriate magnification factor was selected which would give an adequate number of intercepts on the resulting 4" x 5" photograph, see Figure 3.2 for an example. Photographs were taken traversing along the centerline of the sample to cover the sample from bottom to top. The template was then successively applied to five blindly selected positions per photograph, separately recording the count of intercepts for each. Using the values recorded a mean intercept count was calculated for each section.

With the mean of the intercepts for each photograph useful quantities pertaining to grain size were calculated. On the scale that the measurements were taken a single phase microstructure assumption was used because the amount of the second phase (eutectic) was minimal compared to the primary phase. Important quantities were derived from the lineal density of the grains, N_L. The equation for the lineal density is shown in equation 3.3 and consists of the number of intercepts counted per field, the magnification factor, and the total test line length. Desired quatities were caluated according to Equations 3.4-3.10. Equation 3.4 is the mean lineal intercept length, $\bar{\ell}$, which is the inverse of the lineal density. Equation 3.5 is the number of grains per unit area calculated as a function of the lineal density. Equation 3.6 is the mean grain cross sectional area, $\bar{A}$. Equation 3.7 is the number of grains per unit volume calculated as a function of the lineal density. Equation 3.8 is the mean grain volume, $\bar{V}$. Equation 3.9 is the mean spatial (volumetric) grain diameter, $\bar{D}$. Finally, Equation 3.10 is the grain boundary surface area per unit volume, S_V.

$$\bar{N}_L = \frac{\bar{N}_i}{L/M} \qquad \left(\frac{\text{intercepts}}{\text{mm}}\right) \tag{3.3}$$

$$\bar{\ell} = \frac{1}{\bar{N}_L} \qquad \left(\frac{\text{mm}}{\text{intercept}}\right) \tag{3.4}$$

$$\bar{N}_A = 0.735\bar{N}_L^{\,2} \qquad \left(\frac{\text{grains}}{\text{mm}^2}\right) \tag{3.5}$$

$$\bar{A} = \frac{1}{\bar{N}_A} \qquad \left(\frac{\text{mm}^2}{\text{grain}}\right) \tag{3.6}$$

$$\bar{N}_V = 0.422\bar{N}_L^{\,3} \qquad \left(\frac{\text{grains}}{\text{mm}^3}\right) \tag{3.7}$$

$$\bar{V} = \frac{1}{\bar{N}_V} \qquad \left(\frac{\text{mm}^3}{\text{grain}}\right) \tag{3.8}$$

$$\bar{D} = 1.571 \cdot \bar{\ell} \qquad (\text{mm}) \tag{3.9}$$

$$S_V = 2 \cdot \bar{N}_L \qquad \left(\frac{1}{\text{mm}}\right) \tag{3.10}$$

The preceding equations were taken from DeHoff and Rhines (1968). The constants shown in equations 3.5, 3.7, and 3.9 are based on an assumed geometric shape for the grains and relate the number of intercepts to the number of grains. It is assumed that the actual grain shape approximates closely to the shape of a truncated octahedron or tetrakaidecahedron. The reasoning for the geometric model and the statistical basis for the selection of the constants is discussed by DeHoff and Rhines. The geometric model is based on surface-tension considerations, supported by excellent agreement between theory and observation.

3.4 Segregation Measurements

Another important quantitative measurement is the degree of the segregation in the sample. Segregation is caused by the incorporation or rejection of a constituent during solidification resulting in concentration gradients in the sample. Segregation occurs on the microscopic scale, but can result in segregation on a macroscopic scale due to movement of grains or interdendritic liquid from thermal and solutal gradients in the melt. The top cooled experiments performed are the most susceptible to macrosegregation due to the thermal instability introduced from cooling above. Based on this and economic reasons, the concentration profiles in only two top cooled experiments were measured.

Two sets of metallurgical samples were sent for microprobe analysis at the NASA Glenn Research Center. Each set consisted of four samples cut from a single solidification bar. Four sections from experiment E8, Al-1 wt. pct. Cu alloy refined with 0.45 wt. pct. TiB_2, and four sections from experiment E6, Al-10 wt. pct. Cu alloy refined with 0.045 wt. pct. TiB_2, were analyzed. Both experiments were cooled from the top to the bottom and were selected as the samples that showed the most promise for segregation on a macroscopic scale for each alloy composition.

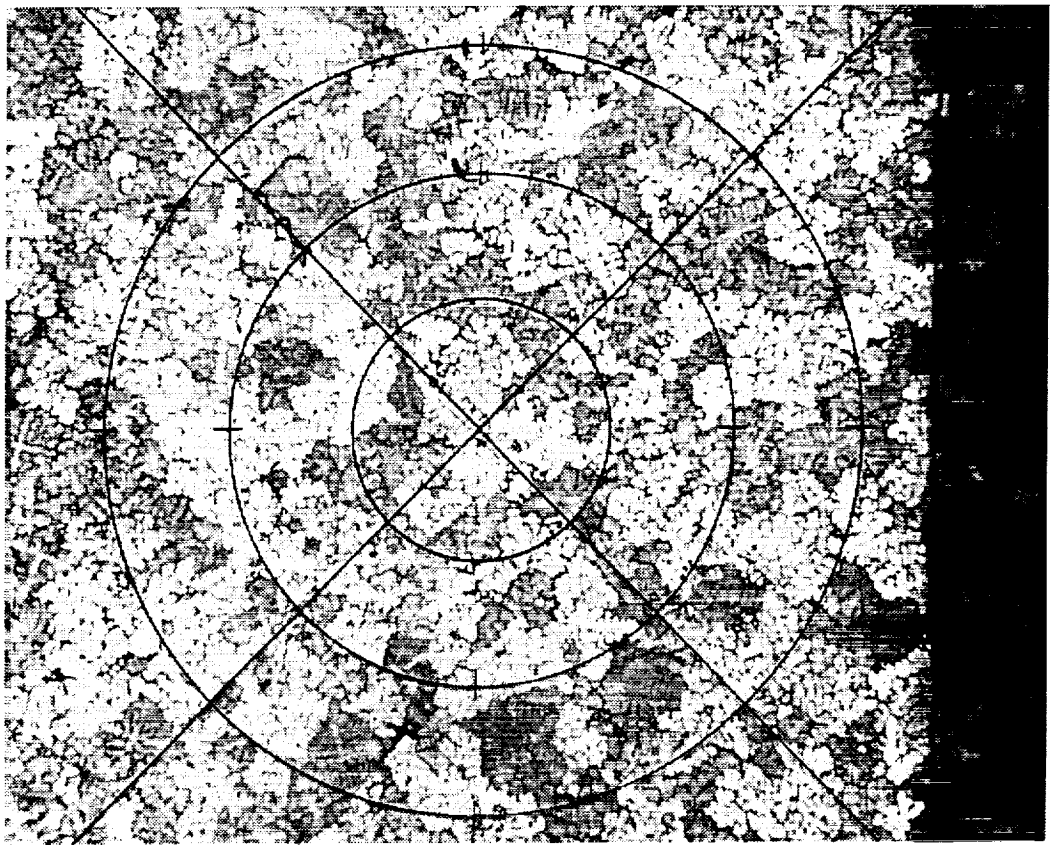

Figure 3.2 Schematic illustrating the testing procedure used to determine the grain size. The number of grains are counted that intercept the three concentric circles.

The microprobe analysis was performed by Jim Smith at NASA Lewis Research Center using wavelength dispersive X-ray spectroscopy on a ARL SEMQ electron microprobe. The procedures that he employed are taken directly from his report and are repeated herein for completeness.

> Final preparation (polishing) of the samples had been done several months prior to submission to perform microsegregation measurements; therefore, the samples were re-polished, lightly coated with evaporated carbon (approximately 100 angstroms) and placed in a dessicator until the individual samples were examined in the electron microprobe. A linear traverse of 20

micron steps down the middle of the section, would give the most reproducible results. The average traverse distance along each sample is 22mm (22,000 microns) which works out to approximately 1100-1200 points per sample. Even though stage and analysis modes are automated on the probe, the average time for a two element run using the accepted method of off-peak correction is about fifty seconds which means it would take sixteen and a half hours to complete one run, not counting approximately three to four hours to set up and stabilize the probe, key in the X,Y, Z coordinates, standardize, etc.

Numerous unsuccessful attempts were made to perform the analyses in the preferred manner of using off-peak correction and eventually it became clear that uncorrectable drift in one form or another would creep into the equation over time and non-reproducible data would result. Temperature changes in the room, standardization drift, and even barometric pressure changes due to cold fronts (affects the gas pressure regulators) are just some of the culprits. It soon became apparent that in order to obtain some consistency, the analysis time had to be shortened considerably.

There are two common methods for performing a background correction on WDS X-ray fluorescence data. The method most frequently employed is the off-peak background correction method. Counts are not only measured on the peak but on assigned background locations on either side of the peak and these values are used in the ZAF corrections. This is the primary technique used at NASA since they are involved with high atomic number samples and/or trace concentrations, frequently with peak and background interference's. However, they also have to use the another technique called the MAN (Mean Atomic Number) background correction.. This latter method is based on the fact that most of the background production in a sample is directly proportional to the average atomic number of the sample. If the average atomic number of the sample is low (for example, silicates) and the peak to background ratio is high, then the MAN background correction method works quite well for quantitative analyses down to the minor element concentrations, since the total background is often less than one standard deviation of the x-ray signal. Basically what this means is that once the system is calibrated the off peak measurements are not necessary cutting the analysis time in half.

These samples seemed ideally suited for the MAN technique because there were no interfering x-ray lines for copper and aluminum and the average z-bar was low (~14.3). The advantage of the MAN method is that it requires only a simple calibration of the analyzing channel over a range of atomic number that includes the atomic number range of the standards and/or samples. If many samples are to be measured for their major and even minor element concentrations, then substantial time may be saved using the MAN method. The MAN background correction is an empirical calibration curve correction for background, The technique is based on the fact that background is essentially a function of the average atomic number of the sample often referred to as the Z-bar. The probe program uses an iterated linear or polynomial fit of up to 10 background measurements to provide quantitative correction over a wide range of sample atomic numbers. The following MAN standards and Z-bars were used for the calibration curve: SiC (11.6), Si (14), Ti (22), Fe (26), Co (27), Ni (28), and Zn (30). This covers the entire range form pure aluminum (13) through copper (29).

CHAPTER 4

TEMPERATURE MEASUREMENT RESULTS AND DISCUSSION

4.1 Introduction

Chapter 3 concluded the presentation of the procedures used for analysis of the samples. Before presenting the grain size and segregation results, the thermal results of the experiments conducted in the Bulk Undercooling Furnace are presented. These results include temperature profiles and applicable boundary conditions. Nine experiments were performed using the experimental procedures set forth in Chapter 2. A summary of the experiments performed is presented in Table 4.

Regardless of the details of any effort to model these experiments, it is expected that temperature data will be used as input boundary conditions and that these data will need to be in numerical form, as in a table. Thus the temperature data for all experiments is provided in Appendix C.

4.2 Results and Discussion

Two figures for each experiment illustrate the thermal results. The first figure is a plot of the thermal history of the experiment. This consists of the temperature readings recorded by the thermocouples located in the sample along with the thermocouple located at the base of the crucible. The diagram in the upper right corner of the plot shows the location of the thermocouples on a longitudinal cross-section view of the crucible. The second figure illustrates the adiabatic boundary condition that was enforced on the side walls of the crucible by plotting the thermocouple readings of the adjacent thermocouples in and near the crucible wall. Again, the diagram in the upper right corner of the plot shows the location of the thermocouples on a longitudinal cross-section view of the crucible. As shown in the plots, near adiabatic side wall conditions were achieved in all of the experiments performed. Actually a zero or a slightly positive gradient was present at the side wall to prevent radial heat loss. Only one experiment showed a radial loss and that was experiment E4, Figure 4.8, which shows the bottom outside thermocouple at a lower temperature than wall thermocouple. This one case of radial heat loss could be attributed to thermocouple error. Another anomaly that should be noted can be seen in Figure 4.5. The temperature profile for thermocouple No. 4 shows a rise in temperature of about 50°C over about a minute time period. The sudden jump is not likely explained by recalescence due to the temperature at which it takes place, but most likely is attributed to an error such as a laps in the water flow to the bottom chill. Two other key points should be made about the temperature profiles. First of all, the thermal plateaus during the experiments, refer to Figure 4.2 for an example, show evidence of equiaxed growth at the solidification temperature of the alloy. These thermal arrests take place because the amount of heat that is released by the solidifying grains approximately equals the heat loss in the system. Second, the cooling rates differ between experiments with large differences in cooling rates between the top and bottom cooled experiments. The bottom cooled experiments cool much faster than the top cooled, mainly due to the use of the water cooled copper chill at the bottom compared to the argon gas flow used during

the top cooled experiments. These different cooling rates while making it a little more difficult to compare experiments have no negative effect on providing data for the numerical simulations

4.3 Error in Temperature Measurements

An error analysis was carried out in order to quantify the error in the resulting temperate profiles.

4.3.1 Error in Thermocouple Readings

Error associated with the temperature reading from the thermocouples is ± 5°C. This is based on our observations of the average temperature value that the thermocouples reported during the one hour soak stage of each experiment, from examining the cooling curves, and the published ANSI code of thermocouple error for type K. The soak stage, an extended measurement time at a fixed set point, gave insight to both the amount of bias and precision error associated with the thermocouples. Looking at the cooling curve from the thermocouple closest to the chill, a change in slope is seen when solidification begins due to latent heat being released into the system as a result of the phase change. The point at which the change in slope occurs for this thermocouple should correspond to the solidification temperature of the initial alloy composition, T_o. The result using T_o proved to be a little more difficult to determine due to the resolution of the data, but nonetheless agreed well with the expected solidification temperature.

4.3.2 Error in Thermocouple Positions

Although precautions were taken in the positioning of the thermocouples in the melt, an error associated with these positions should still be acknowledged. As discussed in the experimental procedures, the thermocouples were inserted through the holes in the Boron Nitride crucible cap and were set to a predetermined height using calipers.

The error associated with these positions arises from the handling of the thermocouples during the insertion of the cap and thermocouple assembly into crucible. Recall that the cap/thermocouple assembly was placed into the crucible after the necessary constituents were melted in the Glove Box Casting Facility. Once cooled (air quench) the setup is transferred to the Bulk Undercooling Furnace for remelting and controlled cooling. Prior to remelting the sample, the thermocouples were slightly bent at the top of the crucible cap to try to prevent the thermocouples from sliding under their own weight into the melt. This means that there were two possible times for movement of the thermocouples from there original set position, hence an estimated error of ± 2 mm is associated with their positions.

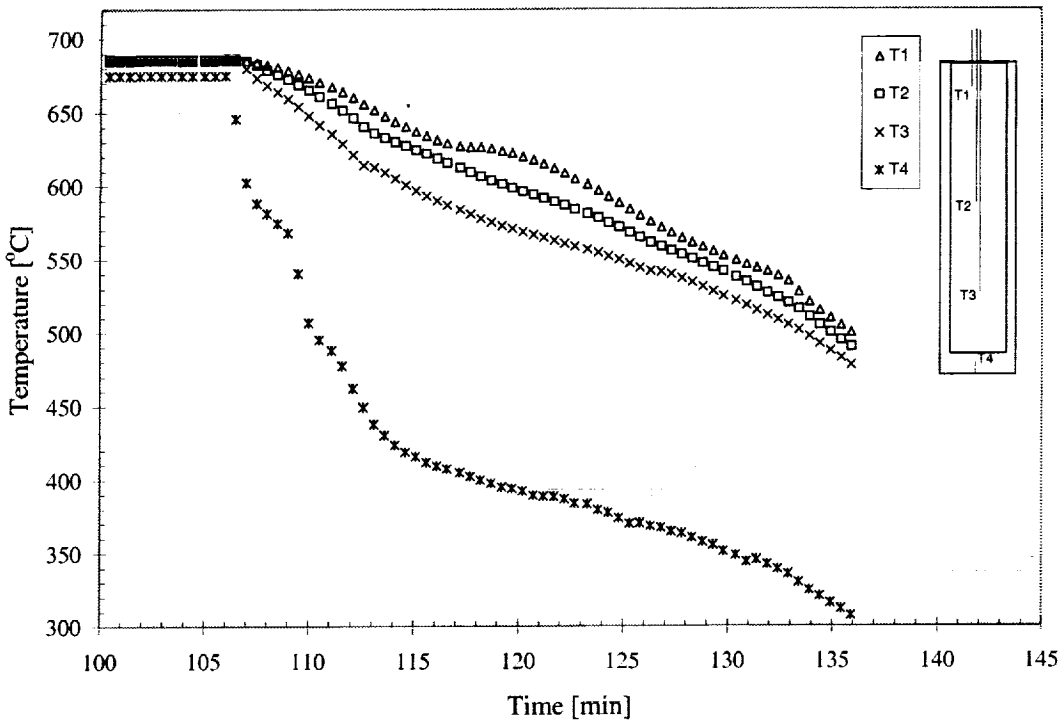

Figure 4.1 Thermocouple readings for experiment E1, bottom cooled Al-10 wt. pct. Cu.

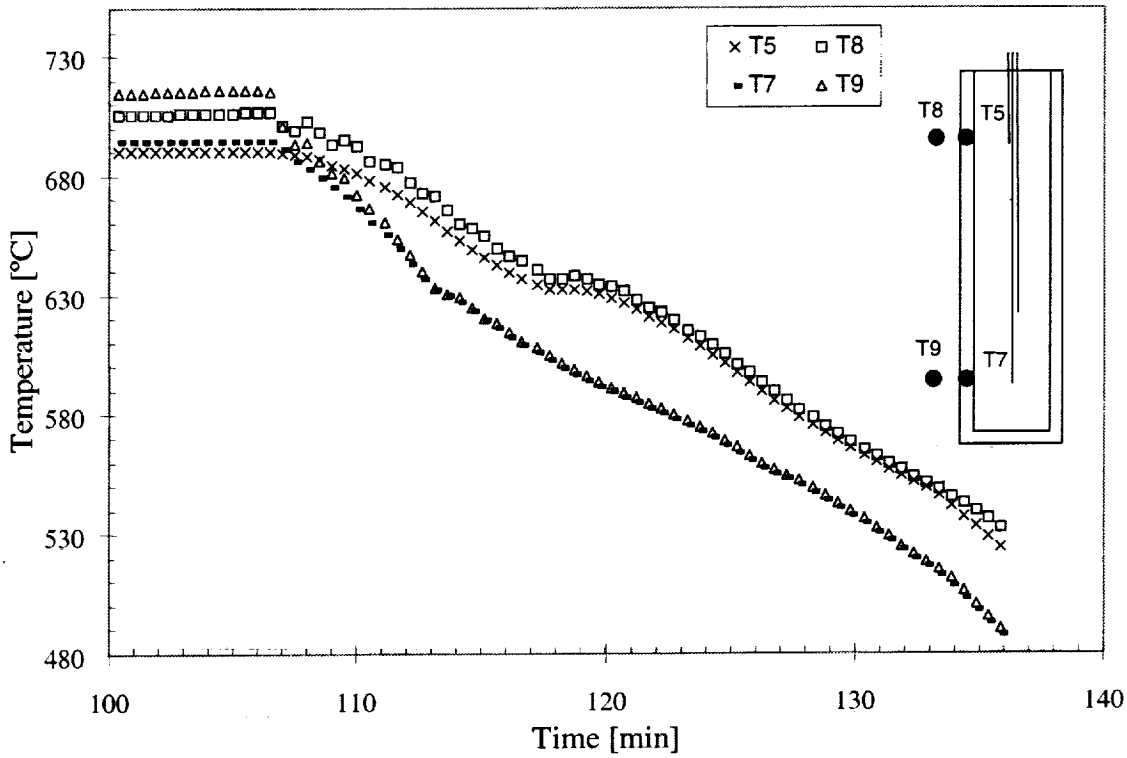

Figure 4.2 Illustration of adiabatic conditions for the radial direction of experiment E1, bottom cooled Al-10 wt. pct. Cu.

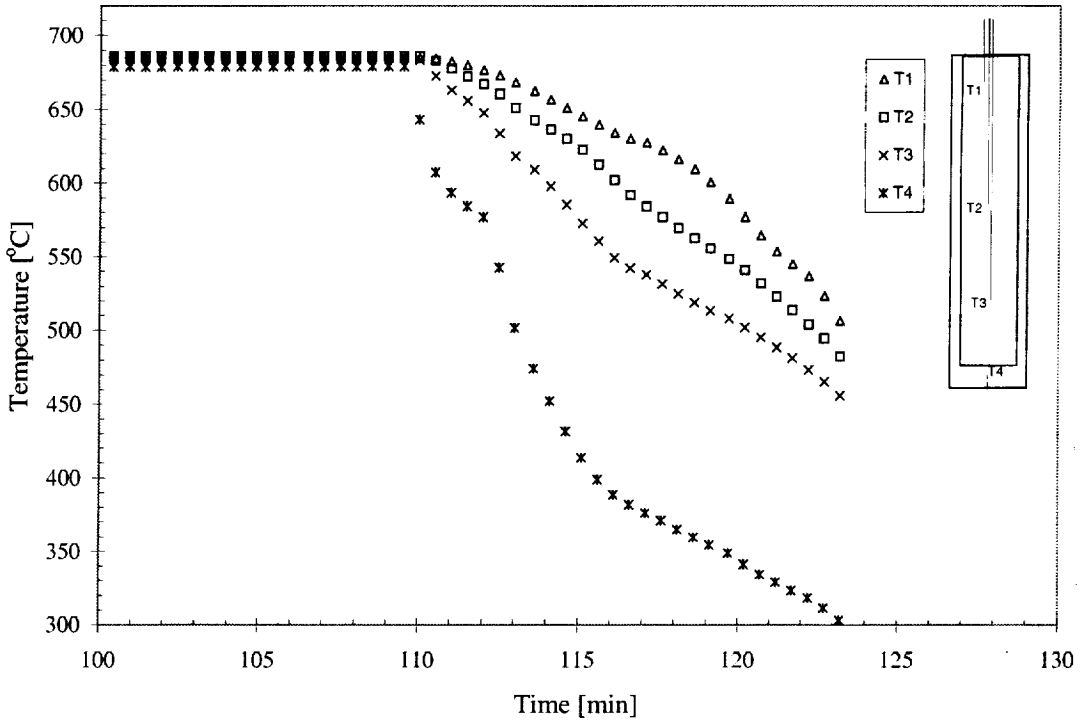

Figure 4.3 Thermocouple readings for experiment E2, bottom cooled Al-10 wt. pct. Cu with 0.045 wt. pct. TiB_2.

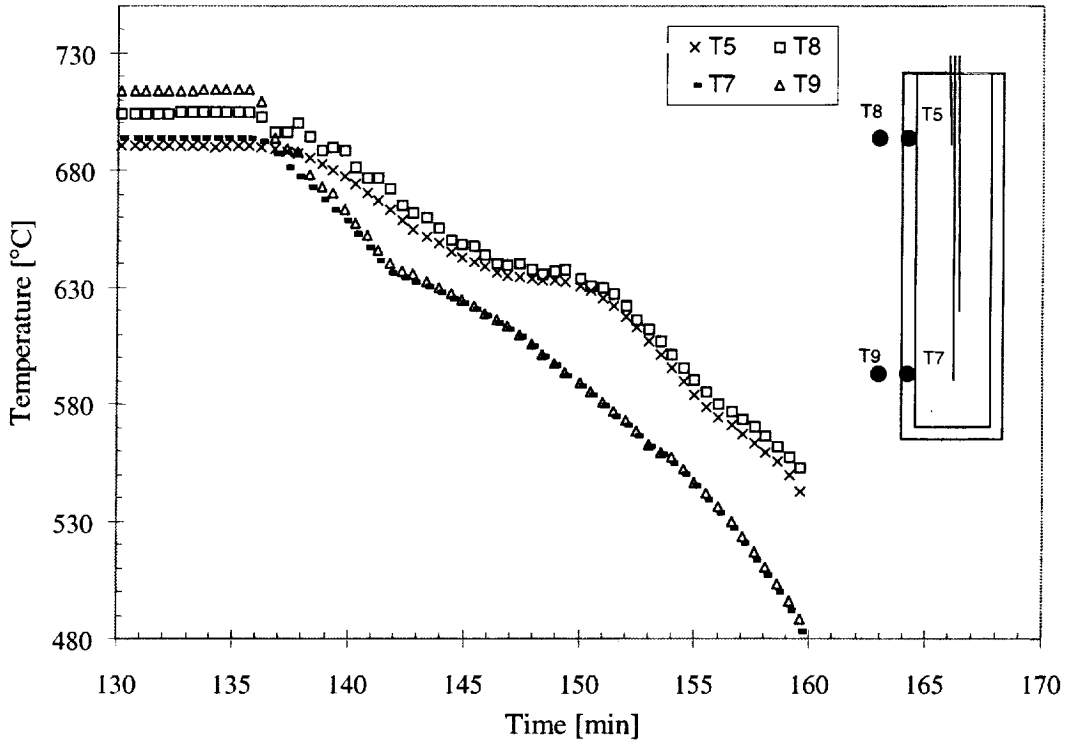

Figure 4.4 Illustration of adiabatic conditions for the radial direction of experiment E2, bottom cooled Al-10 wt. pct. Cu with 0.045 wt. pct. TiB_2.

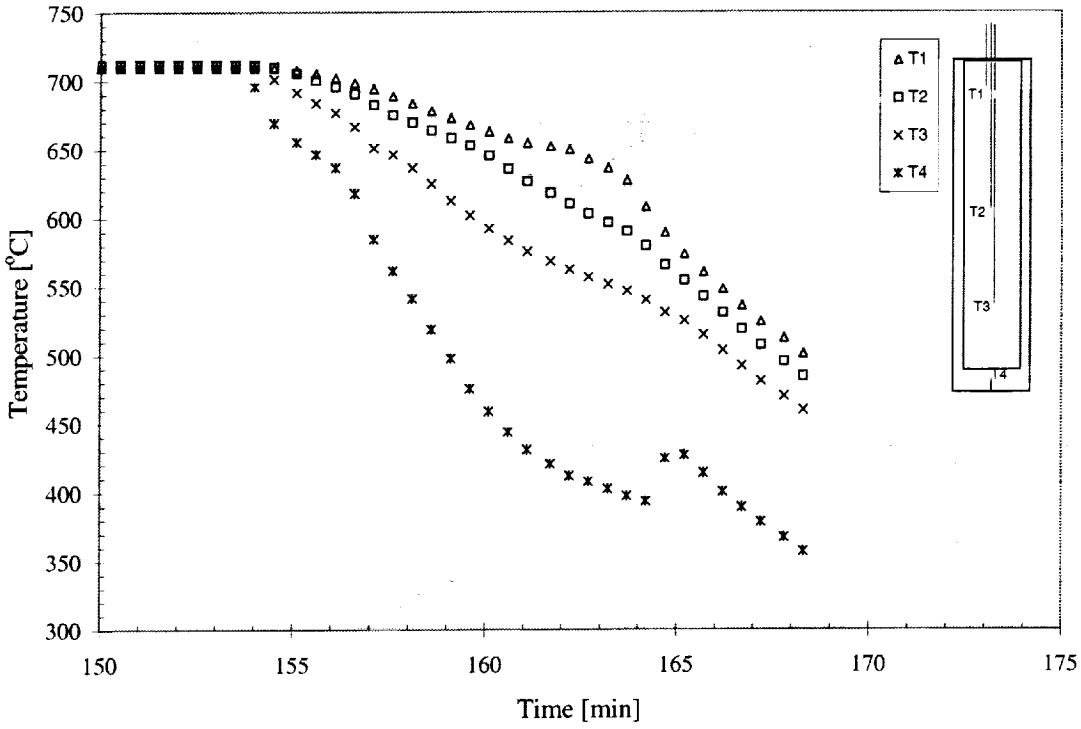

Figure 4.5 Thermocouple readings for experiment E3, bottom cooled Al-1 wt. pct. Cu with 0.45 wt. pct. TiB_2.

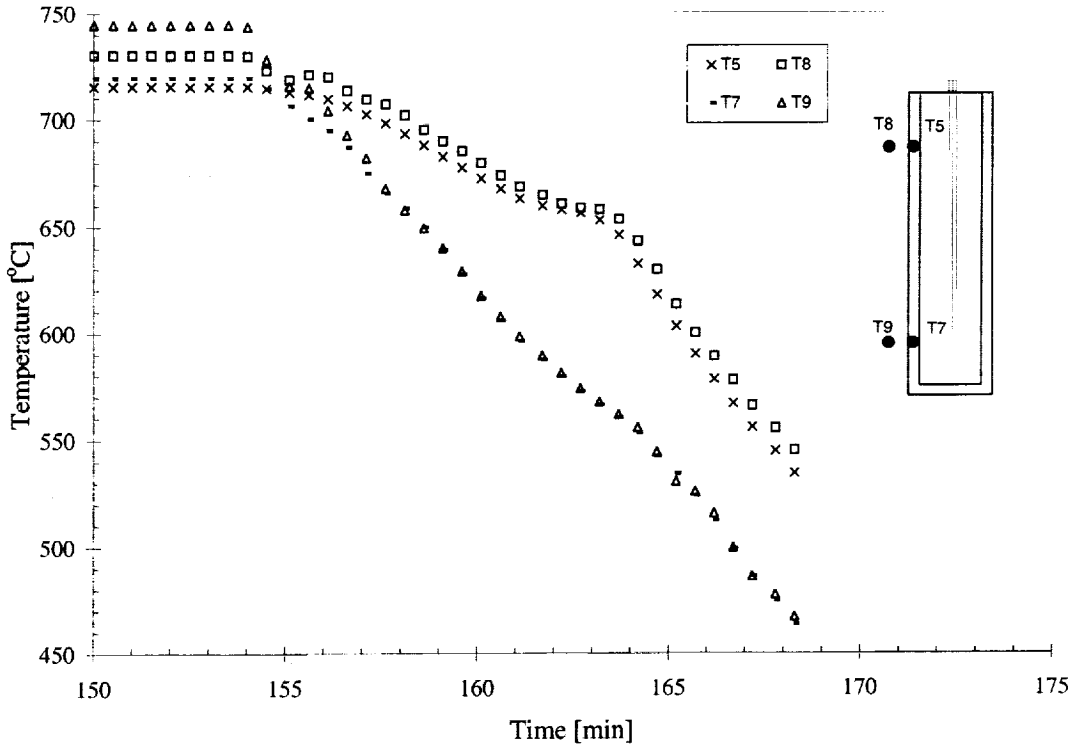

Figure 4.6 Illustration of adiabatic conditions for the radial direction of experiment E3, bottom cooled Al-1 wt. pct. Cu with 0.45 wt. pct. TiB_2.

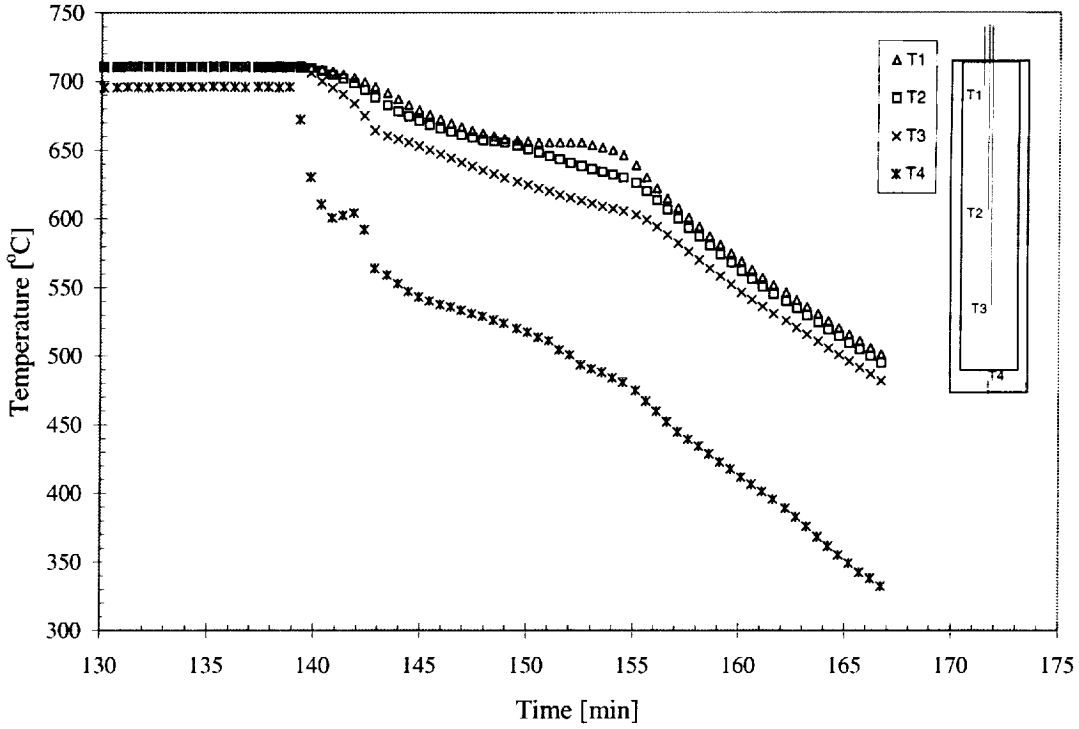

Figure 4.7 Thermocouple readings for experiment E4, bottom cooled Al-1 wt. pct. Cu.

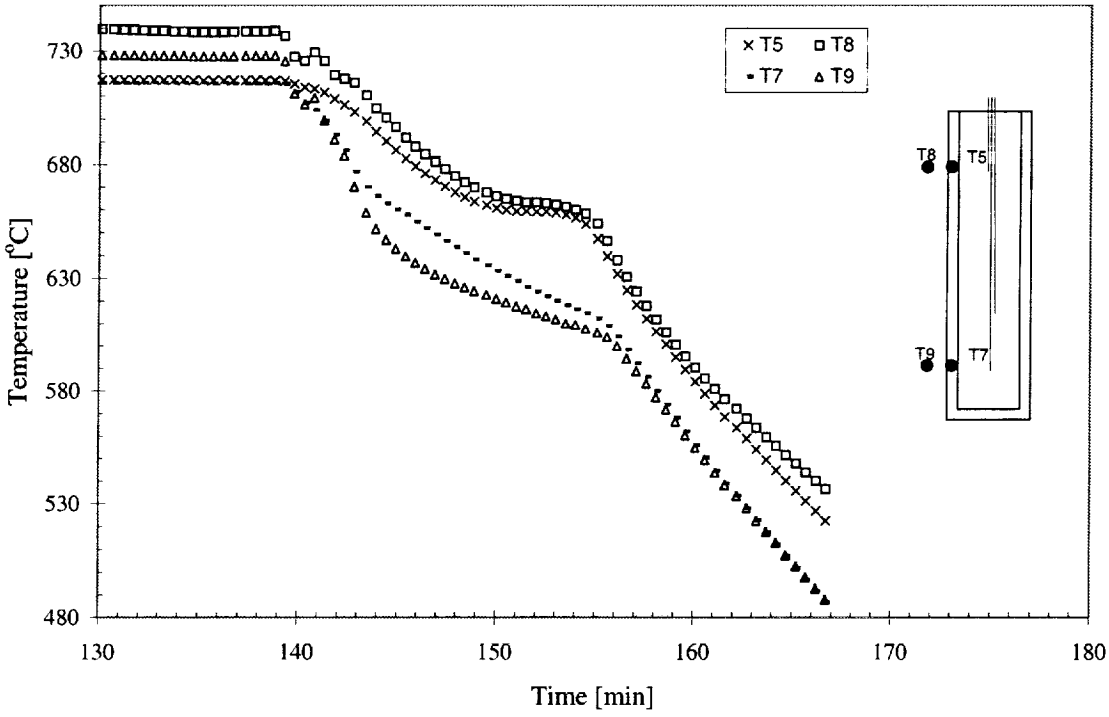

Figure 4.8 Illustration of adiabatic conditions for the radial direction of experiment E4, bottom cooled Al-1 wt. pct. Cu.

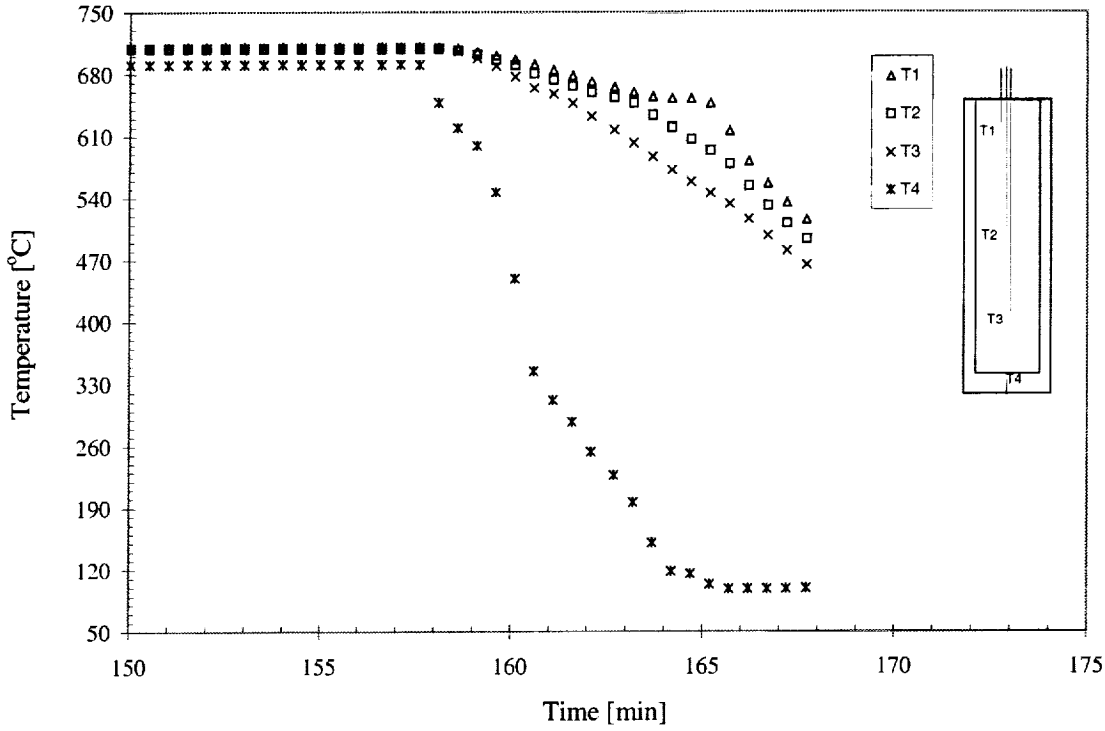

Figure 4.9 Thermocouple readings for experiment E5, bottom cooled Al-1 wt. pct. Cu with 0.67 wt. pct. TiB_2.

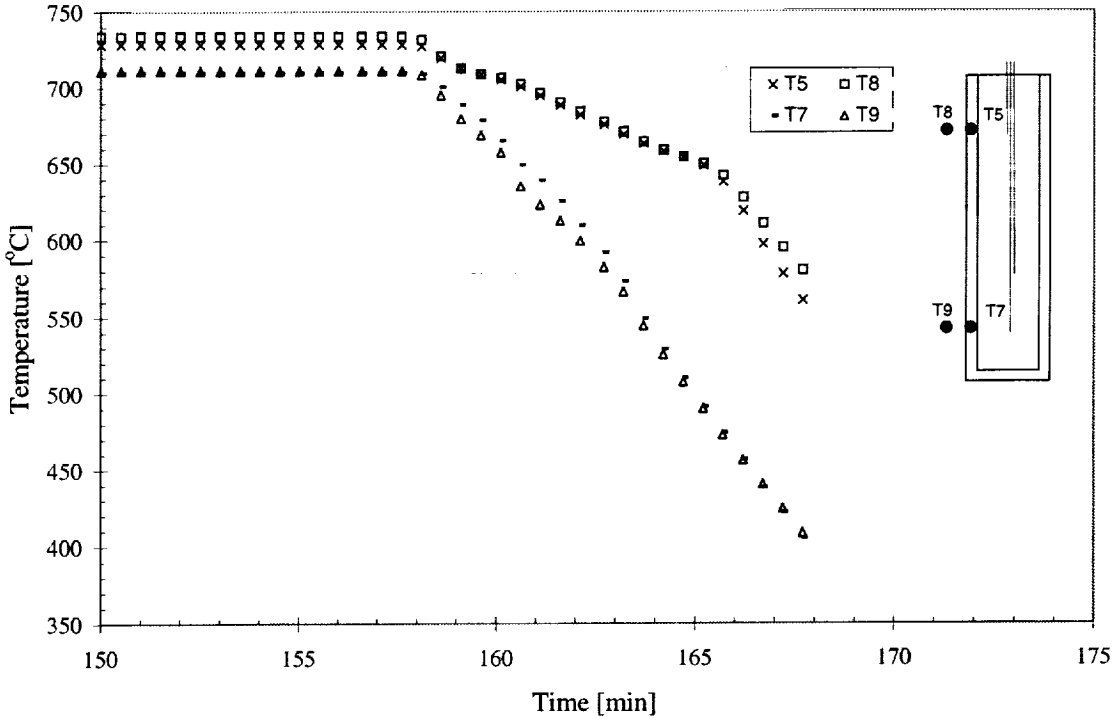

Figure 4.10 Illustration of adiabatic conditions for the radial direction of experiment E5, bottom cooled Al-1 wt. pct. Cu with 0.67 wt. pct. TiB_2.

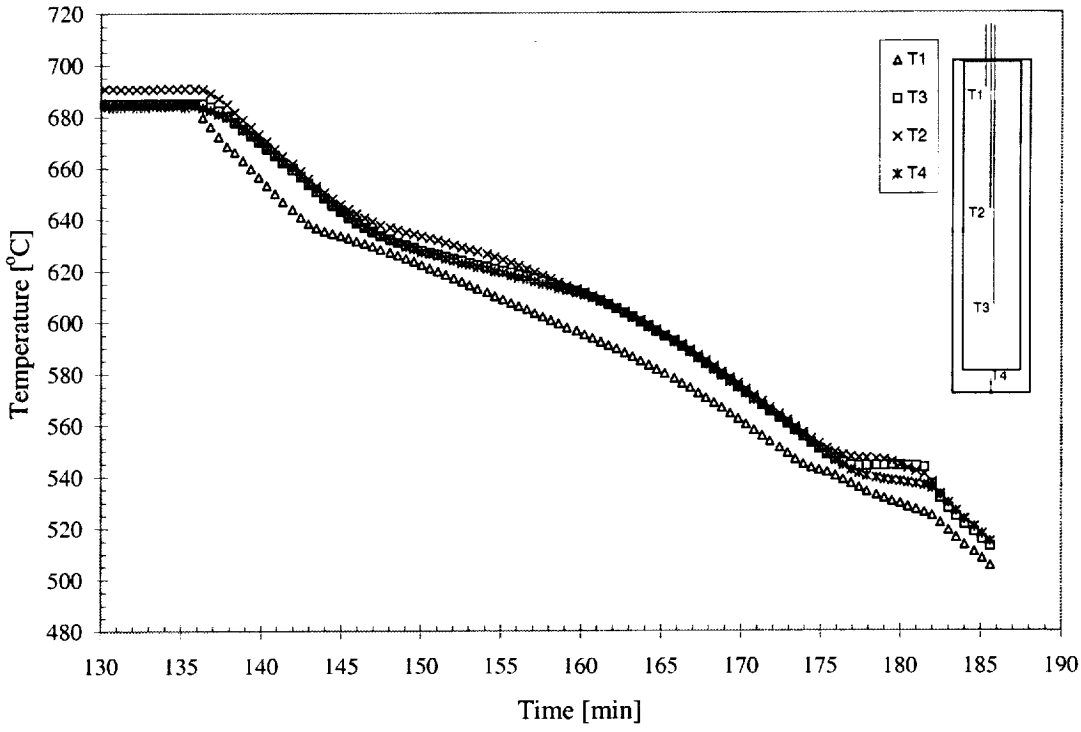

Figure 4.11 Thermocouple readings for experiment E6, top cooled Al-10 wt. pct. Cu with 0.045 wt. pct. TiB_2.

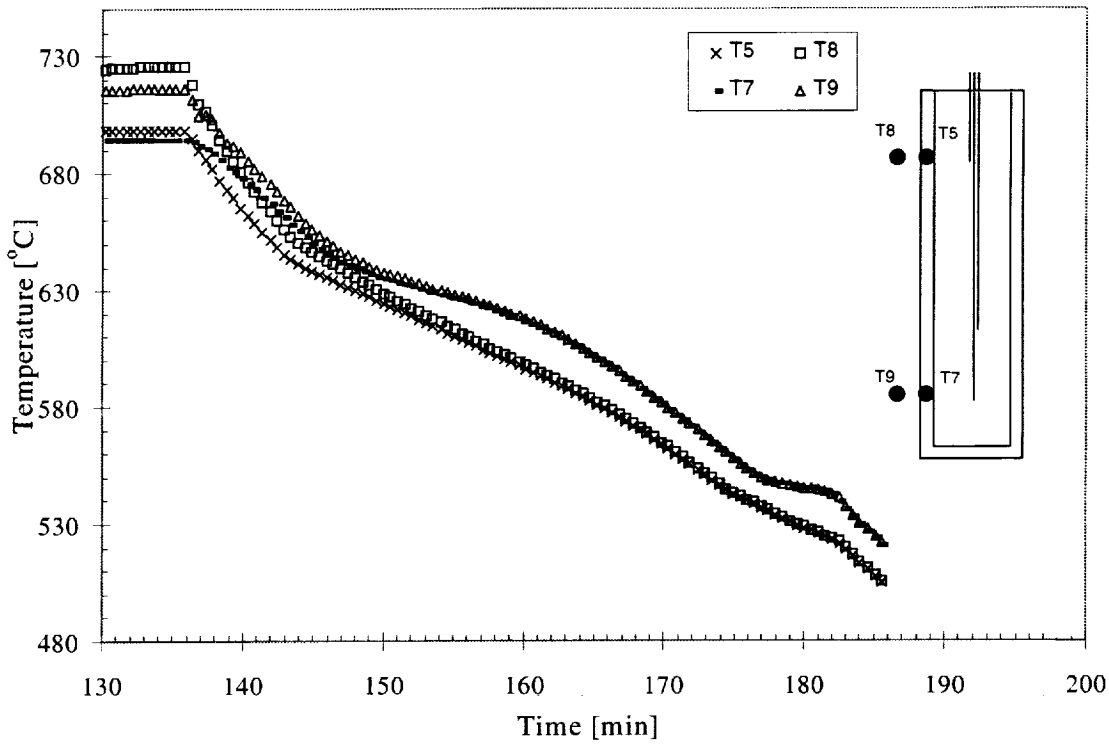

Figure 4.12 Illustration of adiabatic conditions for the radial direction of experiment E6, top cooled Al-10 wt. pct. Cu with 0.045 wt. pct. TiB_2.

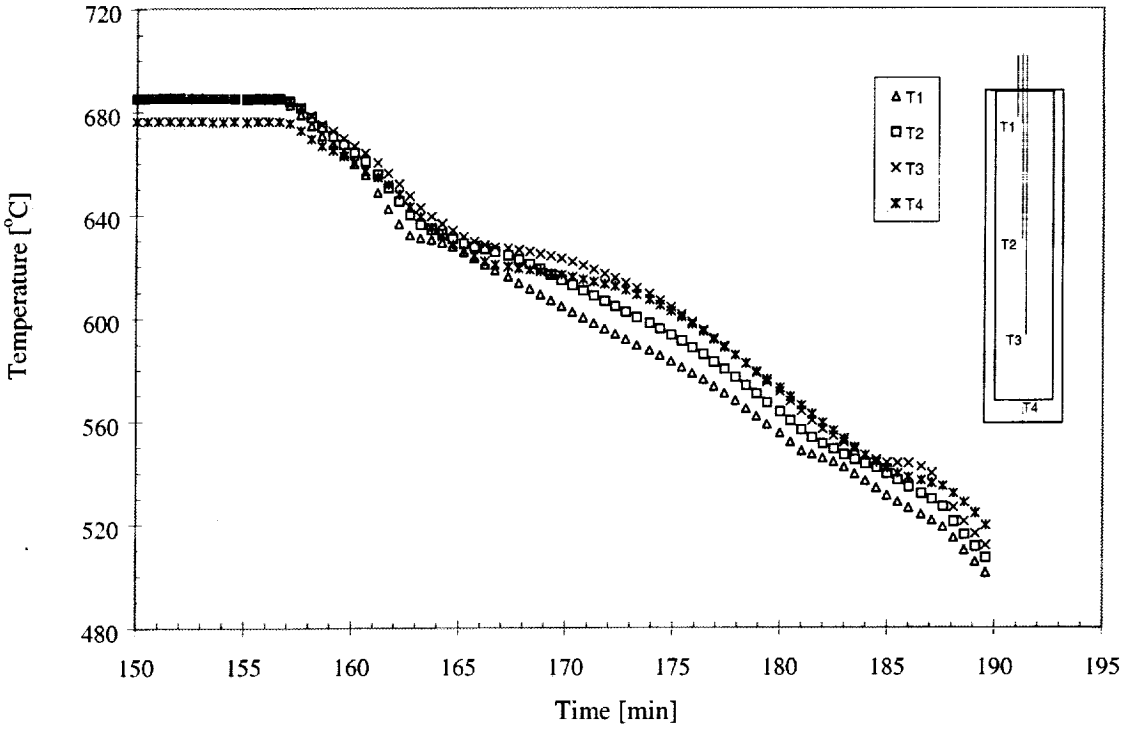

Figure 4.13 Thermocouple readings for experiment E7, top cooled Al-10 wt. pct. Cu with 0.067 wt. pct. TiB_2.

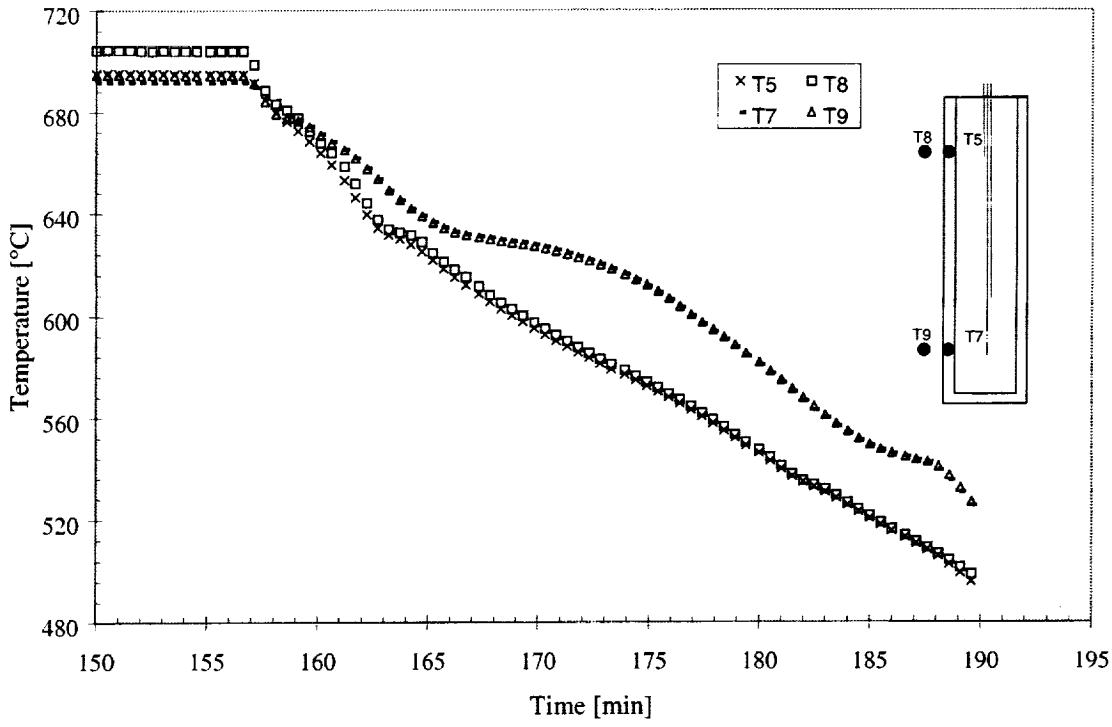

Figure 4.14 Illustration of adiabatic conditions for the radial direction of experiment E7, top cooled Al-10 wt. pct. Cu with 0.067 wt. pct. TiB_2.

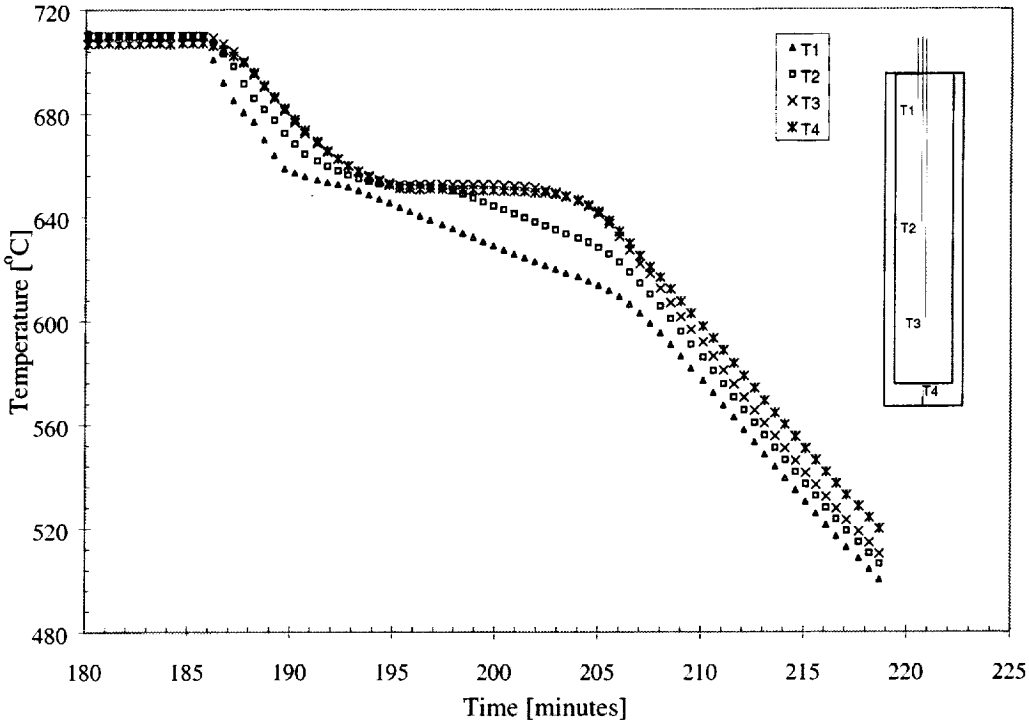

Figure 4.15 Thermocouple readings for experiment E8, top cooled Al-1 wt. pct. Cu with 0.45 wt. pct. TiB_2.

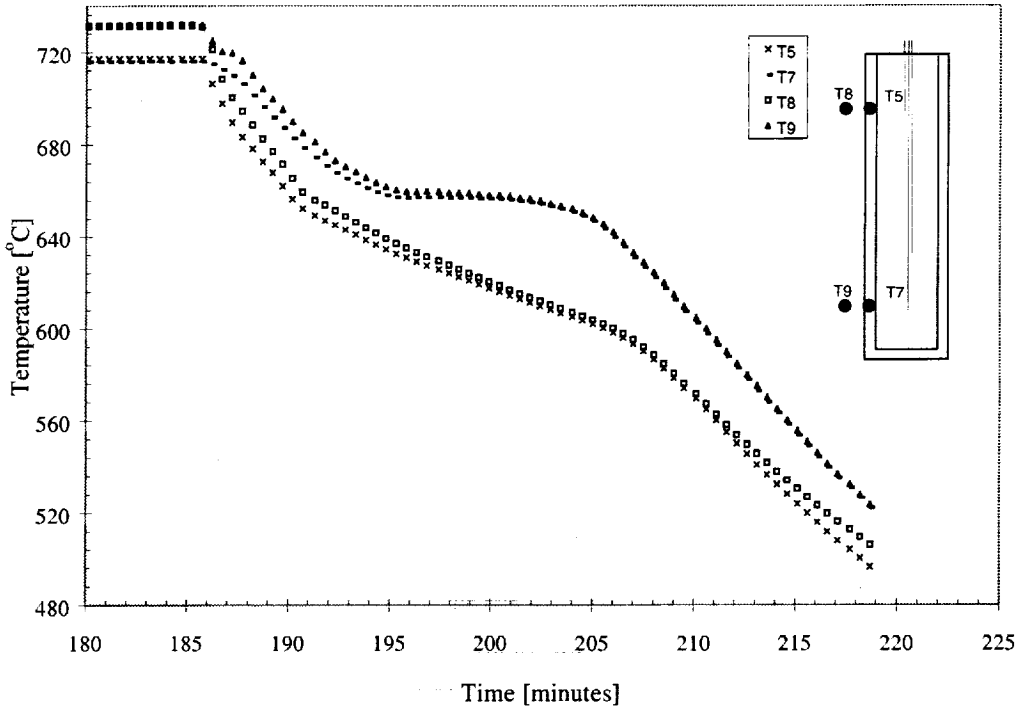

Figure 4.16 Illustration of adiabatic conditions for the radial direction of experiment E8, top cooled Al-1 wt. pct. Cu with 0.45 wt. pct. TiB_2.

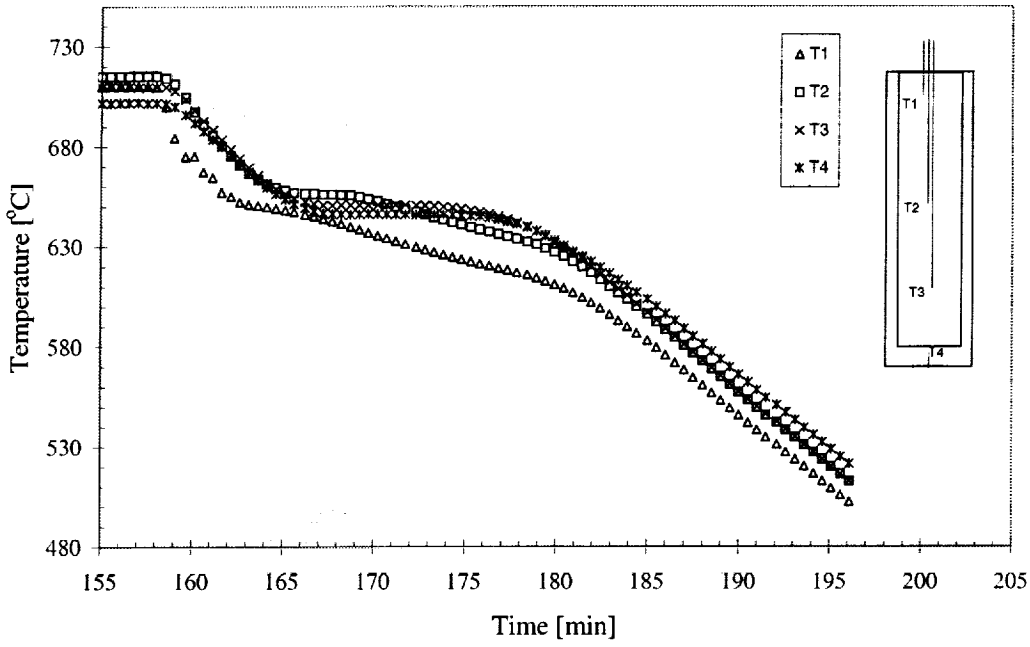

Figure 4.17 Thermocouple readings for experiment E9, top cooled Al-1 wt. pct. Cu with 0.67 wt. pct. TiB_2.

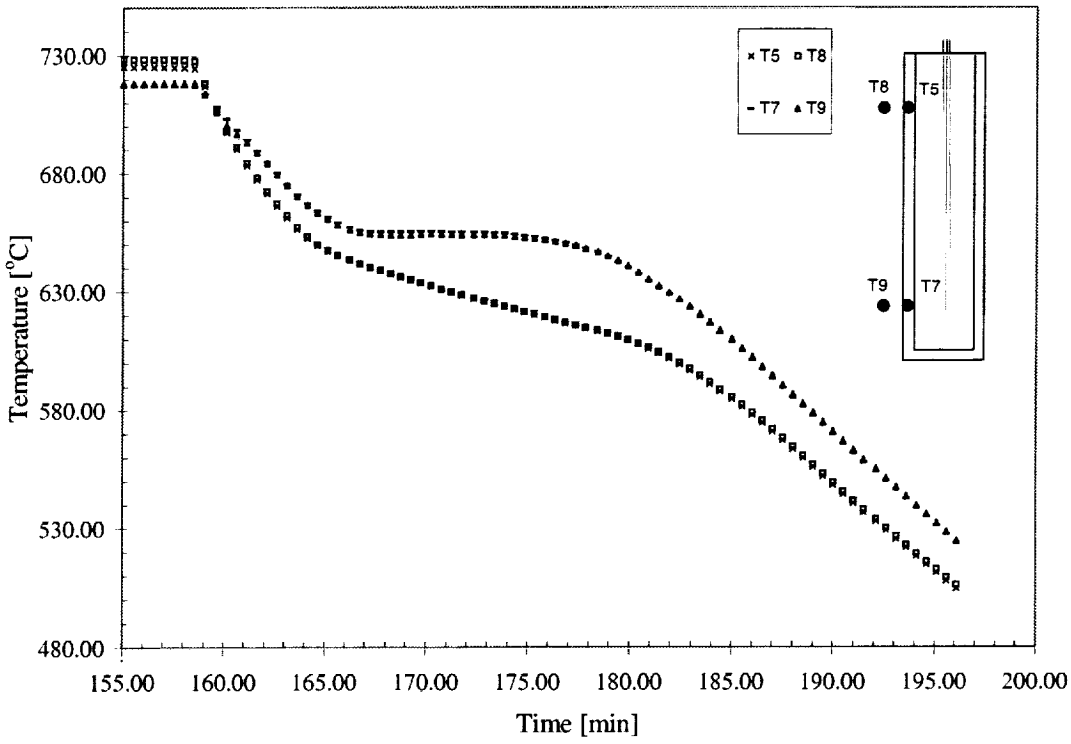

Figure 4.18 Illustration of adiabatic conditions for the radial direction of experiment E9, top cooled Al-1 wt. pct. Cu with 0.67 wt. pct. TiB_2.

CHAPTER 5

GRAIN SIZE MEASUREMENT RESULTS AND DISCUSSION

5.1 Introduction

The following chapter presents the results of the grain size measurements. The results were obtained by following the procedures outlined in Chapter 3 Section 2. Illustrations of the overall grain structure are presented for each experiment followed by plots of the grain size measurements for experiments which exhibited an equiaxed grain structure. For each grain size variable calculated, the results are presented in groups according to the initial copper content of the alloy (10 wt. pct. and 1 wt. pct.). This was done to illustrate the effects of the different cooling directions and amounts of grain refiner added.

5.2 Results and Discussion

The first set of figures presented are longitudinally cut views of the ingots for each experiment showing the overall grain size distribution. Figure 5.1 is a photograph taken of experiment E1, bottom cooled Al-10 wt pct. Cu alloy. No grain refiner was used in experiment E1. The resulting grain structure consists of large equiaxed grains with elongated grains in the middle of the ingot. Experiment E2, Figure 5.2, consisting of Al-10 wt. pct. Cu refined with 0.045 wt. pct. TiB_2 and cooled from the bottom to top, exhibited fine equiaxed grains with some larger grains near the top and bottom. Experiment E3, Figure 5.3, consisting of Al-1 wt. pct. Cu refined with 0.45 wt. pct. TiB_2 and cooled from the bottom to top was fully columnar containing less than twenty grains. No further analysis was done on this experiment. Experiment E4, consisting of Al-1 wt. pct. Cu cooled from the bottom to top with no grain refiner added also exhibited a fully columnar grain structure as expected based on the results of experiment E3. No picture of the grain structure was taken for this experiment. Experiment E5, Figure 5.4, consisting of Al-1 wt. pct. Cu refined with 0.67 wt. pct. TiB_2 and cooled from the bottom to top showed a mixed columnar and equiaxed grain structure. Experiment E6, Figure 5.5, consisting of Al-10 wt. pct. Cu refined with 0.045 wt. pct. TiB_2 and cooled from the top to the bottom contained equiaxed grains that were approximately twice the size at the top compared to the bottom. Experiment E7, Figure 5.6, consisting of Al-10 wt. pct. Cu refined with 0.067 wt. pct. TiB_2 and cooled from the top to the bottom contained fine equiaxed grains with some variations in grain size. Experiment E8, Figure 5.7, consisting of Al-1 wt. pct. Cu refined with 0.45 wt. pct. TiB_2 and cooled from the top to the bottom exhibited a large grain size which was uniform throughout the ingot. Experiment E9, Figure 5.8, consisting of Al-1 wt. pct. Cu refined with 0.670 wt. pct. TiB_2 and cooled from the top to the bottom contained coarse equiaxed grains with some grain size variation.

Of the nine experiments performed, five experiments exhibited an equiaxed grain structure as desired. For these five experiments, grain size measurements are presented. The Al-10 wt. pct. Cu alloy top cooled experiments are presented first followed by the

bottom cooled experiment. The top and bottom cooled experiments were not presented together due to the much larger grains present in the top cooled experiment compared with the bottom cooled experiment. Figure 5.9 shows the lineal density of the grains for the top cooled Al-10 wt. pct. Cu alloys. The measured quantity, lineal density, is the number of intercepts of grains per unit length. Figures 5.10-5.13 show the average number of grains per area, average number of grains per volume, the volumetric grain diameter, and the grain surface to volume ratio for the top cooled Al- 10 wt. pct. Cu alloys, respectively. All of these values are derived from the lineal density measurement. Figures 5.14 through 5.18 report the same quantities but for the bottom cooled Al-10 wt. pct. Cu alloy. Figures 5.19 through 5.23 present the grain size results for the refined, top cooled Al-1wt. pct. Cu alloys (E8 and E9).

In comparing the top and bottom cooled experiments for the Al-10 wt. pct. Cu alloy it can be seen that the grain size in the top cooled experiments (E6 and E7) are approximately three times larger than as those of the bottom cooled experiment (E2). This grain size difference between the Al-10wt. pct. Cu ingots cooled from the top and bottom is an important result and is a trend that a competent solidification simulation should reproduce. This large difference in grain size - about 0.7 mm in E2 versus about 2.1mm in E6 and E7 - is not due to differences in cooling rate. Though cooling rate is an important consideration, as Rhines et al., 1983, has shown that a decrease in grain size is expected as freezing rate is increased. Under our conditions, in the presence of the grain refiner - E6 and E7 show the grain size to be largely insensitive to cooling rate (E6 cooling rate was 5.3 K/min., E7 cooling rate was 12 K/min.). The 125% increase in cooling plus the additional TiB_2 grain refiner used in E7 resulted in a grain size decline of only about 32%, compared to E6. The cooling rate in E2 was only about 35% more than the rate of cooling in E7, yet the E2 average grain diameter (about 0.75mm) is 60% less than in E7 (which had a grain size of about 1.9mm). We believe the difference in grain size between E2 and E7 to be primarily due to grain annihilation that takes place in the top cooled experiments. Due to the alloy composition (Al-10wt. pct. Cu) in E2 and E7 the Al grains which form are nearly neutrally buoyant, thus on their own they neither sink or float. But these grains should be easily carried with any convective flow. In E2 cooling is from the bottom and Cu is rejected into the liquid thus there is little convective flow since the system is (longitudinally) both thermally and solutally stable. In E2 the grain refiner induces lots of nucleation and these nucleated grains, for the most part, do not move and do create an equiaxed structure. In E7 on the other hand, cooling is from the top, thus the system is thermally and solutally unstable; thus lots of flow is expected and many of the grains which nucleated in the upper, cooler regions of the ingot, can be expected to be carried to warmer regions in lower portions of the ingot where some remelt. This process of equiaxed grain transport and subsequent annihilation is responsible for the large grain size in E7 compared to E2. It is expected that any attempt to completely simulate the solidification processes taking place in E7 will require inclusion of equiaxed grain transport via settling and advection.

Both the top and bottom cooled experiments depict a variation in grain size showing evidence of different nucleation rates during the experiment which can be attributed to solid movement and thermosolutal convection. For instance, the top cooled Al-10 wt. pct. Cu alloy with 0.045 wt. pct. TiB_2 shows a trend of large equiaxed grains at

the top transitioning to finer grains in the middle and bottom. For this experiment at the start of solidification, the thermal and solutal gradients are unstable leading to convection in the melt. The convection caused by these instabilities transports nucleated grains into the hot liquid where they melt. As a deep mushy zone develops the amount of grain transport and grain destruction decreases. Since more nucleated grains are now present and in competition with each other in the mushy zone the resulting grain size decreases. As the sample solidifies, the local cooling rate at the leading edge of the mushy zone decreases due to the distance from the chill. The lower freezing rate and possibly the exhaustion of active refiner results in the slightly larger grains at the bottom of the ingot. Experiment 7, the top cooled Al-10 wt. pct. Cu with 0.067 wt. pct., used more grain refiner and a higher cooling rate (compared to E6). The increased grain refiner provided more nucleating sites for grains which resulted in smaller grains throughout most of the ingot compared to the 0.045 TiB_2 experiment, E6. The bottom cooled Al-10 wt. pct. Cu with 0.045 wt. pct. TiB_2 experiment, E2, showed the same trend as the top cooled experiment of the same alloy composition, E6, but not for the same reasons. The bottom cooled experiment was both thermally and solutally stable therefore the convection in the melt would not be that substantial. The general trend from small equiaxed grains at the bottom to larger equiaxed grains at the top is attributed to the lower cooling rate as the experiment proceeded. The few larger equiaxed grains that appear near the bottom of the ingot can not be easily explained and could be a topic of further investigation. It should be kept in mind that these experiments are not ideal and that , for example, convection caused by radial temperature gradients may cause some grain transport and destruction in the early stages of E2. The temperature measurements we provide for use as input boundary conditions may not be exhaustive enough for such nuances to be simulated.

For the Al-1 wt. pct. Cu alloy none of the bottom cooled experiments had a sufficiently equiaxed grain structure for further analysis. The top cooled Al-1wt. pct. Cu experiment did however, result in an equiaxed structure; Figures 5.19 through 5.23 show the grain size quantities for the top cooled Al-1 wt. pct. Cu alloys. Comparison of the bottom versus top cooled Al-1wt. pct. Cu experiments, E3 and 5 versus E8 and E9, may have utility in the examination of numerical codes. The transition from columnar to equiaxed growth was related by Tiller, 1965, to the volume of the constitutionally undercooled zone "X" ahead of the columnar front, "ΔT_{max}" - the maximum undercooling, and "G" - the temperature gradient. The nucleation rate is higher, and thus the onset of equiaxed growth more likely, with increasing X, and ΔT_{max}, and decreasing G. For the bottom cooled Al-1wt. pct. Cu alloys, G was relatively high due to the higher cooling rates in these bottom quenched experiments, and both X and ΔT_{max} were relatively low due to the low alloy content and high G. All these work against the onset of equiaxed growth thus E3 and E5 resulted in columnar structures. The grain refiner was largely not effective at the lower Al-1wt. pct. Cu concentration, perhaps due to interfacial energy differences between the 1 and 10wt. pct. alloys.

The question now arises, why did the top cooled Al-1wt. pct. Cu experiments (E8 and E9) result in equiaxed structures. The lower cooling rate in E8 and E9 contributed to the production of their equiaxed structure since the resulting lower thermal gradients present enabled higher ΔT_{max} and X levels. Convection is also stronger in the top cooled

experiments (compared to bottom cooling); this convection should exacerbate the settling and advection of nucleated equiaxed grains as well as the production of additional free grains resulting from fragmented dendrites (Jackson, 1966; Paradies, 1993). It is still expected that grain annihilation takes place when primary grains from the cooler top are transported to the hotter lower ingot regions. However, the convection and the concomitant production and transport of grains and grain fragments may contribute to the disruption of columnar growth and the resulting equiaxed structure. These Al-1wt. pct. Cu experiments (E3, E4, E5, E8, and E9) may have utility in the examination and development of a numerical code which includes prediction of the columnar to equiaxed transition, free grain settling and advection, and nucleation due to dendrite fragmentation.

The top cooled Al-1 wt. pct. Cu alloy with 0.67 wt. pct. TiB_2 exhibited slightly larger grains than the top cooled Al-1 wt. pct. Cu with 0.45 wt. pct. TiB_2. This is not expected based on the normal trend that the more the grain refiner the finer the grains; however, this is only with other factors being equal. In E8 the initial cooling rate was 12 K/min., in E9 it was 11.3 K/minutes. The Al-1 wt. pct. Cu alloy with 0.67 wt. pct. TiB_2 took approximately 19 min. to solidify while E8 solidified in about 17 minutes. The lower cooling rate for E9 resulted in the development of the relatively larger grains.

In addition to the other observations, in comparing the top cooled experiments of the two alloy compositions, it can be seen that the 1 wt. pct. Cu alloy resulted in grains that were approximately 2.5 times larger than those of the 10 wt. pct. Cu alloy. Since strong natural convection and complete mixing are expected, this grain size difference is not believed to be due to any difference in grain remelting caused by the settling or advection of free solid in these top cooled experiments. The grain size difference is likely to be due to the different nucleation rates achieved by the grain refiner in the different Al compositions. Since the refined Al-10wt. pct. Cu, bottom cooled ingot, E2, was fully equiaxed and the Al-1wt. pct. Cu, bottom cooled ingots E3 and E5 were fully columnar, it can be concluded that the grain refiner in the Al-1 wt. pct. Cu alloys was not effective. Thus grain size differences between the Al-1wt. pct. Cu and 10wt. pct. Cu, top cooled experiments (E6 and E7 versus E8 and E9) are believed to be due to the different grain refinement characteristics of the alloys. This basic dependence of equiaxed growth on alloy content is detailed in work due to Plaskett and Winegard, 1950, who showed that nucleation occurs ahead of an advancing interface when the temperature gradient divided by the square root of solidification rate is less than a value that is roughly proportional to solute content. Thus in general, at a lower solute content - less nucleation is expected.

5.3 Uncertainty Analysis

5.3.1 Error in Measured Quantities

A statistical analysis was performed to determine the precision with which the observed size may, with normal confidence, be considered to represent the actual grain size of the specimen examined. Normal confidence implies the expectation that the actual error will be within the stated uncertainty 95% of the time. As stated in Chapter 3, the template to measure the number of grain intercepts was randomly applied to the test

region five successive times. From the count obtained during each application, a mean and standard deviation were calculated according to equations 5.1 and 5.2:

$$\overline{X} = \frac{\sum X_i}{n} \tag{5.1}$$

$$s = \left[\frac{\sum (X_i - \overline{X})^2}{n-1} \right]^{\frac{1}{2}} \tag{5.2}$$

where X_i represents an individual value, $\overline{X}$ is the mean, n is the number of fields measured, and s is the standard deviation. A 95% confidence interval was then calculated from equation 5.3:

$$95\%CI = \frac{t \cdot s}{\sqrt{n}} \tag{5.3}$$

where t is a multiplier determined from the number of fields measured.

With n equal to five the t multiplier was determined to be 2.776 from a table of 95% confidence interval multipliers in ASTM standard E112. Finally, a percent relative accuracy, %RA, was calculated according to equation 5.4.

$$\%RA = \frac{95\%CI}{\overline{X}} \cdot 100 \tag{5.4}$$

It is recommended from the ASTM standard that a value of 10 %RA (or lower) be obtained to ensure an acceptable level of precision. This condition was met for all measured fields.

5.3.2 Error in Derived Quantities

Since all of the remaining quantities were a function of the number of intercepts counted, the uncertainties for these quantities were found in the same manner as discussed in section 5.3.1. The desired formula was applied to each of the five recorded values for the number of intercepts then a mean and standard deviation was calculated. From the mean and standard deviation the 95% CI and %RA were calculated as previously discussed.

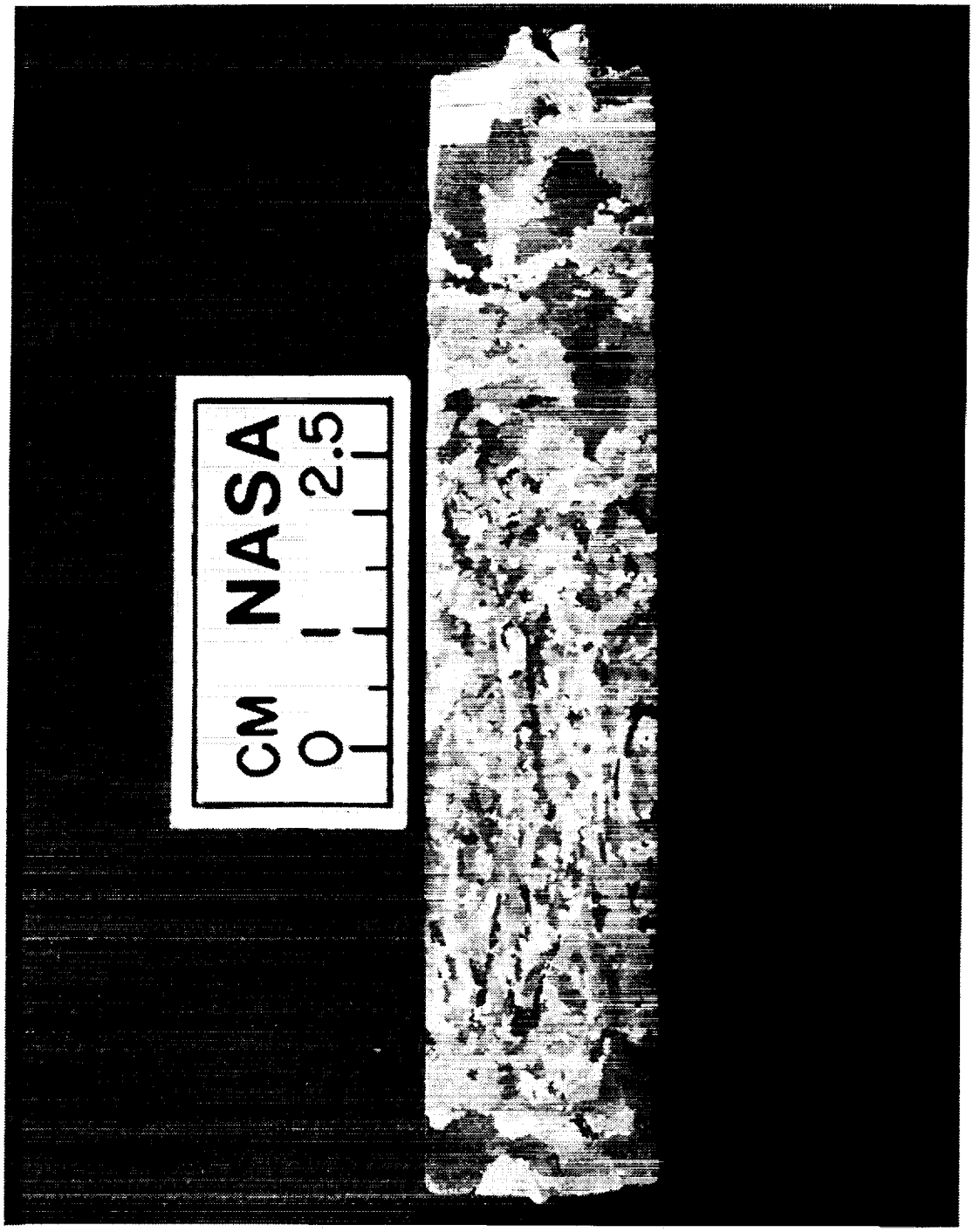

Figure 5.1 Cross-sectional view showing the grain structure of ingot from experiment E1, bottom cooled, 12.4 K/min. initial cooling, Al-10 wt. pct. Cu alloy.

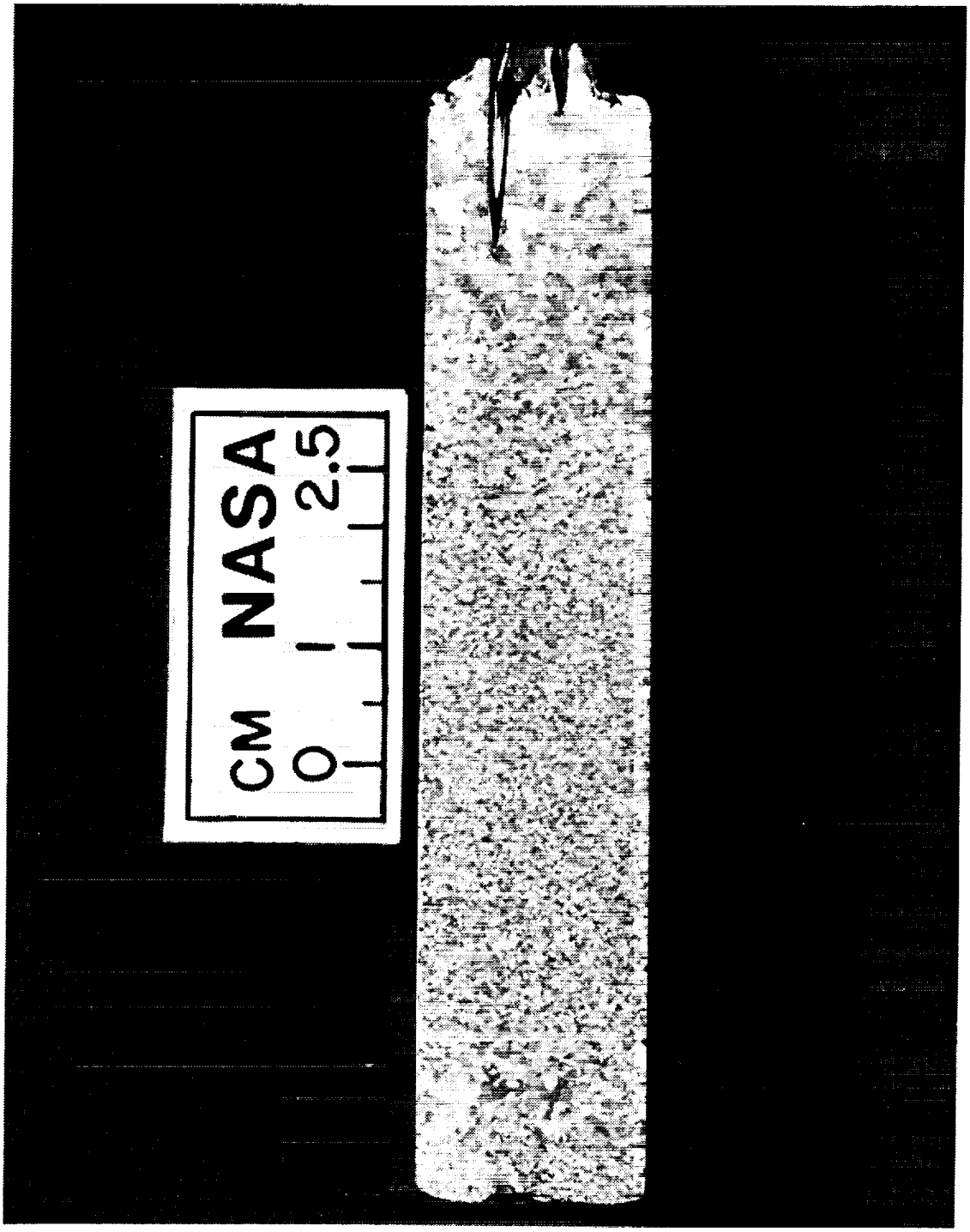

Figure 5.2 Cross-sectional view showing the grain structure of ingot from experiment E2, bottom cooled, 16 K/min. initial cooling, Al-10 wt. pct. Cu alloy with 0.045 wt. pct. TiB_2.

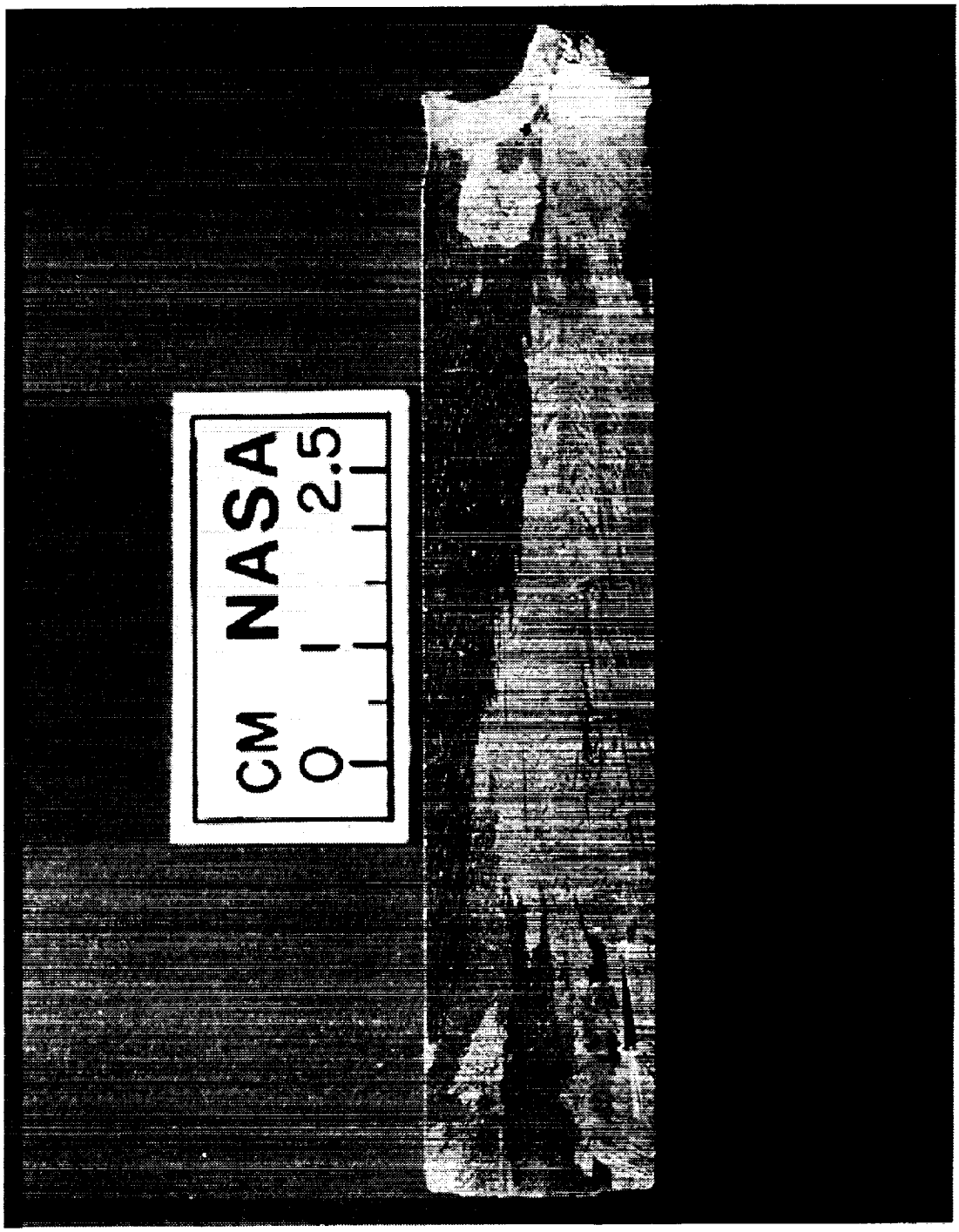

Figure 5.3 Cross-sectional view showing the grain structure of ingot from experiment E3, bottom cooled, 18.5 K/min. initial cooling, Al-1 wt. pct. Cu with 0.45 wt. pct. TiB_2.

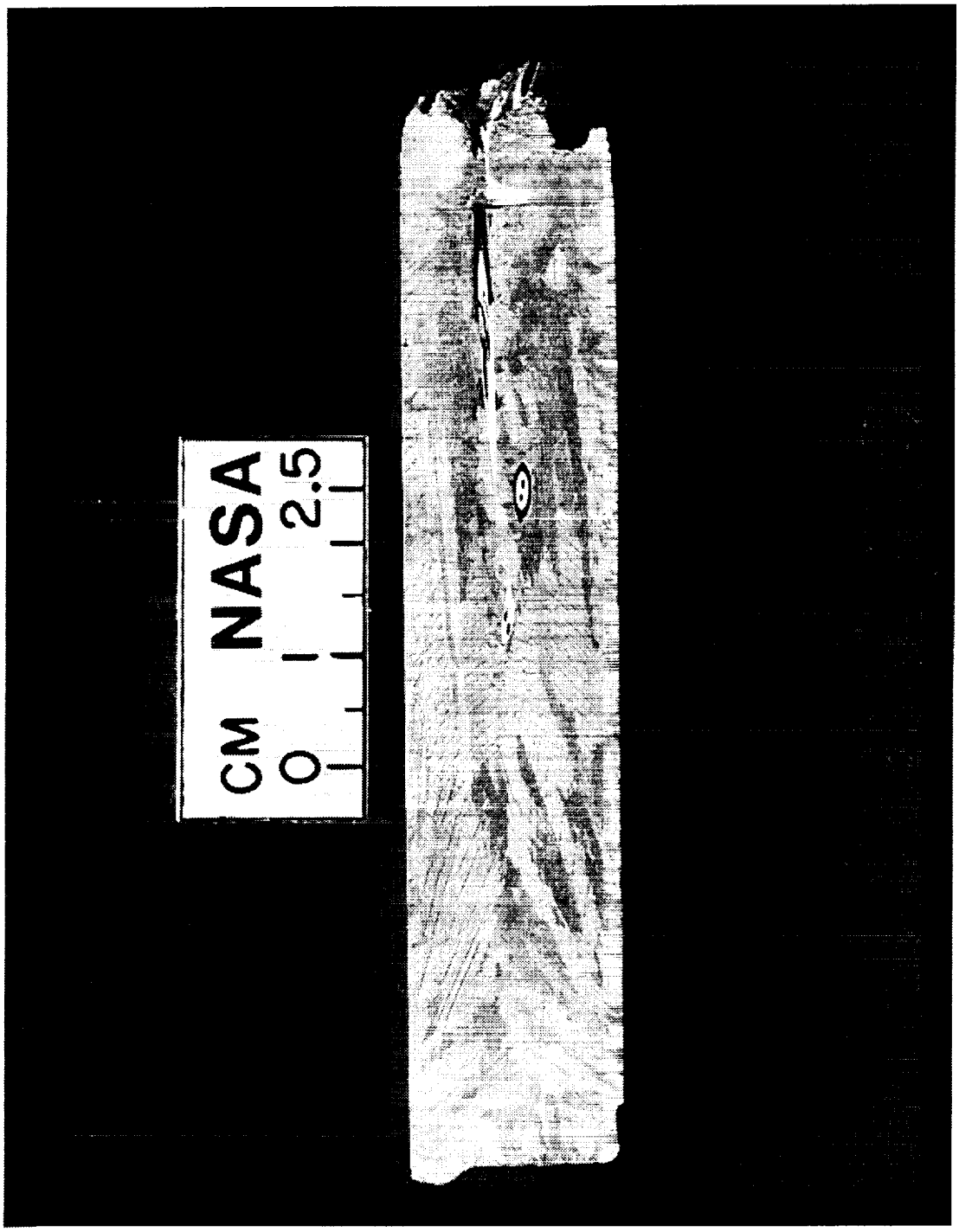

Figure 5.4 Cross-sectional view showing the grain structure of ingot from experiment E5, bottom cooled, 24 K/min. initial cooling, Al-1 wt. pct. Cu with 0.67 wt. pct. TiB_2.

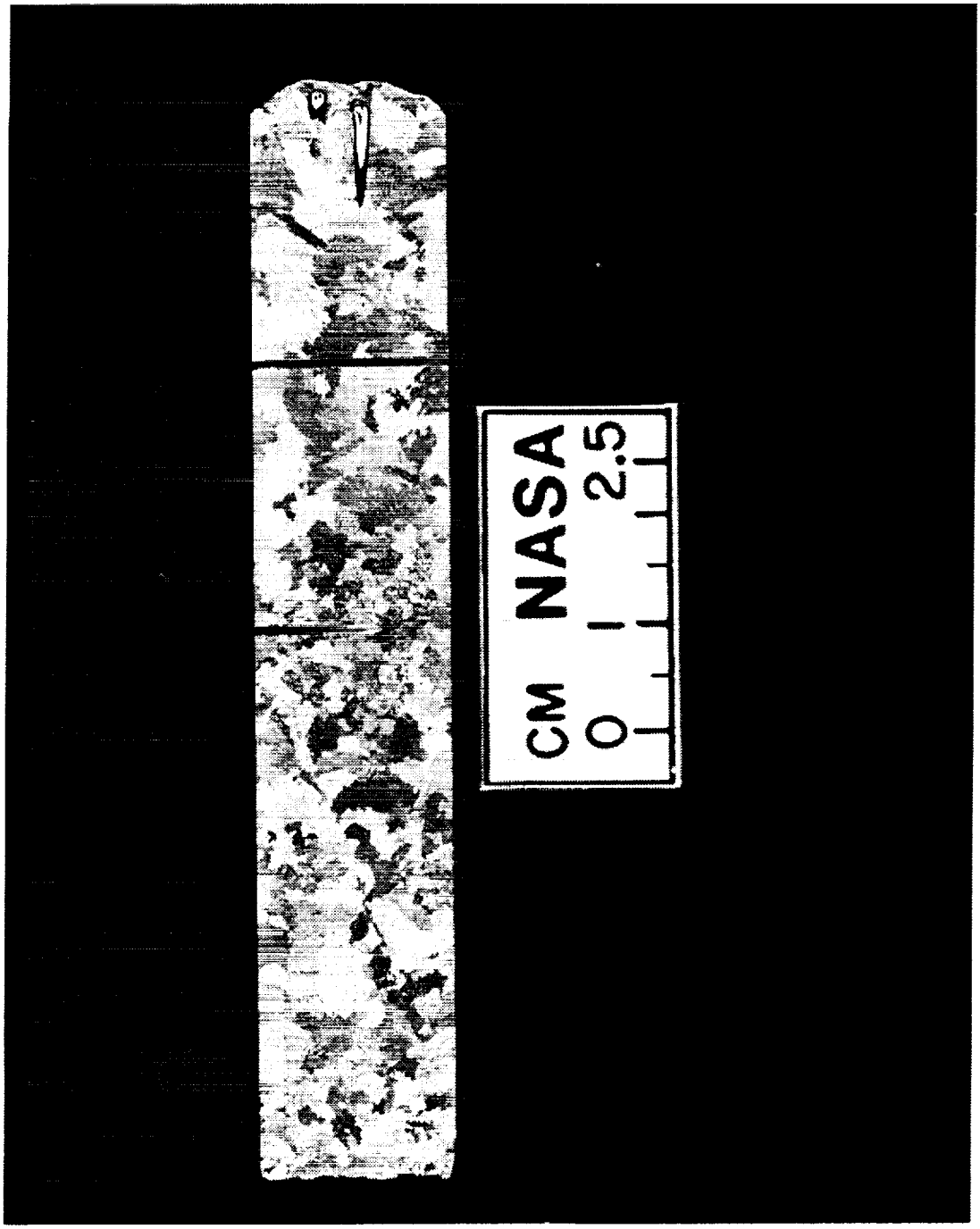

Figure 5.5 Cross-sectional view showing the grain structure of ingot from experiment E6, top cooled, 5.3 K/min. initial cooling, Al-10 wt. pct. Cu with 0.045 wt. pct. TiB_2.

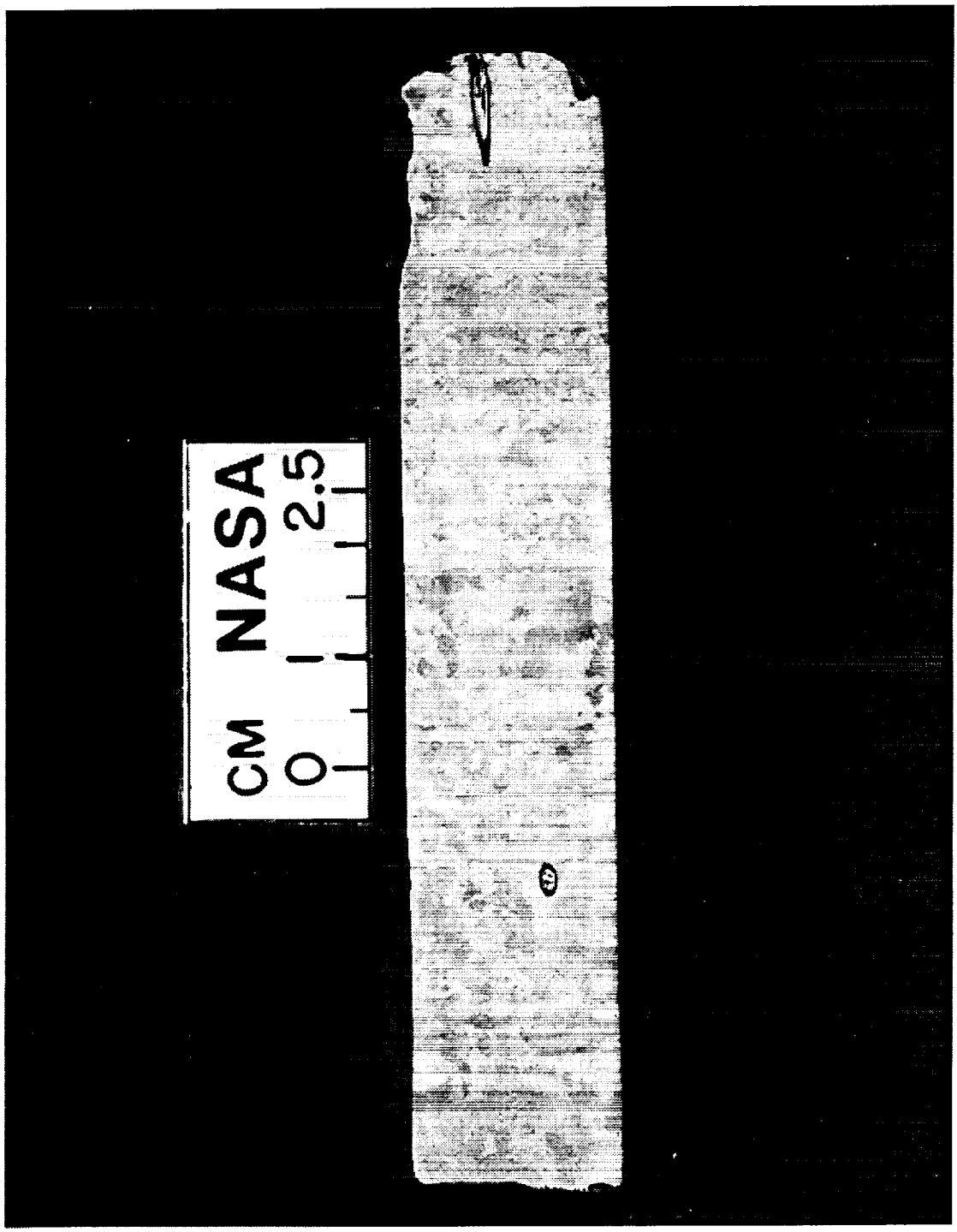

Figure 5.6 Cross-sectional view showing the grain structure of ingot from experiment E7, top cooled, 11.9 K/min. initial cooling, Al-10 wt. pct. Cu with 0.067 wt. pct. TiB_2.

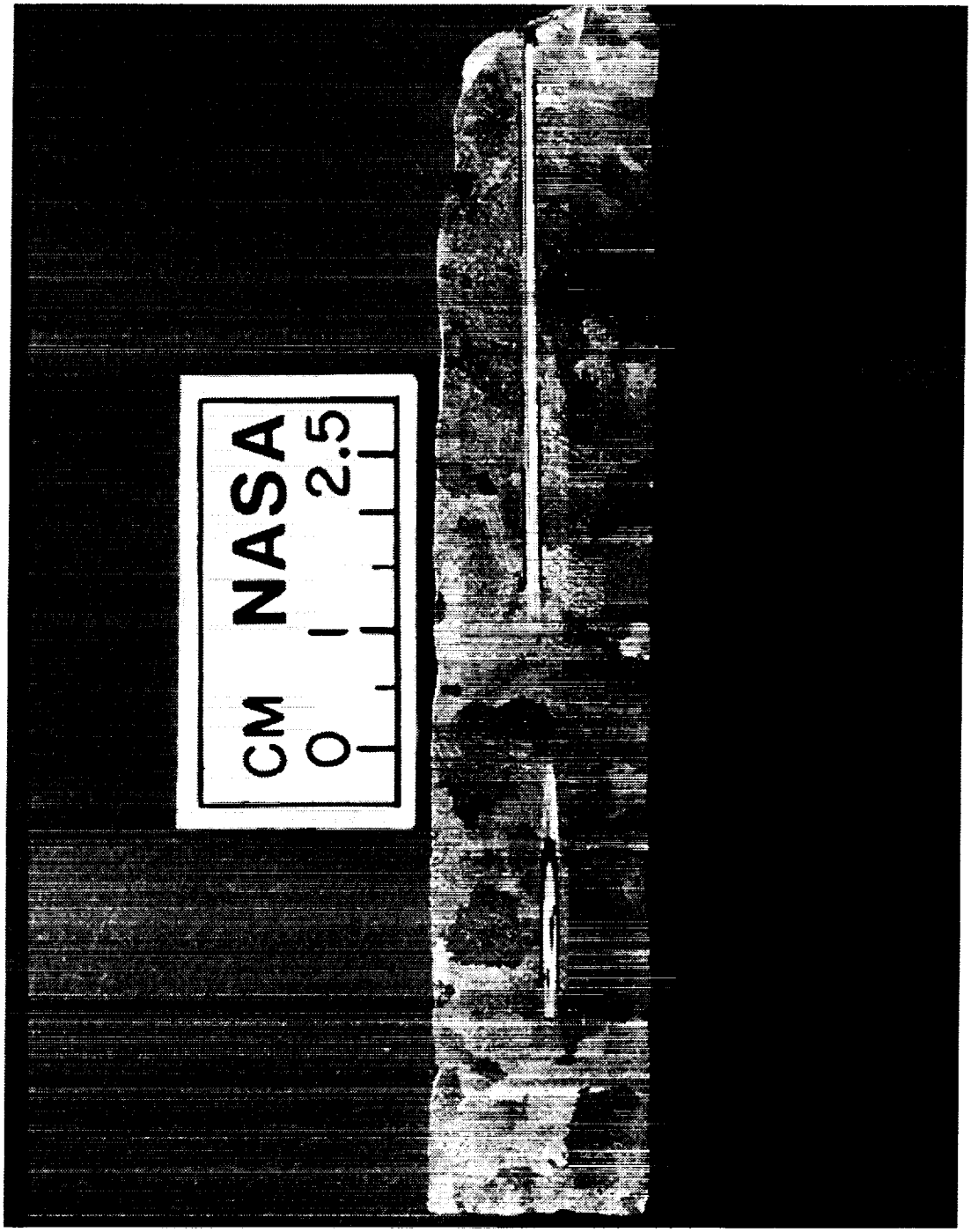

Figure 5.7 Cross-sectional view showing the grain structure of ingot from experiment E8, top cooled, 12 K/min. initial cooling, Al-1 wt. pct. Cu with 0.45 wt. pct. TiB_2.

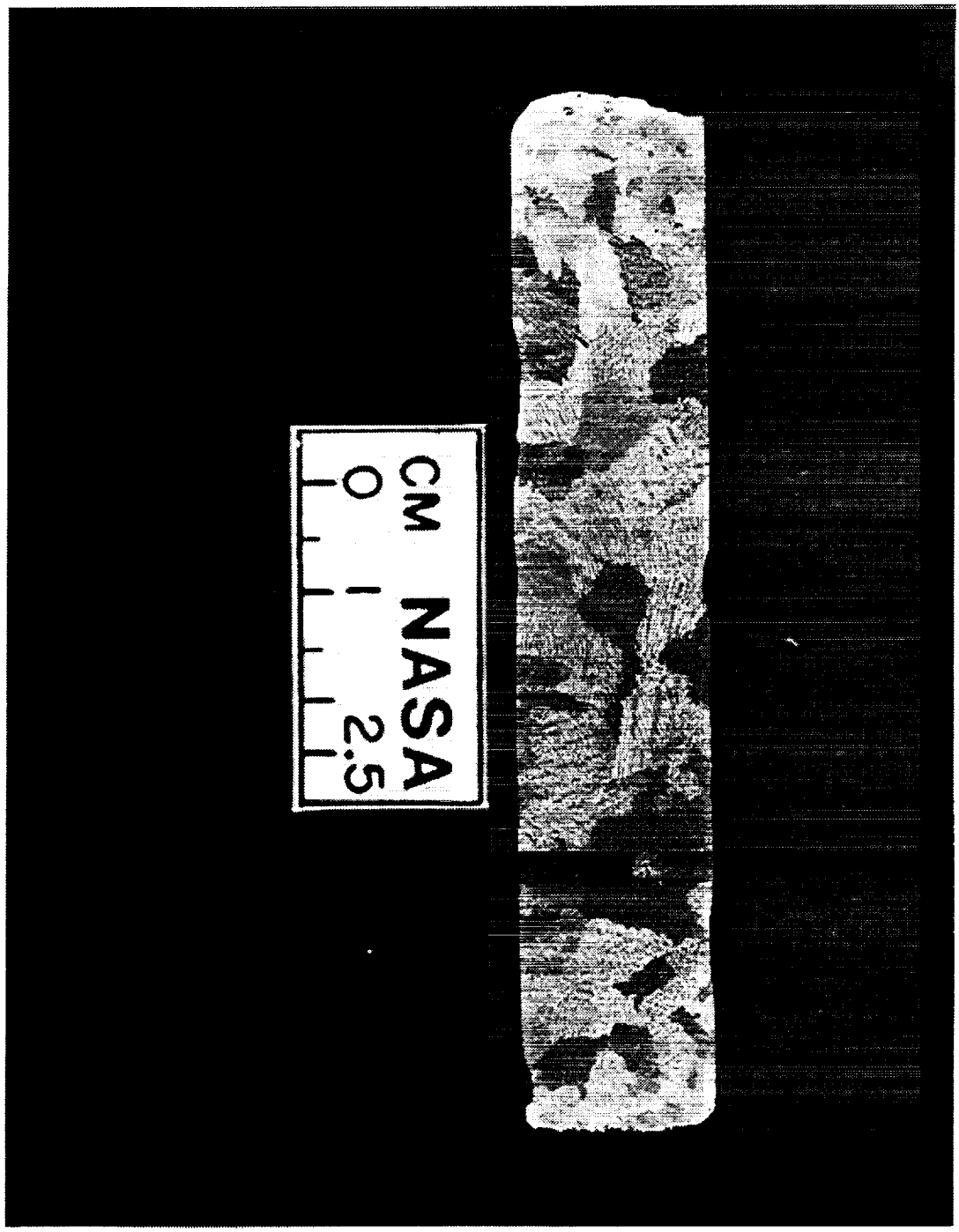

Figure 5.8 Cross-sectional view showing the grain structure of ingot from experiment E9, top cooled, 11.3 K/min. initial cooling, Al-1 wt. pct. Cu with 0.67 wt. pct. TiB_2.

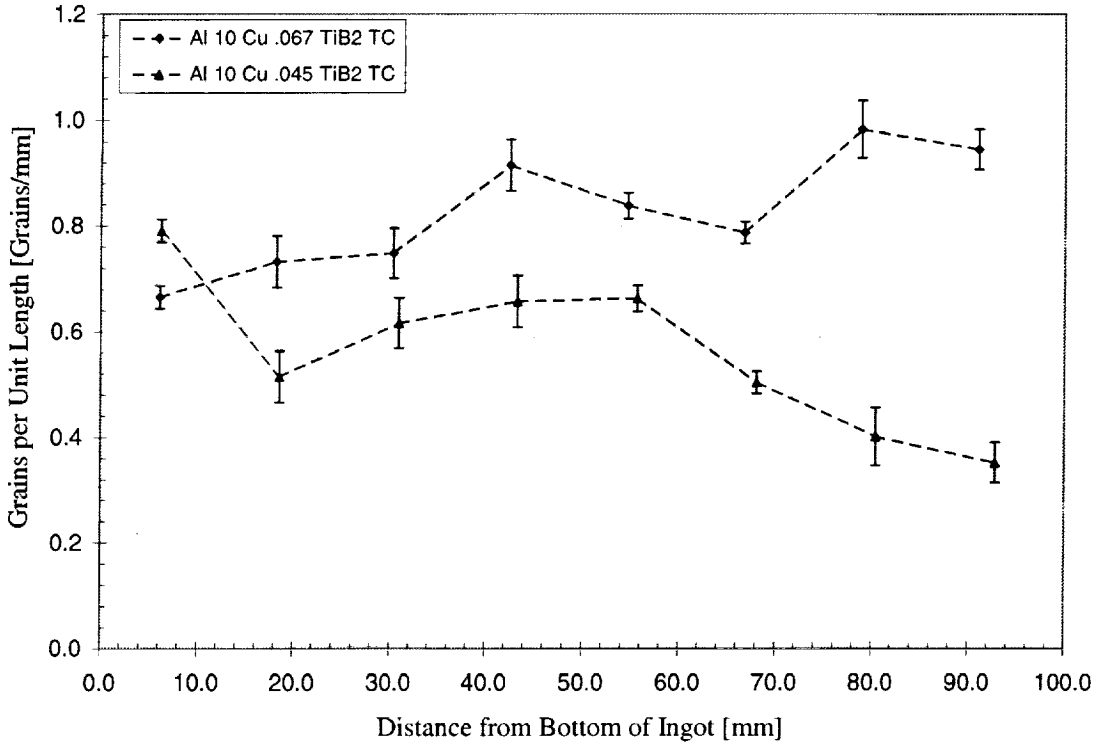

Figure 5.9 Plot of the lineal density of the grains for the top cooled Al-10 wt. pct. Cu experiments which exhibited an equiaxed grain structure, E6 and E7.

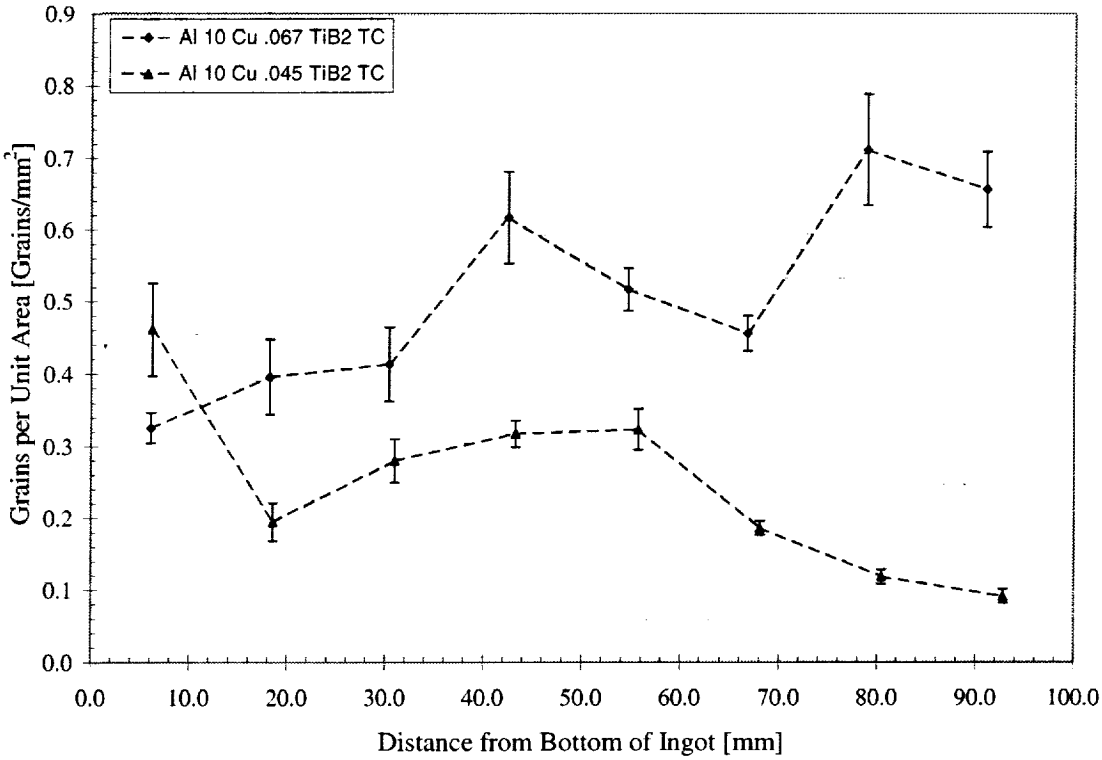

Figure 5.10 Plot of the average number of grains per unit area for the top cooled Al-10 wt. pct. Cu experiments which exhibited an equiaxed grain structure, E6 and E7.

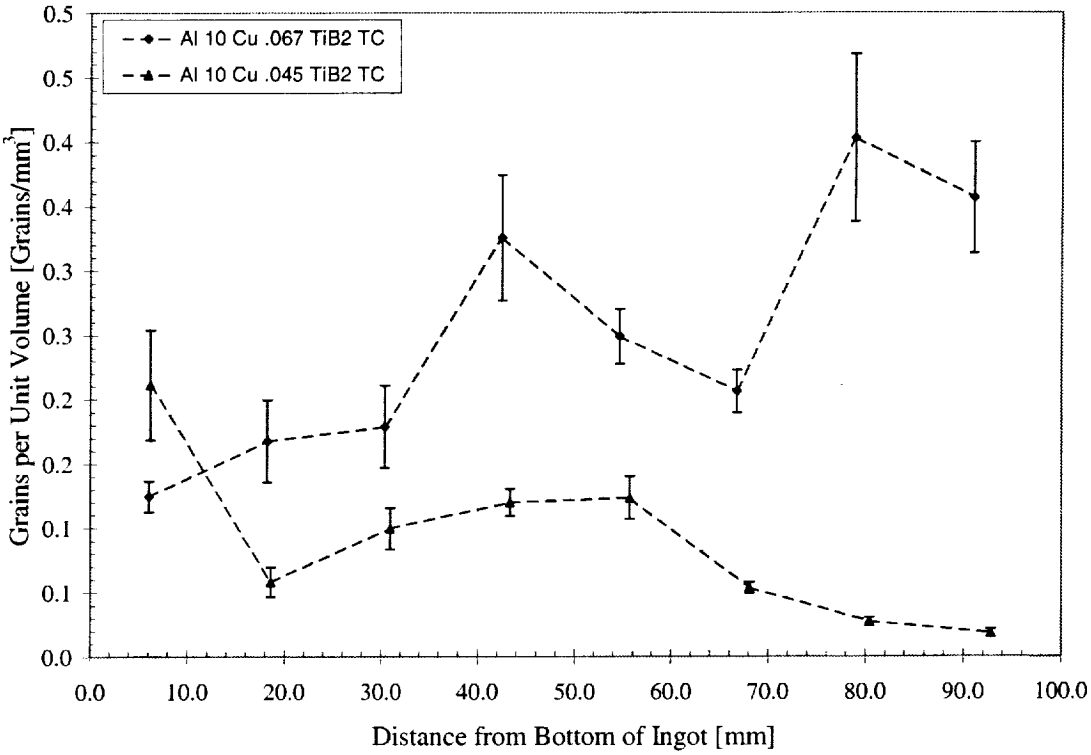

Figure 5.11 Plot of the average number of grains per unit volume for the top cooled Al-10 wt. pct. Cu experiments which exhibited an equiaxed grain structure, E6 and E7.

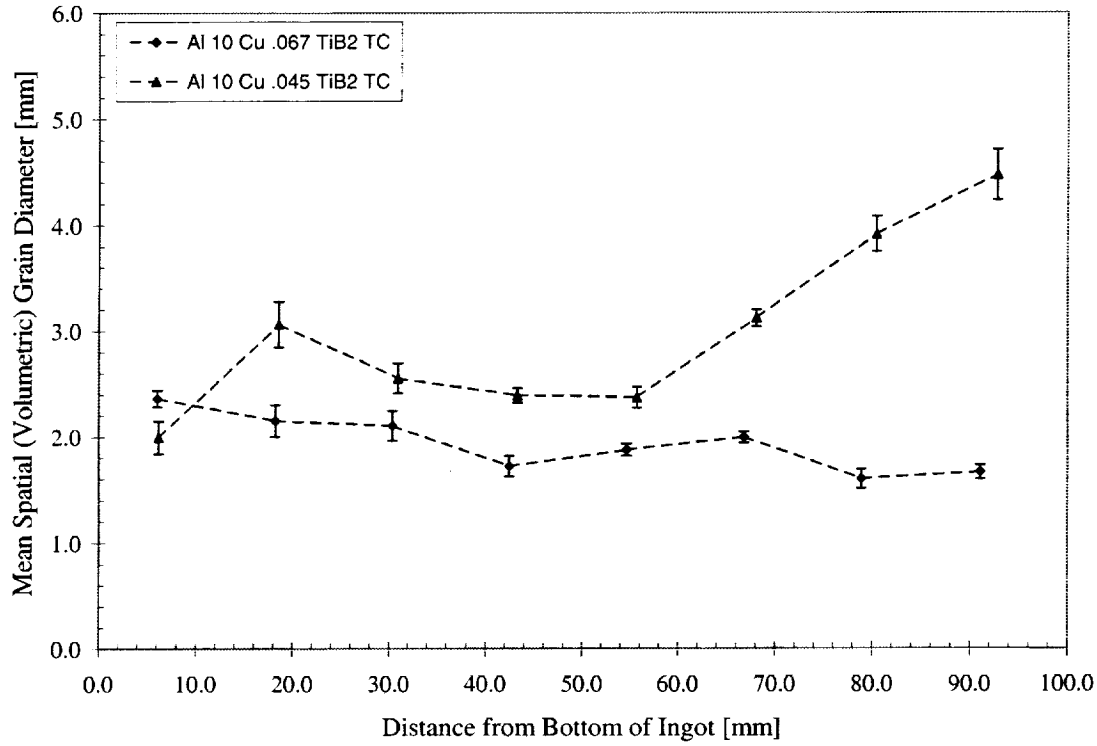

Figure 5.12 Plot of the volumetric grain diameter for the top cooled Al-10 wt. pct. Cu experiments which exhibited an equiaxed grain structure, E6 and E7.

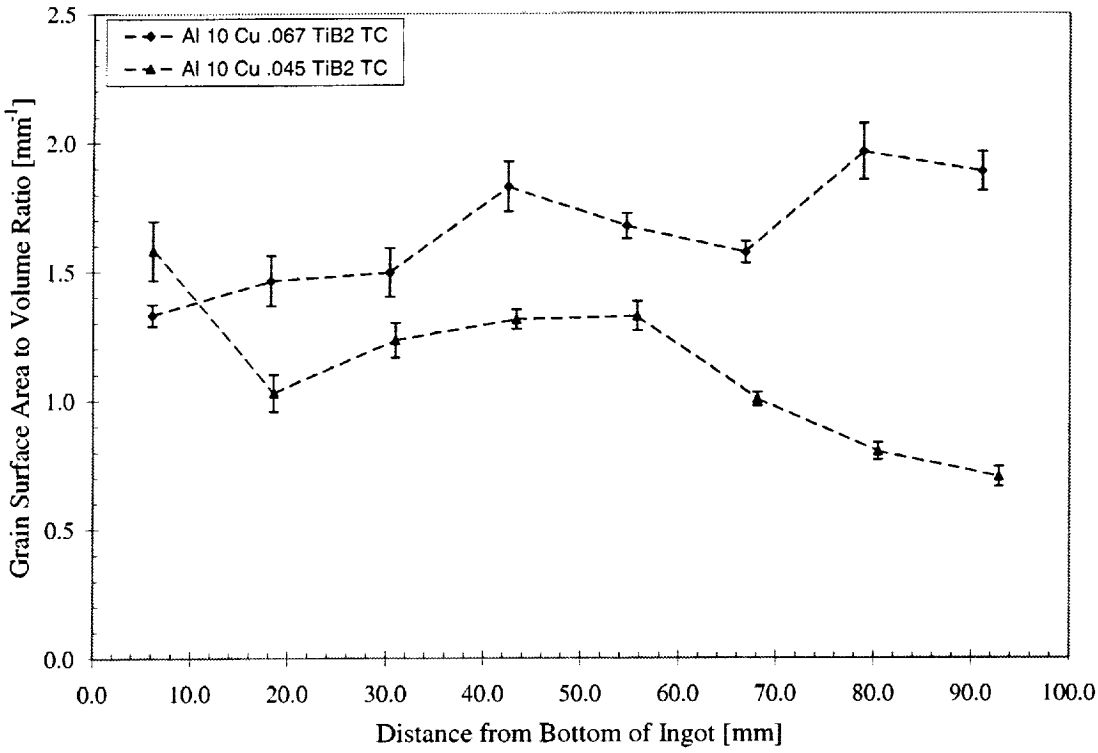

Figure 5.13 Plot of the grain surface area to volume ratio for the top cooled Al-10 wt. pct. Cu experiments which exhibited an equiaxed grain structure, E6 and E7.

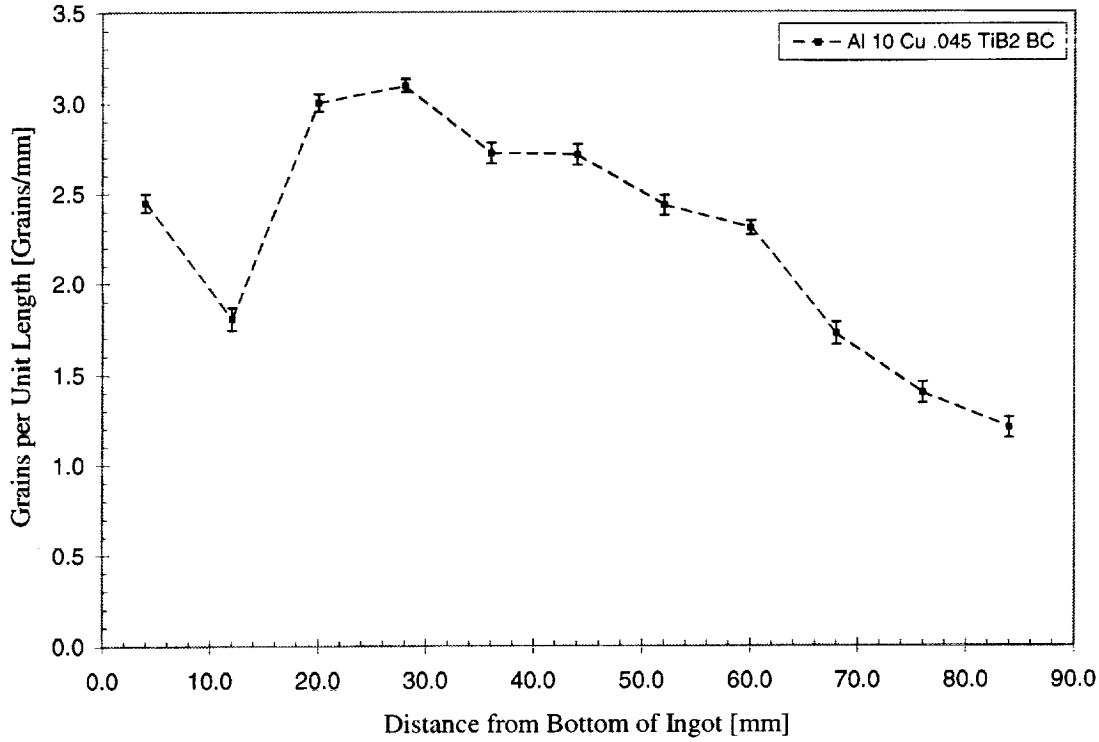

Figure 5.14 Plot of the lineal density of the grains for the bottom cooled Al-10 wt. pct. Cu experiment which exhibited an equiaxed grain structure, E2.

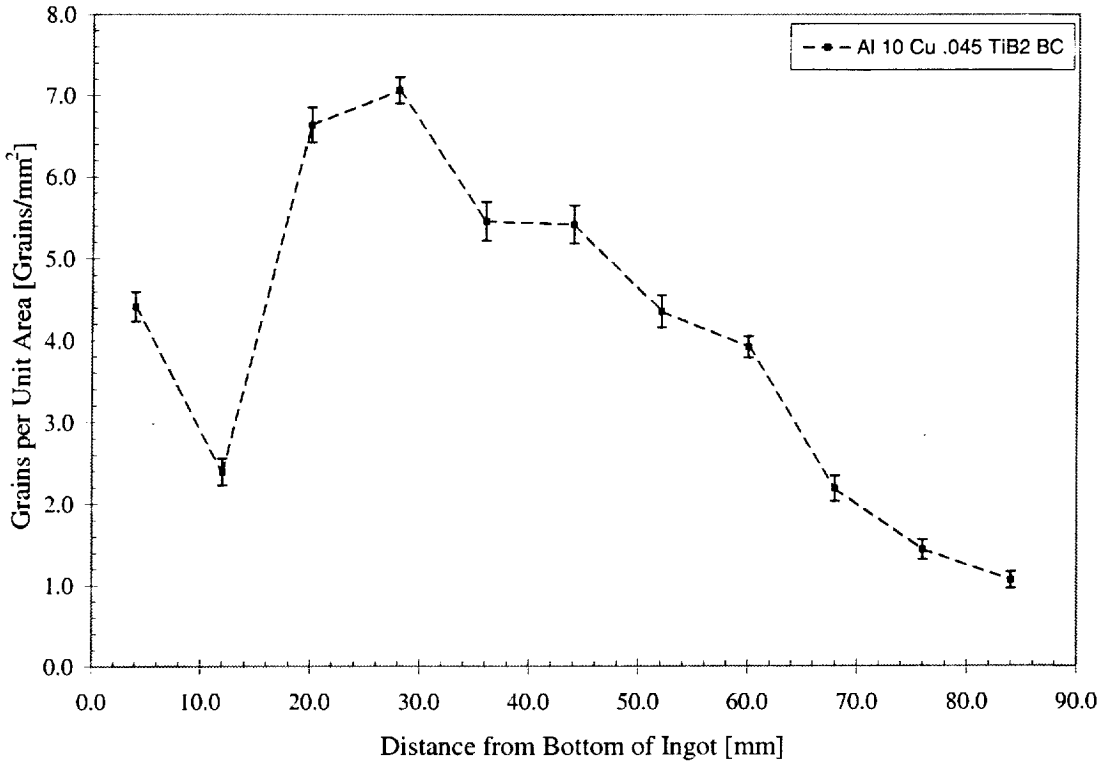

Figure 5.15 Plot of the average number of grains per unit area for the bottom cooled Al-10 wt. pct. Cu experiment which exhibited an equiaxed grain structure, E2.

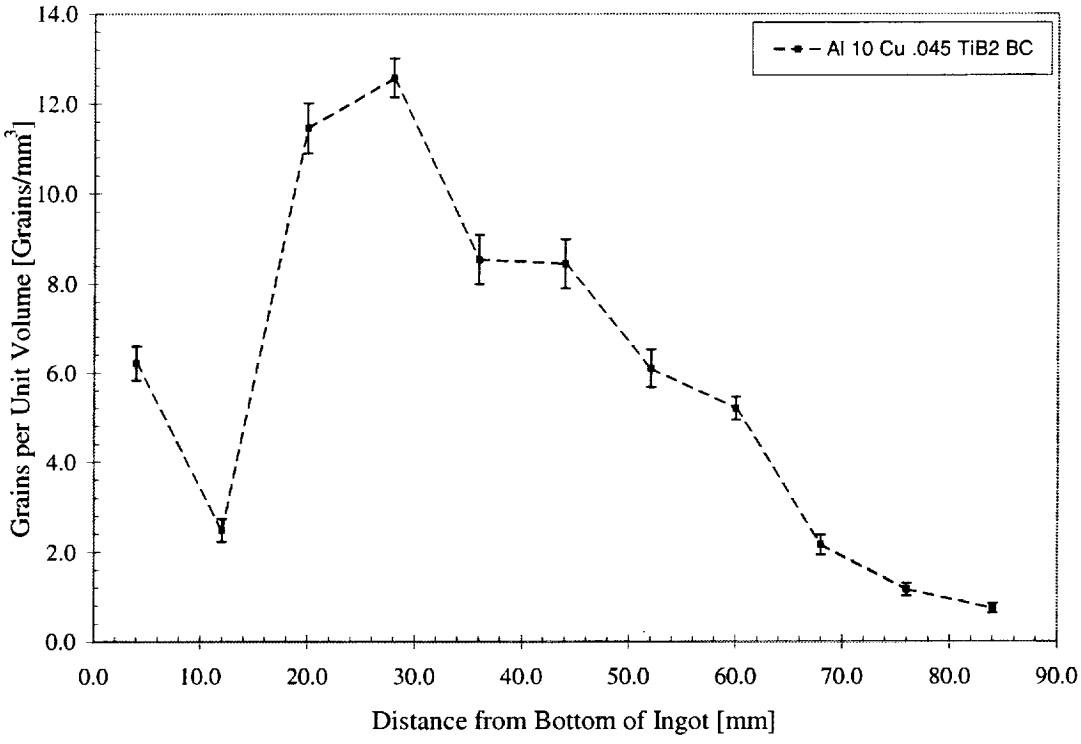

Figure 5.16 Plot of the average number of grains per unit volume for the bottom cooled Al-10 wt. pct. Cu experiment which exhibited an equiaxed grain structure, E2.

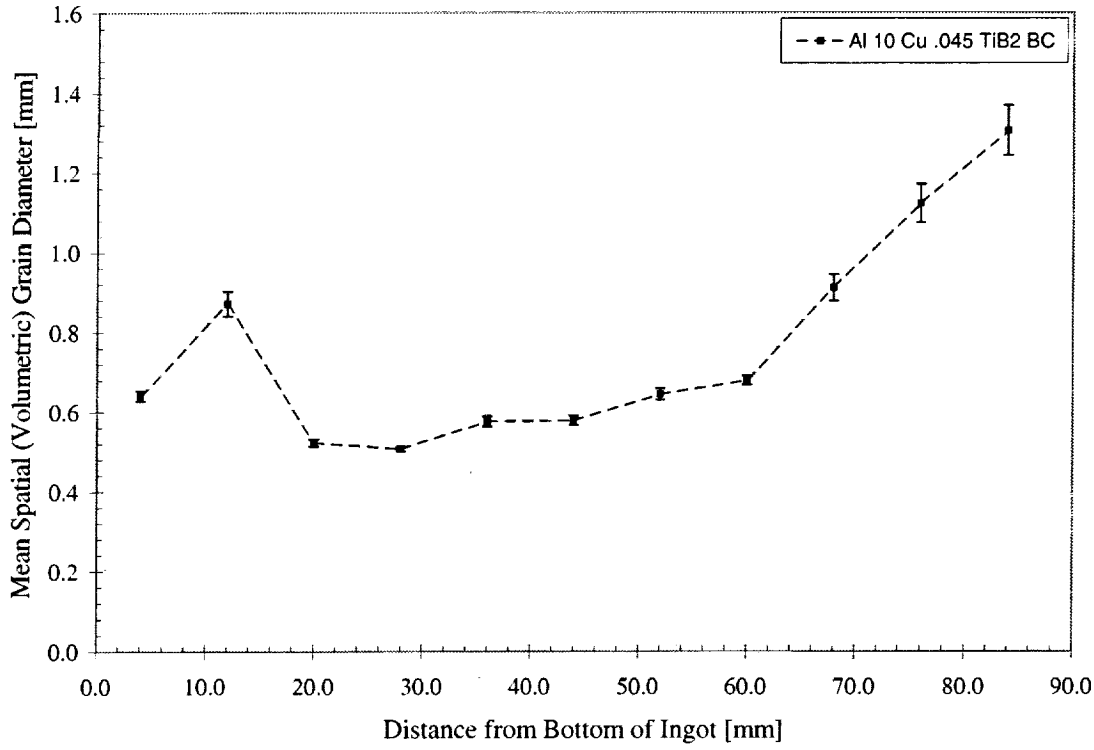

Figure 5.17 Plot of the volumetric grain diameter for the bottom cooled Al-10 wt. pct. Cu experiment which exhibited an equiaxed grain structure, E2.

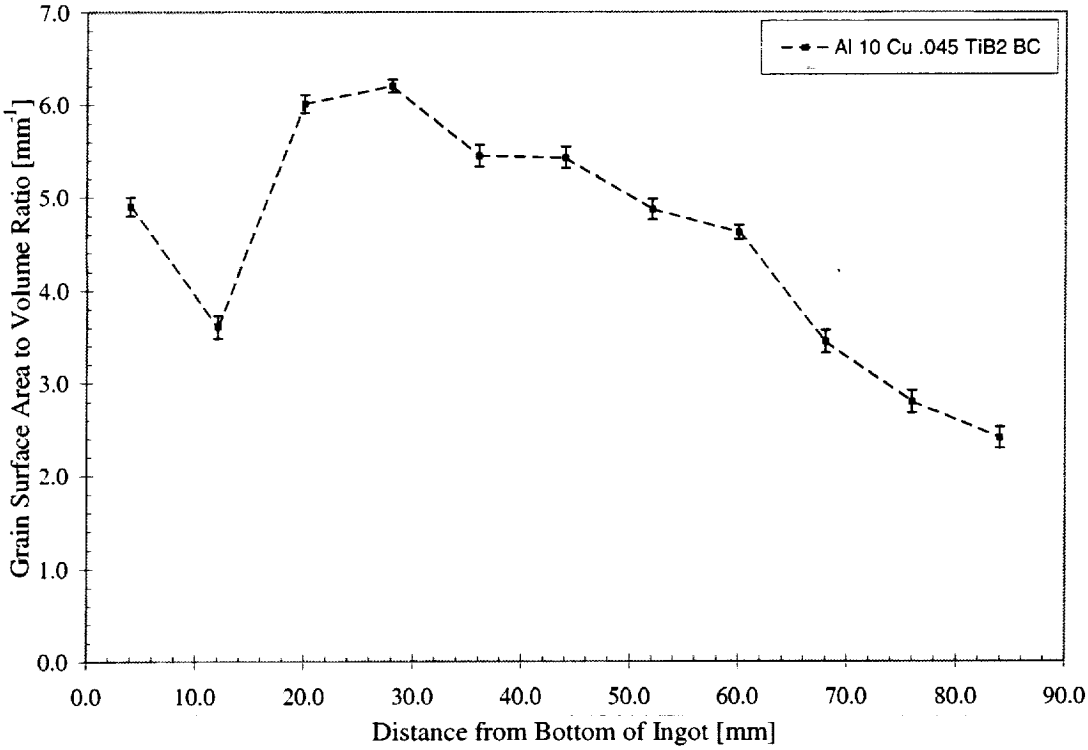

Figure 5.18 Plot of the grain surface area to volume ratio for the bottom cooled Al-10 wt. pct. Cu experiment which exhibited an equiaxed grain structure, E2.

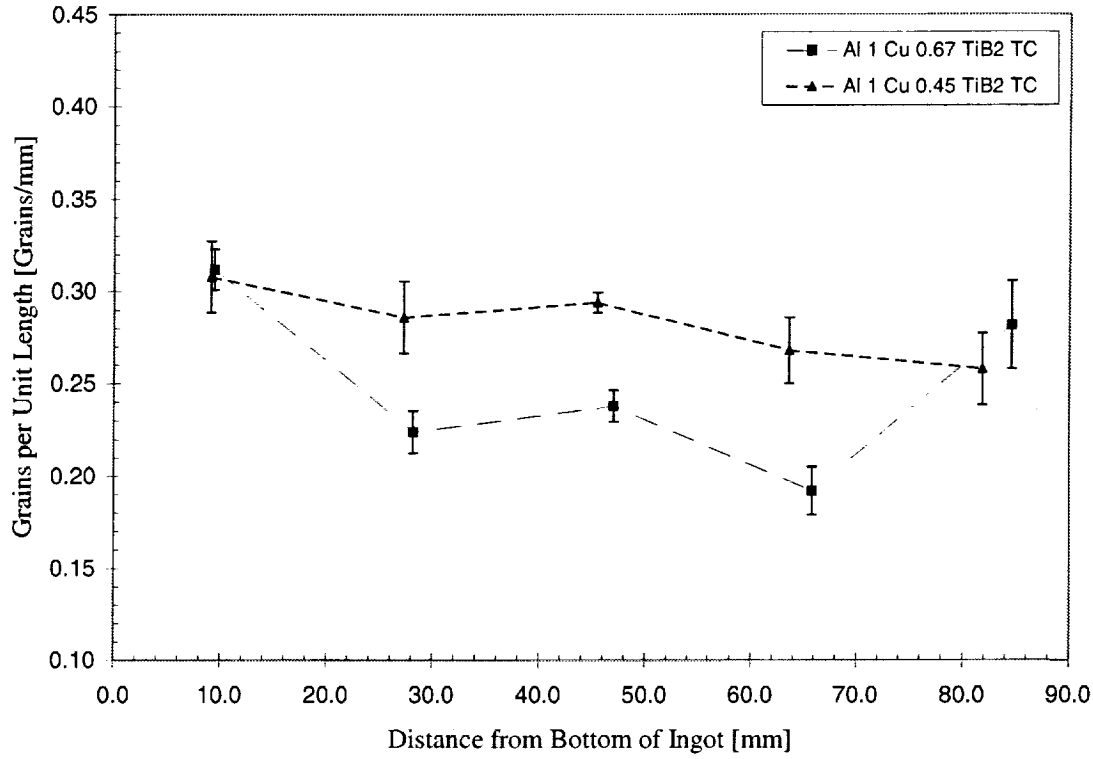

Figure 5.19 Plot of the lineal density of the grains for the top cooled Al-1 wt. pct. Cu experiments which exhibited an equiaxed grain structure, E8 and E9.

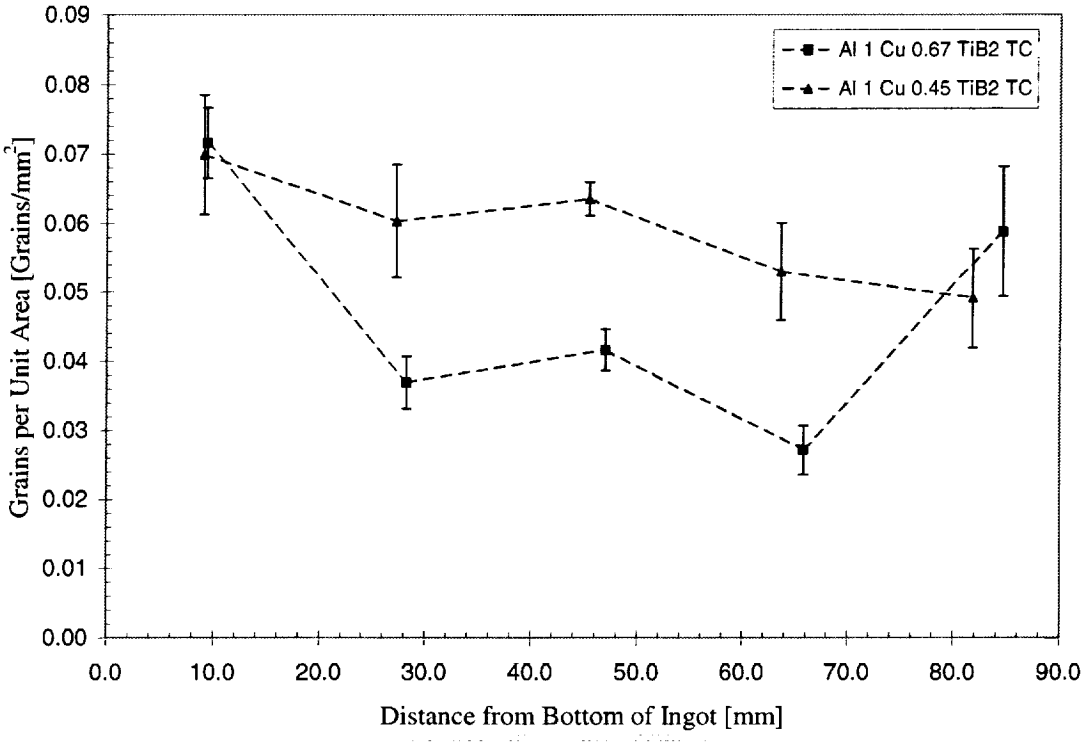

Figure 5.20 Plot of the average number of grains per unit area for the top cooled Al-1 wt. pct. Cu experiments which exhibited an equiaxed grain structure, E8 and E9.

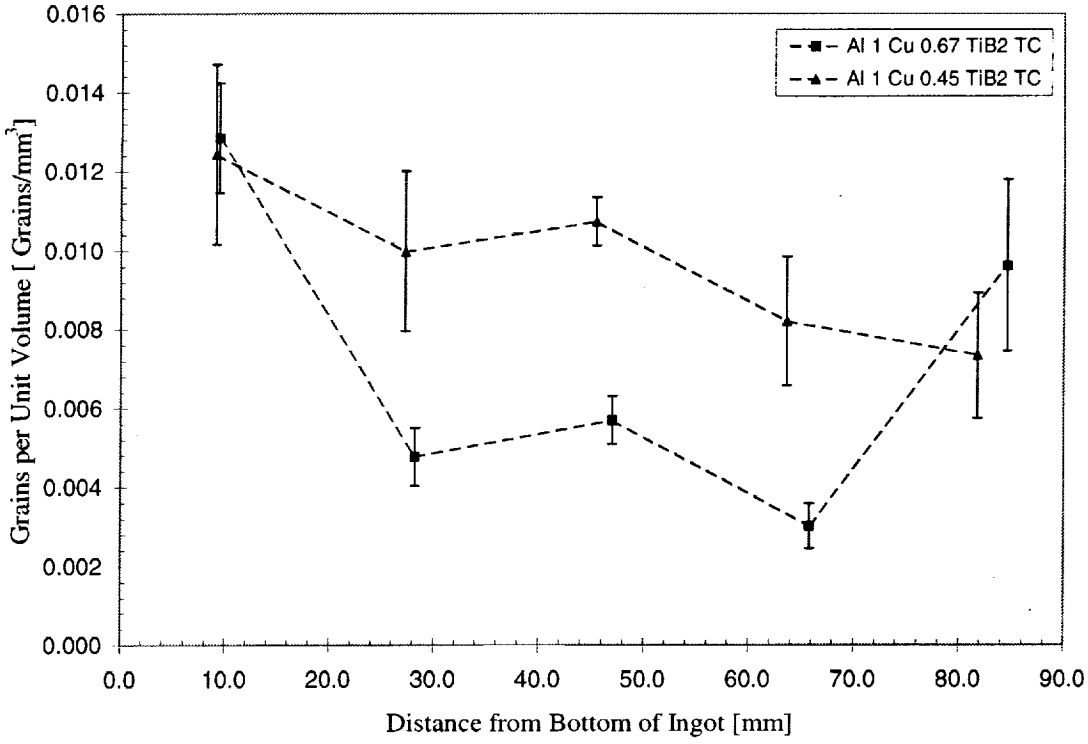

Figure 5.21 Plot of average number of grains per unit volume for the top cooled Al-1 wt. pct. Cu experiments which exhibited an equiaxed grain structure, E8 and E9.

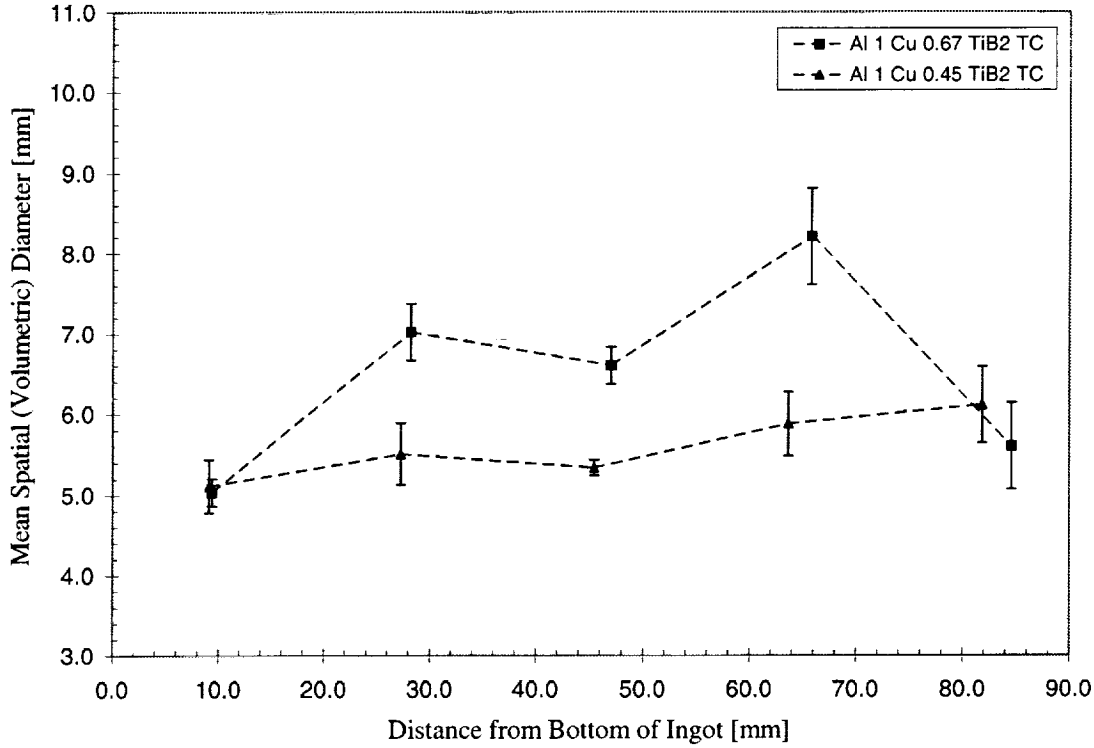

Figure 5.22 Plot of the volumetric diameter of the grains for the top cooled Al-1 wt. pct. Cu experiments which exhibited an equiaxed grain structure, E8 and E9.

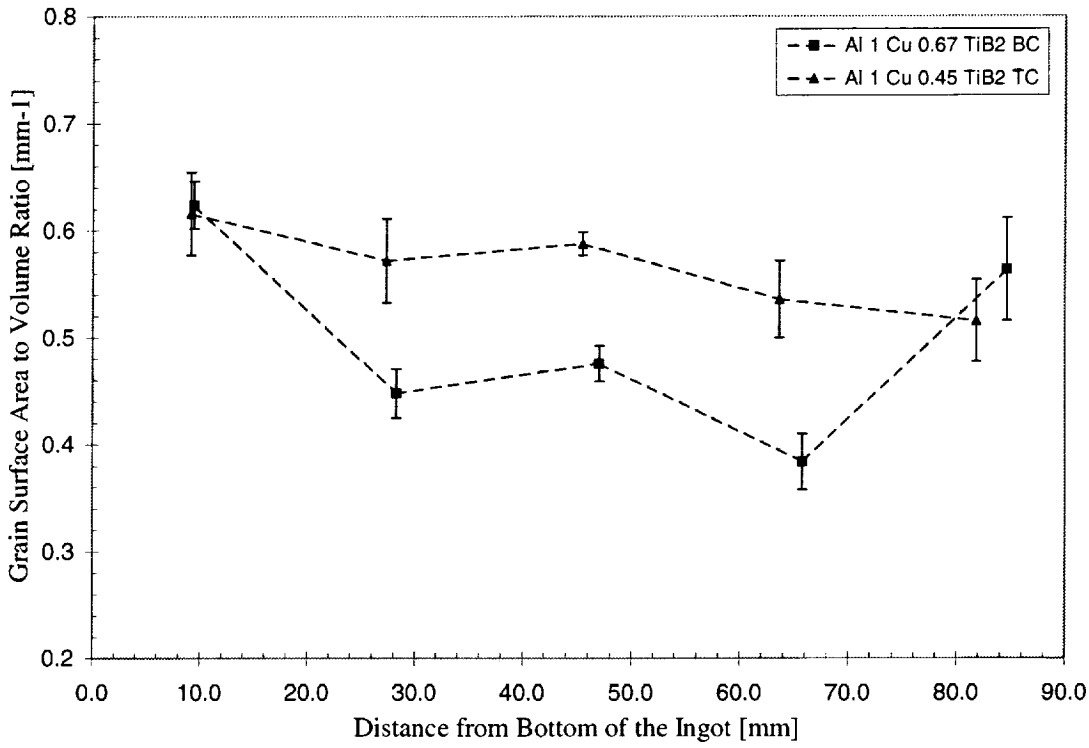

Figure 5.23 Plot of the grain surface area to volume ratio for the top cooled Al-1 wt. pct. Cu experiments which exhibited an equiaxed grain structure, E8 and E9.

CHAPTER 6

SEGREGATION MEASUREMENT RESULTS AND DISCUSSION

6.1 Introduction

This chapter discusses the findings of the segregation measurements on ingots E6 and E8 that were performed by Jim Smith at NASA Lewis Research Center. For an overview of the procedures used, refer to Chapter 3 Section 3. The segregation results provide a clear trend that may assist in the development and verification of numerical codes. A genuine simulation of Experiments 6 and 8 would also be of value in determining the segregation mechanisms active in these experiments.

6.2 Results and Discussion

It should be noted that the intent of the segregation measurements are to determine segregation on a macroscopic scale (compared to the size of the ingot). This presented some difficulty in performing the segregation measurements since the probe used took readings approximately every 20 microns. On the microscopic scale the samples can all be characterized as very inhomogeneous, two and three phase alloys. Figure 6.1 is a low magnification optical micrograph taken of experiment E6, Al-10 wt. pct. Cu alloy refined with 0.45 wt. pct. TiB_2 and illustrates a two-phase eutectic microstructure. At higher magnification, (Figure 6.2) the boundary phase is also observed to exhibit a binary structure. The bright phase has a composition of approximately Al50-Cu50 in the 10 wt. pct. Cu alloy. The darker phase in the two-phase boundary is the same composition as the grain, approximately Al98-Cu2. Figure 6.3 shows a 1000x magnification of the grain boundary.

The chemical inhomogeneities on this scale caused complications in so much as the matrix corrections applied to the measured x-rays are different to the matrix corrections necessary for the individual phases, causing the chemistry and final totals to be in error. These effects were minimized through the selection of a small probe size, 5 microns. The preliminary tests for the Mean Atomic Number (MAN) analyses were consistent with earlier off-peak corrected analyses performed under stable conditions. The analysis time of each sample traverse was shortened from 16.5 hours for the off-peak correction method to about 6.5 hours for the MAN method. The traverse for each sample began at a point approximately 4 mm from the top of the section and proceeded to the base in increments of 20 microns per point. The traverse for each sample was divided into two parts, traverse a1 and traverse a2. Traverse a1 began at the upper portion of each sample and ended in the approximate center of the section. Traverse a2 began at a point 20 microns from the approximate center and ended at the base of the sample. This was done to recalibrate the Z coordinate direction of the stage (focus) in the approximate center of the sample. In samples of size 2.0 x 2.5 cm there are subtle changes in the height along the section due to rounding of the sample during polishing. The middle of the sample is slightly higher than the edges which adversely affects the measurements.

Since the objective of the microprobe measurements is to determine the segregation on a macroscopic scale, the data obtained from Smith's analysis was mapped

to the entire uncut ingot. To do this the results of the four samples (8 traverses in total) were combined into one database. Starting from the bottom edge of the sample, the traverses were converted into global coordinates by taking into account the sections overall position from the bottom and the amount of material that was removed during cutting. The distance that was skipped at the top of each section (4mm) during the microprobe analysis was also taken into account. The resulting composite is shown in Figure 6.4 for the Al-10 wt. pct. Cu alloy, E6 and Figure 6.5 for the Al-1 wt. pct. Cu alloy, E8. These figures show every measurement taken starting from the bottom of the ingot. The empty spaces illustrate where material was removed during cutting. To clearly see segregation on a macroscopic scale, averaging was used across partitions of the ingot and the results were reported as one value for each partition. The averaging was done for 8, 16, 32, and 64 partitions. The partitions were determined by dividing the regions measured into an equal number. The regions which did not contain data were excluded in the averaging. Figures 6.6-6.9 show the results of the averaging for the Al-10 wt. pct. Cu alloy. Figures 6.10-6.13 show the results of the averaging for the Al-1 wt. pct. Cu alloy.

The results for the Al-10 wt. pct. Cu alloy cooled directionally downward, depicted in Figures 6.6-6.9 clearly show a progression from negative segregation at the top (solute poor) to a positive segregation (solute rich) at the bottom or end of solidification. This trend can be explained by taking a closer look at the density of the solid and liquid phases. As discussed in Chapter 2, the Al-10 wt. pct. Cu alloy was selected due to the neutral buoyancy of the grains compared to the bulk liquid at the start of solidification. Thus some of the primary grains are expected to remain in there initial positions, with some others being advected to lower portions of the ingot. During solidification solute is rejected causing the interdendritic liquid to become more rich in copper. Copper has approximately three times the density of aluminum and thus the interdendritic liquid tends to sink, being replaced by bulk liquid of a lower density. Between there two competing transport mechanisms, 1) transport of solute poor solid, and 2) sinking of solute rich liquid, it appears from the segregation data that settling of Cu rich liquid dominates in E6. As solidification proceeds the copper content of the bulk liquid would continue to increase resulting in more solute at the bottom of the ingot. The compositional differences act in conjunction with the inverted temperature field in the ingot resulting in thermosolutal convection, a major contributor to the occurrence of segregation on the macroscopic scale. Furthermore, Figure 6.4 shows a higher concentration of eutectic at the bottom of the ingot, illustrated by the higher concentration of data points at the eutectic composition (33.3 wt. pct. Cu). This non-uniform eutectic distribution is also an indication of positive segregation at the bottom of the ingot since more copper would need to be present for the additional formation of eutectic.

Figures 6.10-6.13, illustrating the Al-1 wt. pct. Cu Alloy cooled directionally downward, show a very flat segregation profile. Looking at the start of solidification, grains form which tend to sink because the solid density of the aluminum dendrite is higher than that of the bulk liquid due to the bulk liquid's low copper content and solidification shrinkage. The relatively higher copper concentration that is in the interdendritic liquid causes the interdendritic liquid to sink as well. With solute poor

dendrites moving downward, and solute rich liquid moving downward concurrently, their effects on segregation tend to cancel each other out.

The grand average of the segregation measurements is shown in Table 5 below along with the nominal composition of the alloys. Since the values are within an acceptable range, both are less than 10% different from nominal, the segregation data taken represents the sample well. The nominal and grand average totals do differ though because the measurements were only taken on the centerline of the ingot not taking into account the true three-dimensional macrosegregation pattern.

Table 5. For experiments E6 and E8, average of all composition measurements, percent difference from the initial composition (C_o), and composition at longitudinal locations from the bottom from averaging the original data into 32 partitions.

Experiment number	E6		E8	
Grand Average	9.18		0.924	
% Difference from C_o	8.2		7.6	
	mm	wt. pct. Cu	mm	wt. pct. Cu
	96.11471	5.780422	98.47328	0.84356
	93.48432	8.270404	95.76858	0.79752
	90.87391	6.243174	93.06389	1.14243
	88.25341	5.420585	90.35919	1.00288
	85.6318	7.31606	87.69566	1.08715
	83.00736	6.811044	85.08311	0.82987
	80.3828	5.935465	82.48056	0.70957
	77.75823	9.374065	79.87802	0.95491
	70.93458	6.803506	72.27484	0.99707
	68.47174	7.517873	69.64106	1.02655
	66.00891	6.776104	67.01730	0.93245
	63.55608	6.779968	64.39354	0.84531
	61.10371	7.883594	61.75164	0.82521
	58.65207	10.42025	59.10146	0.70837
	56.20044	7.350051	56.46130	0.80263
	53.74883	7.104513	53.82113	1.28219
	46.91796	8.725023	46.14082	0.99614
	44.26794	7.134746	43.38045	0.93242
	41.62798	8.249467	40.62008	1.00481
	38.98798	8.273994	37.86932	0.87927
	36.34568	8.439878	35.10907	0.71635
	33.70089	9.896277	32.32913	0.88638
	31.0561	9.711535	29.54917	1.02829
	28.4113	12.02457	26.76918	0.82971
	21.38882	8.464236	19.07673	1.00552
	18.54864	15.35453	16.44175	0.87581
	15.70841	12.92813	13.81678	0.94212
	12.86821	11.86752	11.19184	0.87590
	10.02589	11.90768	8.64835	0.85152
	7.181371	12.18351	6.16451	0.84691
	4.336853	16.32267	3.68355	1.24286
	1.420682	13.3024	1.23115	0.86347

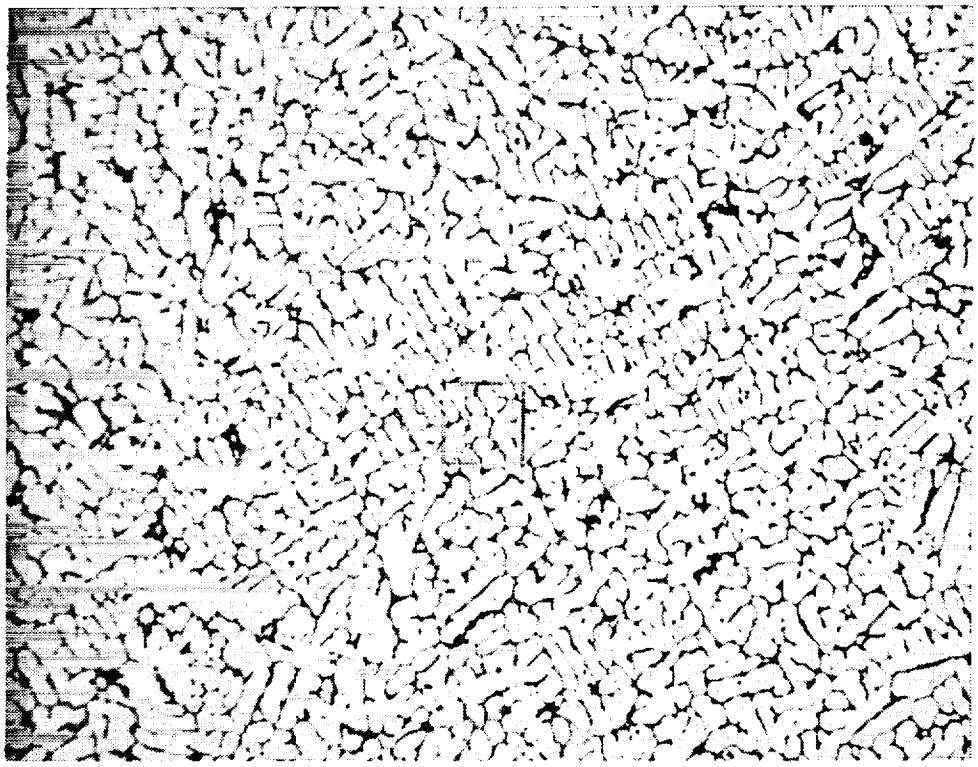

Figure 6.1 Sample optical micrograph, 16x magnification, of experiment E6, top cooled Al-10 wt. pct. Cu alloy refined with 0.045 wt. pct. TiB_2.

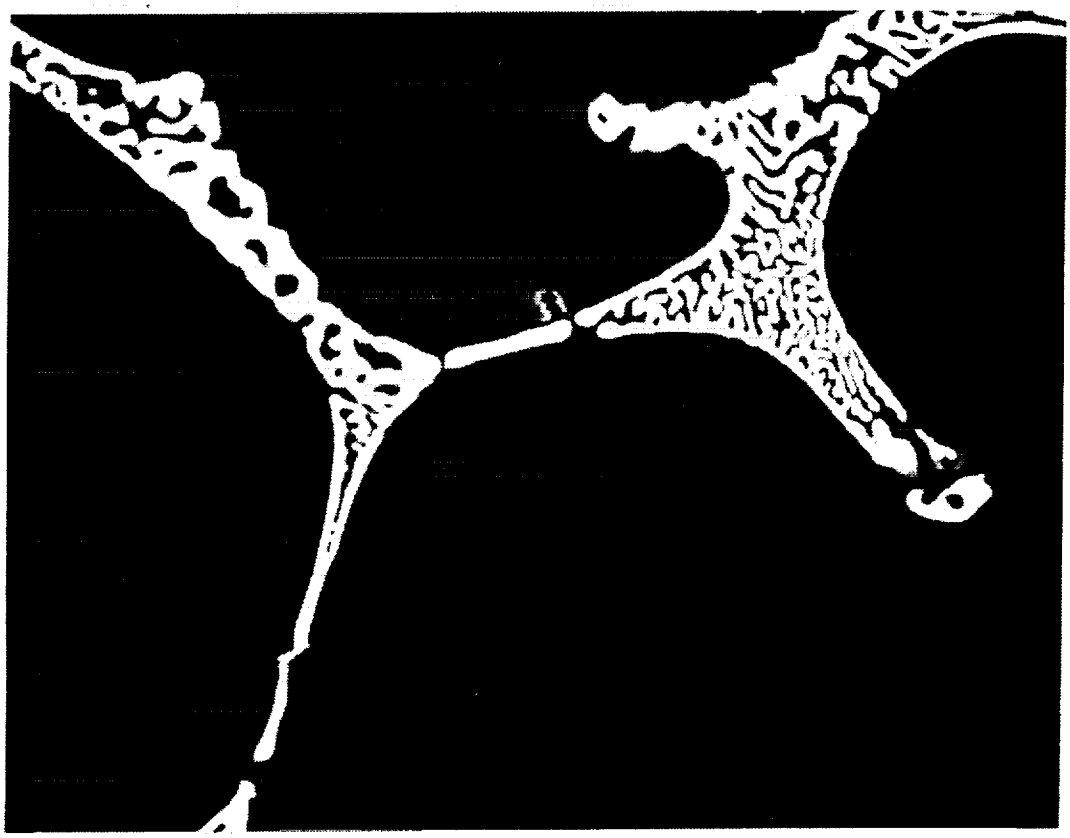

Figure 6.2 Sample optical micrograph, 500x magnification, of experiment E6, top cooled Al-10 wt. pct. Cu alloy refined with 0.045 wt. pct. TiB_2.

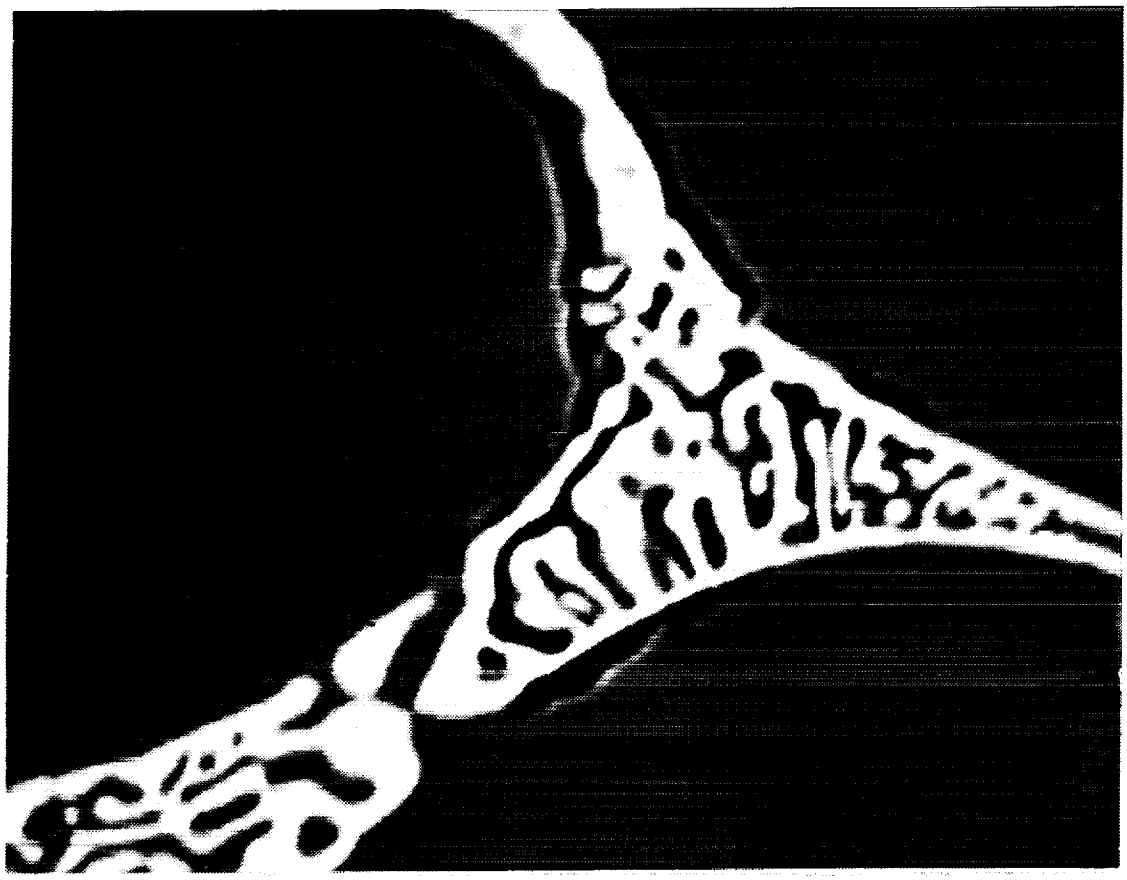

Figure 6.3 Sample micrograph of eutectic at grain boundary, 1000x magnification, of experiment E6, top cooled Al-10 wt. pct. Cu alloy refined with 0.045 wt. pct. TiB_2.

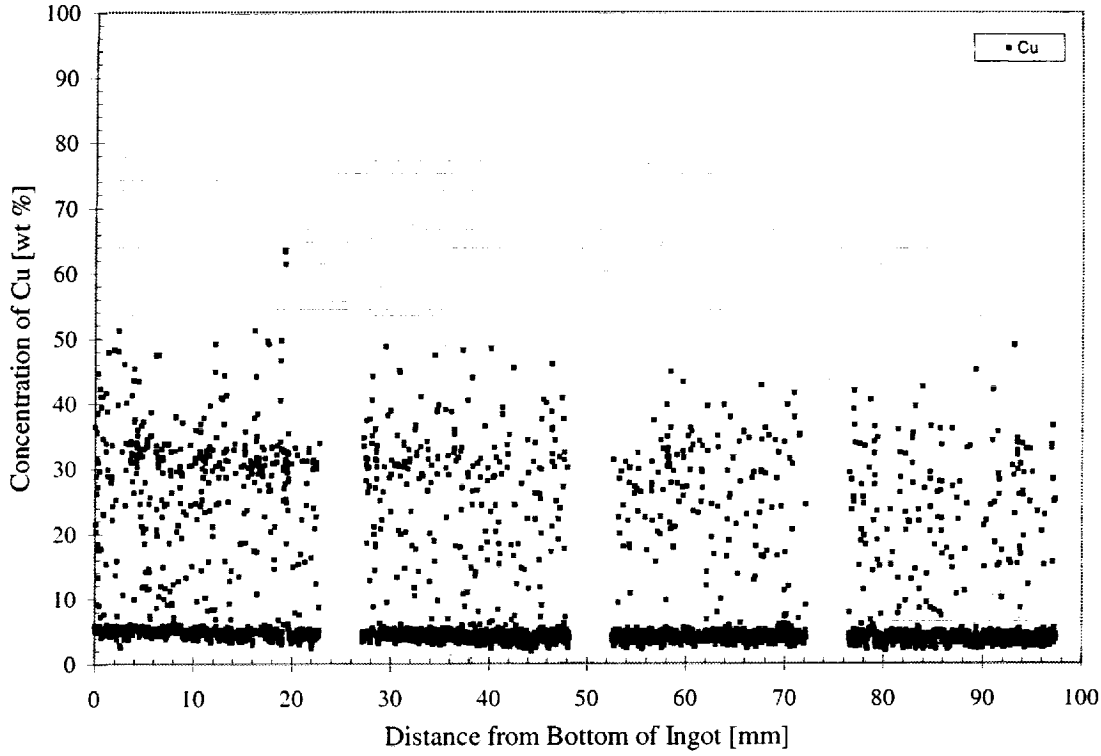

Figure 6.4 Plot of the original microprobe measurement data taken from experiment E6, top cooled Al-10 wt. pct. Cu alloy with 0.045 wt. pct. TiB_2.

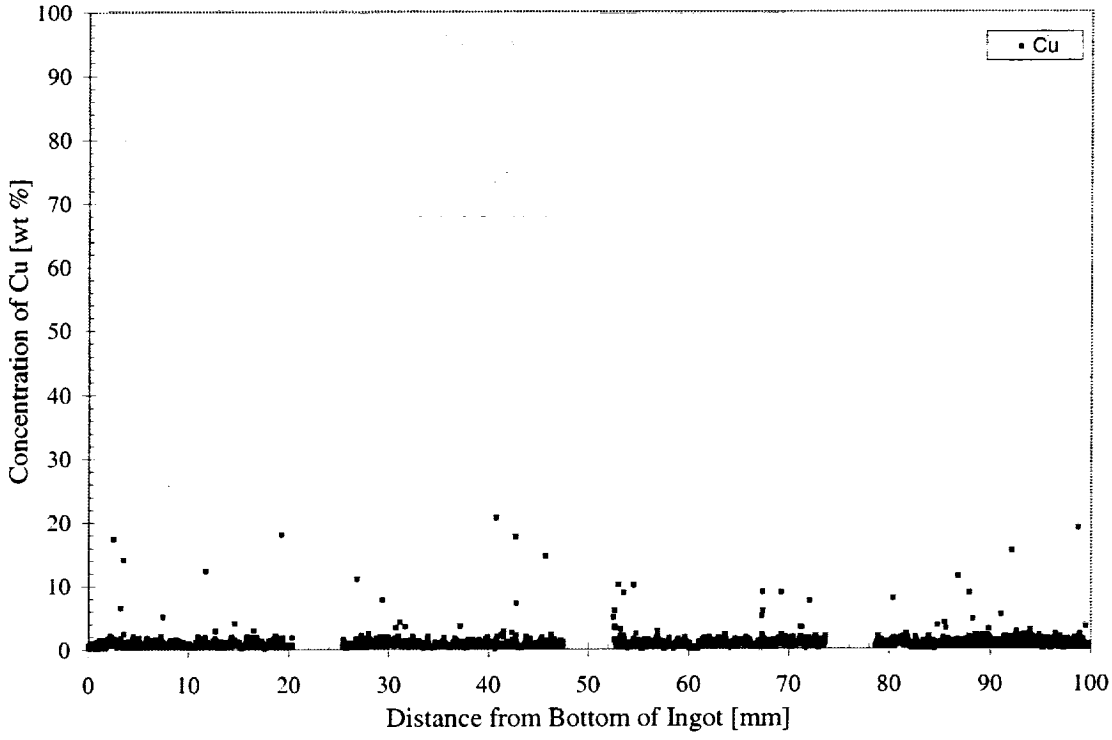

Figure 6.5 Plot of original microprobe measurements taken from experiment E8, top cooled Al-1 wt. Pct. Cu with 0.45 wt. Pct. TiB_2.

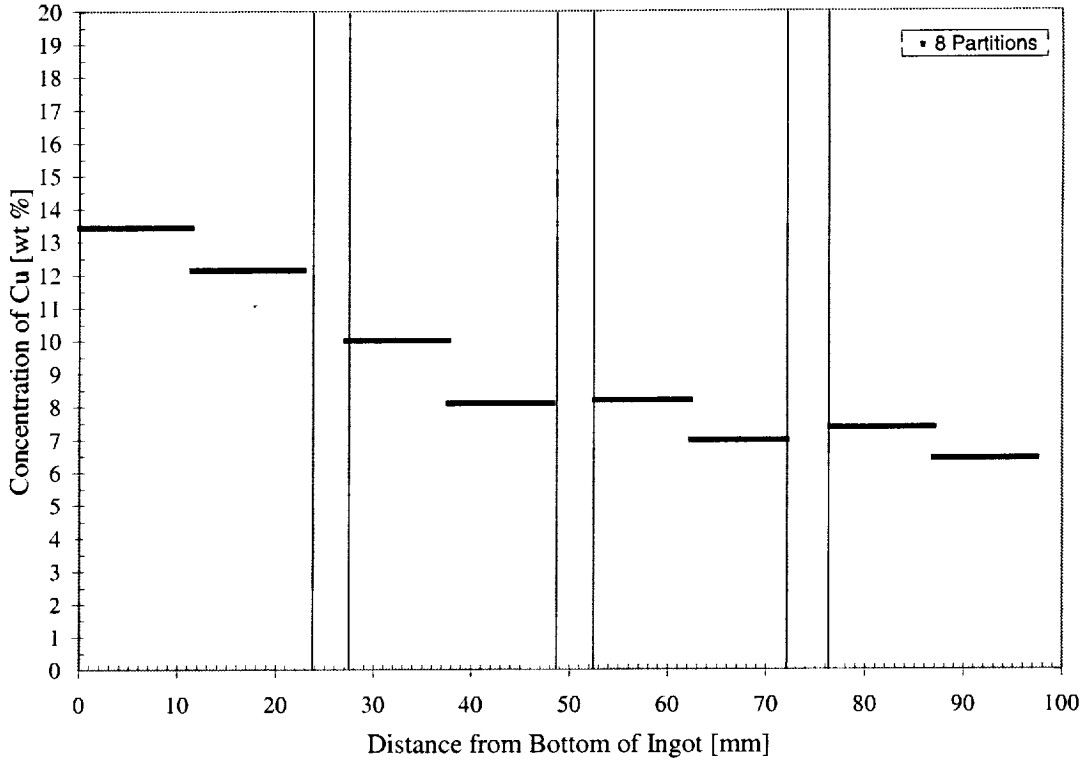

Figure 6.6 Plot showing compositional variation of experiment E6, top cooled Al-10 wt. pct. Cu alloy with 0.045 wt. pct. TiB_2, by averaging original data over 8 partitions.

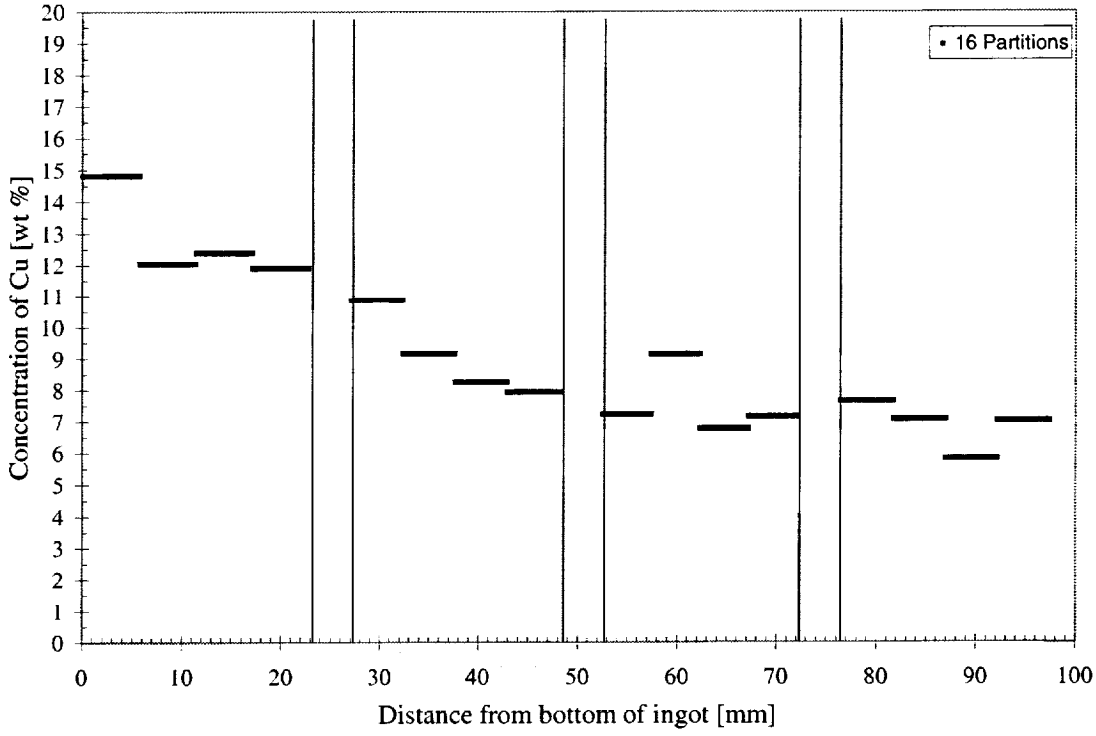

Figure 6.7 Plot showing compositional variation of experiment E6, top cooled Al-10 wt. pct. Cu alloy with 0.045 wt. pct. TiB_2, by averaging the original data into 16 partitions.

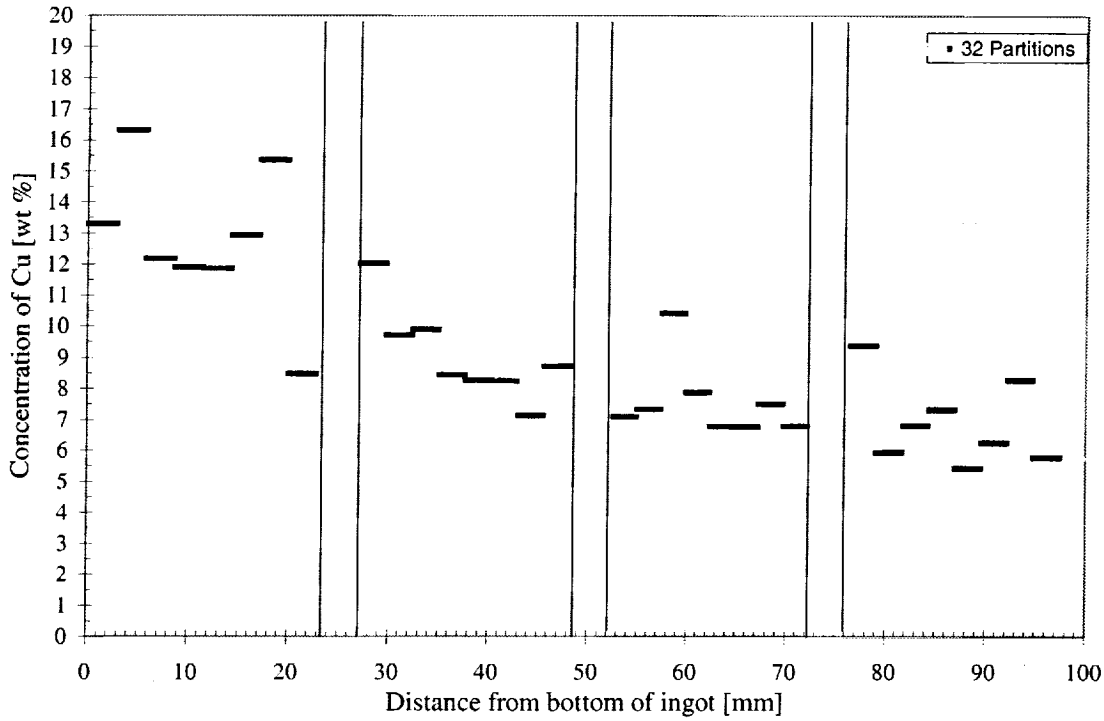

Figure 6.8 Plot showing compositional variation of experiment E6, top cooled Al-10 wt. pct. Cu alloy with 0.045 wt. pct. TiB_2, by averaging the original data into 32 partitions.

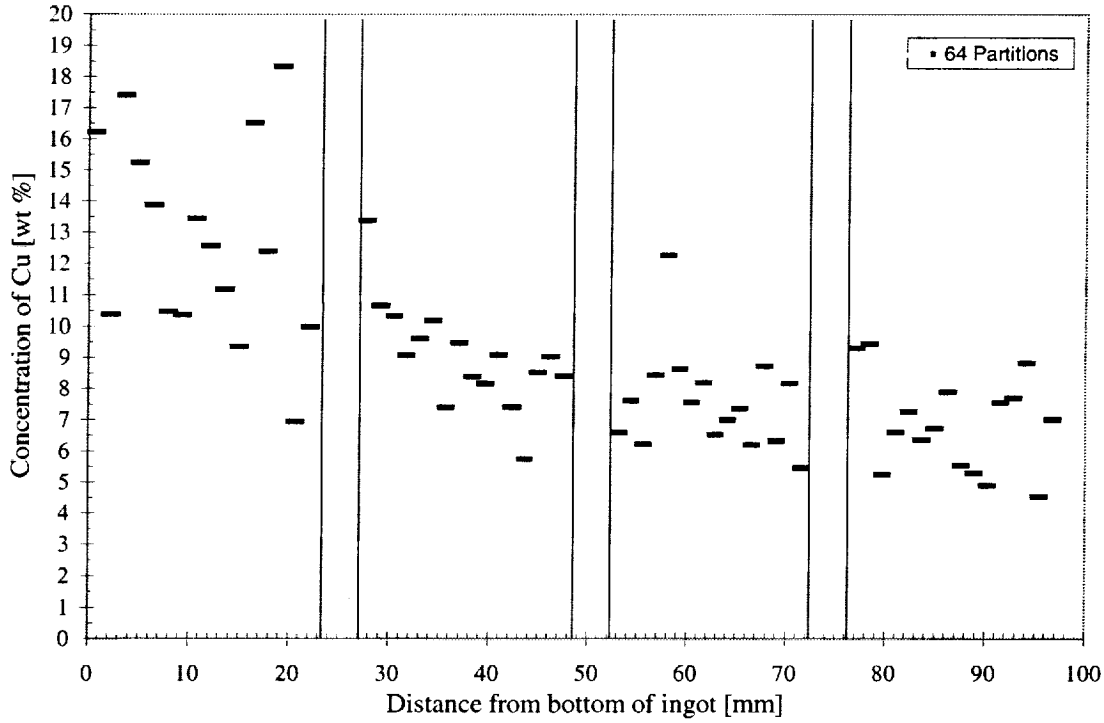

Figure 6.9 Plot showing compositional variation of experiment E6, top cooled Al-10 wt. pct. Cu alloy with 0.045 wt. pct. TiB_2, by averaging the original data into 64 partitions.

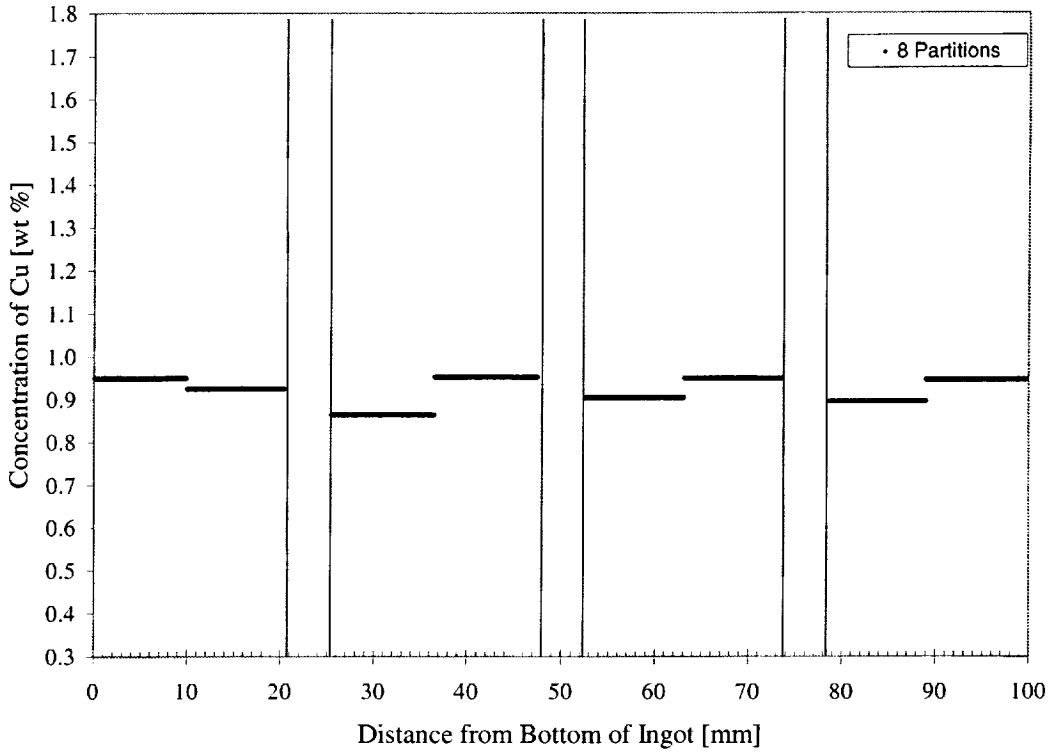

Figure 6.10 Plot showing compositional variation of experiment E8, top cooled Al-1 wt. pct. Cu with 0.45 wt. pct. TiB_2, by averaging original data into 8 partitions.

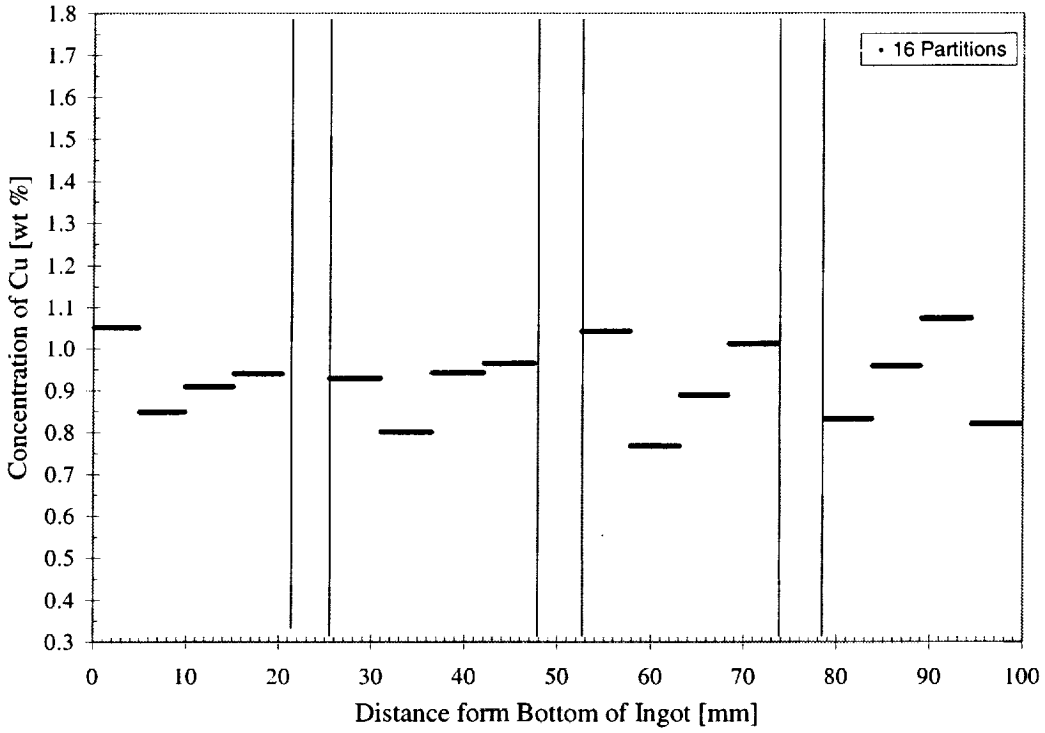

Figure 6.11 Figure showing compositional variation of experiment E8, top cooled Al-1 wt. Pct. Cu with 0.45 wt. Pct. TiB_2, by averaging original data into 16 partitions.

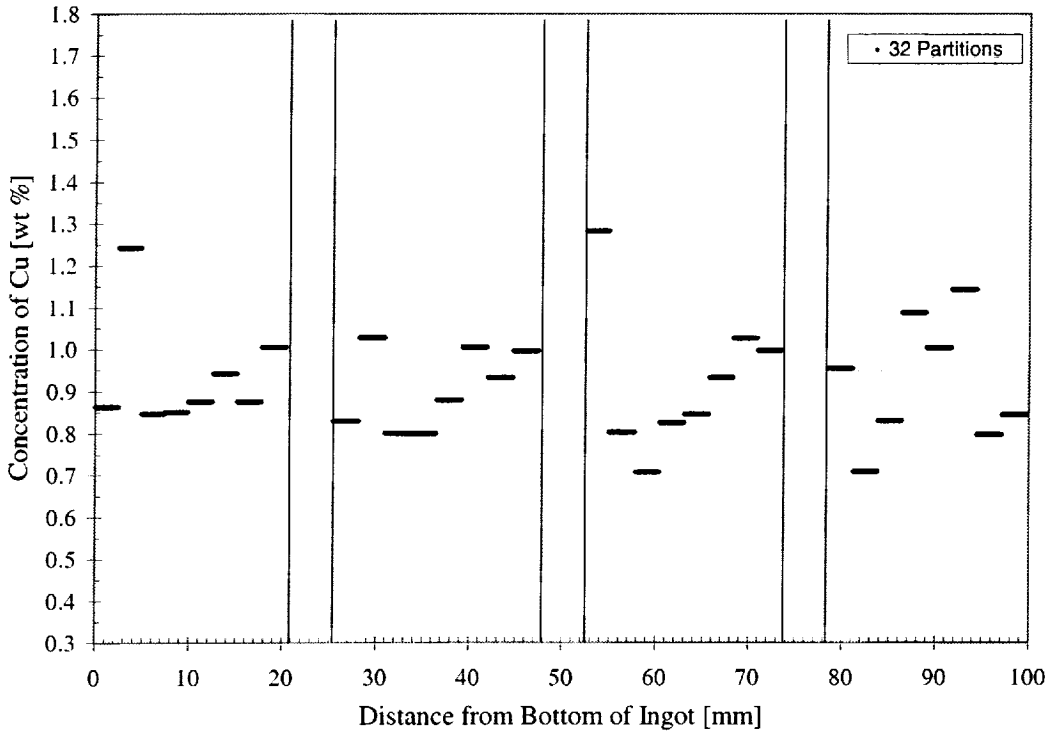

Figure 6.12 Figure showing compositional variation of experiment E8, top cooled Al-1 wt. Pct. Cu with 0.45 wt. Pct. TiB_2, by averaging original data into 32 partitions.

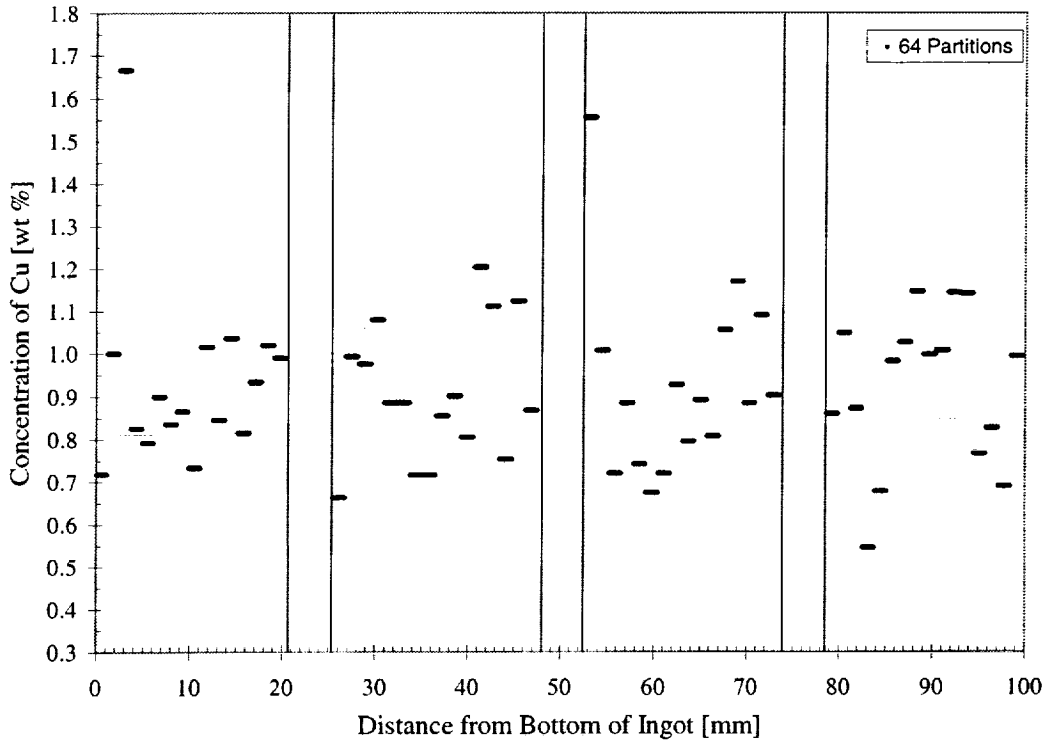

Figure 6.13 Figure showing compositional variation of experiment E8, top cooled Al-1 wt. Pct. Cu with 0.45 wt. Pct. TiB_2, by averaging original data into 64 partitions.

CHAPTER 7

NUMERICAL SIMULATION WORK

7.1 Introduction

Preliminary simulation work was done upon completion of the solidification experiments. The purpose of these simulations was to define all of the boundary conditions in preparation of a more detailed analysis and to evaluate property values for the Al-Cu alloy system. The one-dimensional simulations have the same boundary conditions as what might be used in a two-dimensional simulation. This is due to the adiabatic condition imposed on the side walls of the crucible. Only two boundary conditions need to be specified. The top boundary condition is set by the thermocouple placed near the top of the ingot in the melt leaving only the bottom boundary condition to be determined. This bottom boundary condition is the main focus of these simulations since it is located in the crucible wall and not the melt.

7.2 Governing Equations

The modeling approach used for the preliminary model is a rather simplistic one-dimensional formulation that solves for the temperature distribution in the ingot using a differential control volume and the conservation of energy principal. On a rate basis, the general form of the conservation of energy requirement is:

$$\dot{E}_{in} + \dot{E}_g - \dot{E}_{out} = \dot{E}_{st} \tag{7.1}$$

The one-dimensional model assumes heat transfer by conduction only, ignoring convection and movement of solid. With this simplification, the conservation of energy equation comes to the form commonly referred to as the heat diffusion equation. The heat diffusion for one dimension is shown in equation 7.2.

$$\frac{\partial}{\partial x}\left(k\frac{\partial T}{\partial x}\right) + \dot{q} = \rho c_p \frac{\partial T}{\partial t} \tag{7.2}$$

The first term on the left in equation 7.2 is the net conduction heat flux into the control volume. The second term corresponds to the volumetric rate of thermal energy generation. Both of these terms must equal the rate of change of thermal energy stored within the control volume. In order to solve this differential equation it was reduced to an approximate algebraic equation by using an explicit central finite-difference approach. The second order conduction term is approximated as shown in equation 7.3 with the temperature gradient terms evaluated as in equations 7.4 and 7.5.

$$\left.\frac{\partial^2 T}{\partial x^2}\right|_i = \frac{\left.\partial T/\partial x\right|_{i+\frac{1}{2}} - \left.\partial T/\partial x\right|_{i-\frac{1}{2}}}{\Delta x} \tag{7.3}$$

$$\left.\frac{\partial T}{\partial x}\right|_{i+\frac{1}{2}} \cong \frac{T_{i+1}^{p} - T_{i}^{p}}{\Delta x} \tag{7.4}$$

$$\left.\frac{\partial T}{\partial x}\right|_{i-\frac{1}{2}} \cong \frac{T_{i}^{p} - T_{i-1}^{p}}{\Delta x} \tag{7.5}$$

Substituting equations 7.4 and 7.5 into equation 7.3 results in equation 7.6.

$$\left.\frac{\partial^2 T}{\partial x^2}\right|_{i} \cong \frac{T_{i+1}^{p} + T_{i-1}^{p} - 2T_{i}^{p}}{(\Delta x)^2} \tag{7.6}$$

Substituting equation 7.6 into the energy equation of equation 7.2 and solving for the temperature at node i and current time, p+1 results in the following:

$$T_i^{p+1} = Fo\left(T_{i+1}^{P} + T_{i-1}^{p}\right) + \left(1 - 2Fo\right)T_i^{p} - \Delta h \rho_{eu} \frac{\left(\varepsilon_{li}^{p} - \varepsilon_{li}^{p-1}\right)}{dt} \tag{7.7}$$

where the Fourier number, Fo, and the energy generation term, $\dot{q}$, are evaluated as follows.

$$Fo = \frac{\alpha \Delta t}{\Delta x^2} \tag{7.8}$$

$$\dot{q} = -\Delta h \rho_{eu} \frac{\left(\varepsilon_{li}^{p} - \varepsilon_{li}^{p-1}\right)}{dt} \tag{7.9}$$

Equation 7.9 is the latent heat release written in a finite difference form. The term is negative because the equation is written in terms of the liquid fraction. This term adds to the heat diffusion equation as the alloy solidifies. It should be noted that this term is a lagging term, in other words it is evaluated using the liquid fraction from the previous two time steps. The latent heat term, Δh, in equation 7.9 needs to be evaluated at a reference temperature. The eutectic temperature is the temperature selected for this reference; therefore, the density used in this equation is the eutectic density.

In order to determine the liquid fraction the temperature distribution is evaluated at the end of each time step and updated according to the Scheil equation. Equation 7.10

shows the Scheil equation which relates the concentration of the alloy to the solid and liquid fractions.

$$\frac{C_l}{C_o} = \frac{1}{(1-\varepsilon_s)^{1-\kappa}} = \frac{1}{\varepsilon_l^{1-\kappa}} \tag{7.10}$$

In order to simplify the mathematical treatment of solidification, it is generally assumed that the liquidus and solidus lines of the phase diagram are straight, and therefore that the distribution coefficient, κ, and the liquidus slope, m, are constant. With this assumption relationship can be derived from the phase diagram to write the Scheil equation in terms of temperature as shown in Figure 7.11.

$$\varepsilon_{l\ i}^{p} = \left(\frac{T_m^{p+1} - T_{liq}^{p+1}}{T_m^{p+1} - T_i^{p+1}} \right)^{\frac{1}{1-\kappa}} \tag{7.11}$$

The form of the Scheil equation shown in equation 7.11 is used to update the liquid fraction while the temperature is between the liquidus temperature and the eutectic temperature.

7.3 Boundary Conditions

After the governing equations were derived the number of control volumes used for the simulations was set to 85 which corresponds to a control volume size of 1 mm. The size of the control volume was arbitrarily set to 1mm for convenience and the simulations were then tested for grid independence. The boundary conditions for the simulation were also determined. The boundary condition for the top control volume was fixed to the temperature profile from the top thermocouple. At the bottom control volume the bottom thermocouple could not be used directly. This was due to the fact that the bottom thermocouple was not in the melt but in the crucible wall. To compensate for the thermal resistance between the thermocouple and the bottom of the melt, a boundary condition similar to a convection surface condition was used. The boundary condition was written in the form shown in equation 7.12 where the heat transfer coefficient, h, equals the inverse of the thermal resistance between the thermocouple and the bottom control volume, T_4 is the temperature of the bottom thermocouple located in the crucible wall, and T_i the temperature of the bottom control volume.

$$-k \left. \frac{\partial T}{\partial x} \right|_{x=0} = h[T_4 - T_i] \tag{7.12}$$

For all of the simulations performed a heat transfer coefficient of 450 W/K was used. This value was obtained by a trial and error process, but can be justified by approximating the thermal resistance between the bottom thermocouple and the melt. There are two sources for thermal resistance. One source is due to the crucible itself while the other is from any air gap that forms due to solidification shrinkage. Since the thermal conductivity of the crucible is much higher than that of air the crucible resistance will be assumed to be negligible. The thermal conductivity of air in the temperature range of the experiments is approximately 0.06 W/m-K. For a heat transfer coefficient of

450 W/K to be justified an air gap of approximately 0.13 mm would need to be present (h = k/L). An air gap of this size is reasonable.

7.4 Property Values

The material properties that need to be evaluated for the simulations include the thermal conductivity, the specific heat, and the liquid and solid densities. The density values were evaluated as both a function of temperature and concentration for each control volume by using empirical curves (Ganesan and Poirier, 1987) from measurements of pure aluminum and seven binary Al-Cu alloys. The liquid density was evaluated by taking the inverse of the following relation, Equation 7.13, for the specific volume.

$$v_L = 0.3970 - 4.5322x10^{-3} C_L + 4.0924x10^{-5} T + 1.1078x10^{-6} C_L T + 2.7475x10^{-5} C_L^2 \quad [cm^3/g] \qquad (7.13)$$

The solid density was evaluated using the following relations, Equations 7.14 and 7.15, based on the initial concentration of Cu:

$$\rho_s = 2.5593 + 9.5307x10^{-4} C_L \quad [g/cm^3] \qquad (7.14)$$

for C_o = 1 wt pct. Cu

$$\rho_s = 2.5689 + 1.8401x10^{-3} C_L \quad [g/cm^3] \qquad (7.15)$$

for C_o = 10 wt pct. Cu

The thermal conductivity and specific heat were evaluated as a mixture quantity based on the solid fraction in the control volume. Table 6 is a summary of the property values used. Also included in this table are other constants required for the simulation such as the latent heat, and density of the eutectic, as well as other thermophysical properties that might be needed in other more detailed modeling efforts.

For the inclusion of equiaxed grain settling and advection, the drag coefficient for an equiaxed dendrite, C_D, is needed and is given by

$$C_D = \frac{24}{C_{ed}\,\mathrm{Re}_e}$$

where C_{ed} is the settling velocity ratio of the dendrite to the volume-equivalent sphere of the envelope around the dendrite, which has been emperically determined, by Zakhem et al., 1993, de Groh et al., 1993, and Ahuja et al., 1992, to be

$$C_{ed} = 1.26\log\left(\frac{\psi}{0.163}\right) \times \frac{2\beta^2 + 3\left(1 - \tanh(\beta)/\beta\right)}{2\beta^2\left(1 - \tanh(\beta)/\beta\right)}$$

which is equation [4] in de Groh et al., 1993. Briefly: Re_e is Reynolds number equal to $\rho_l U d_e/u$ where ρ_l is melt density, U is terminal velocity, d_e is the envelop volume-equivalent sphere diameter, and u is melt viscosity; ψ is dendrite envelope sphericity equal to $\pi d_e/A_e$, where d_e equals $(6V_e/\pi)^{1/3}$, V_e and A_e are the volume and surface area of

an envelope around the dendrite which can be estimated using equations [9] and [10] in de Groh et al., 1993; β is the normalized radius given by $d_e/2K^{1/2}$ where K is permeability of the interdendritic structure which may be estimated using the Kozeny-Carman equation $K= (1-\varepsilon)^3/5(A_p/V_e)^2$ taken from Scheidegger, 1974, ε is the solid fraction of the dendrite equal to V_p/V_e, and where V_p and A_p are the volume and surface area of the dendrite which can be estimated using a program available from de Groh (de Groh et al., 1993b). An extensive treatment of dendrite drag, covering a wide range of solid fractions, is presented by Wang et al., 1995; these drag models were validated experimentally by Nielsen et al., 1999. The very different growth velocities achieved by settling equiaxed grains were examined by Ramani and Beckermann, 1997.

Table 6. Property Values for the Al-Cu. The volumetric expansion coefficient is approximately three times the linear expansion coefficient (Van Vlack, 1973). β_T is thermal expansion coefficient, $(1/\rho_l)(d\rho_l/dT)$. β_S is solutal expansion coefficient, $(1/\rho_l)(d\rho_l/dC_l)$; C_l must be in units of *volume* fraction Cu. (Beer, 1972; Metals Handbook, 1985; Touloukian et al., 1970)

Property Name, Units	Initial Melt Composition Al-1 wt. pct. Cu	Initial Melt Composition Al-10 wt. pct. Cu
Liquid density, @T_m, g/cm^3	2.397	2.54
Solid linear expansion, cm/cm-K	23.5×10^{-6}	23.3×10^{-6}
β_T, K^{-1}	-114×10^{-6}	-113×10^{-6}
β_S, (volume fraction Cu)$^{-1}$	0.0236	0.0236
Liquid specific heat, J/kg-K	1080.0	1020.0
Solid specific heat, J/kg-K	1140.0	980.0
Liquid thermal conductivity, W/m-K	90.0	82.0
Solid thermal conductivity, W/m-K	180	160
Eutectic density, kg/m^3	3409.0	
Eutectic temperature, K	821.2	
Equilibrium partition coefficient of Cu in Al	0.173	
Liquidus slope, K/wt. pct.	-3.37	
Melting temperature of pure Al, K	933.6	
Latent heat, kJ/kg	395.0	

7.5 Results and Discussion

Before the simulations were performed the transient conduction portion of the code was validated by comparison to an analytical solution of transient conduction in a semi-infinite medium with a surface convection boundary condition. The closed-form solution can be seen in equation 7.16. The initial temperature values of the control volumes were

set to 958 K and thermal properties were set to arbitrary values for the test. The result of the analytical solution and numerical code at the bottom interior surface (x = 0) are shown in Figure 7.1.

$$\frac{T(x,t)-T_i}{T_4-T_i} = erfc\left(\frac{x}{2\sqrt{\alpha t}}\right)-\left[\exp\left(\frac{hx}{k}+\frac{h^2\alpha t}{k^2}\right)\right]\left[erfc\left(\frac{x}{2\sqrt{\alpha t}}+\frac{h\sqrt{\alpha t}}{k}\right)\right] \qquad (7.16)$$

Following validation of the code, the bottom cooled experiments were simulated. The results of the bottom cooled experiments are shown in Figures 7.2 through 7.11. The results include the comparison of measured and predicted temperature profiles and a three-dimensional plot of the solid fraction evolution for each experiment. In the following figures which show the simulated temperature results, Sim1 is the an input boundary condition equal to the temperature measured by the T1 thermocouple (see Figures 2.2 and 2.3), Sim2 is the simulated temperature at the T2 location, Sim3 is the simulated temperature at the T3 location, and Sim4 is an input boundary condition equal to the calculated temperature in the liquid at the bottom of the crucible, T_i.

Only the bottom cooled experiments were used for this initial numerical study. The reason is that in order to evaluate property values and obtain a heat transfer coefficient for the experiments the thermal instabilities, which the model could not predict, needed to be kept to a minimum. Since the top cooled experiments were thermally and solutally unstable they made bad candidates for the purpose of these simulations.

The results obtained for these simulations for the most part agree well with experiments. The most sensitive quantity in these simulations was the heat transfer coefficient, which had by far the most influence on the results. The value selected for these simulations will be a good place to start in future simulation work with more complex models, but further refinement will most likely be needed. The results of the simulations were not sensitive to thermal conductivity, density, and specific heat.

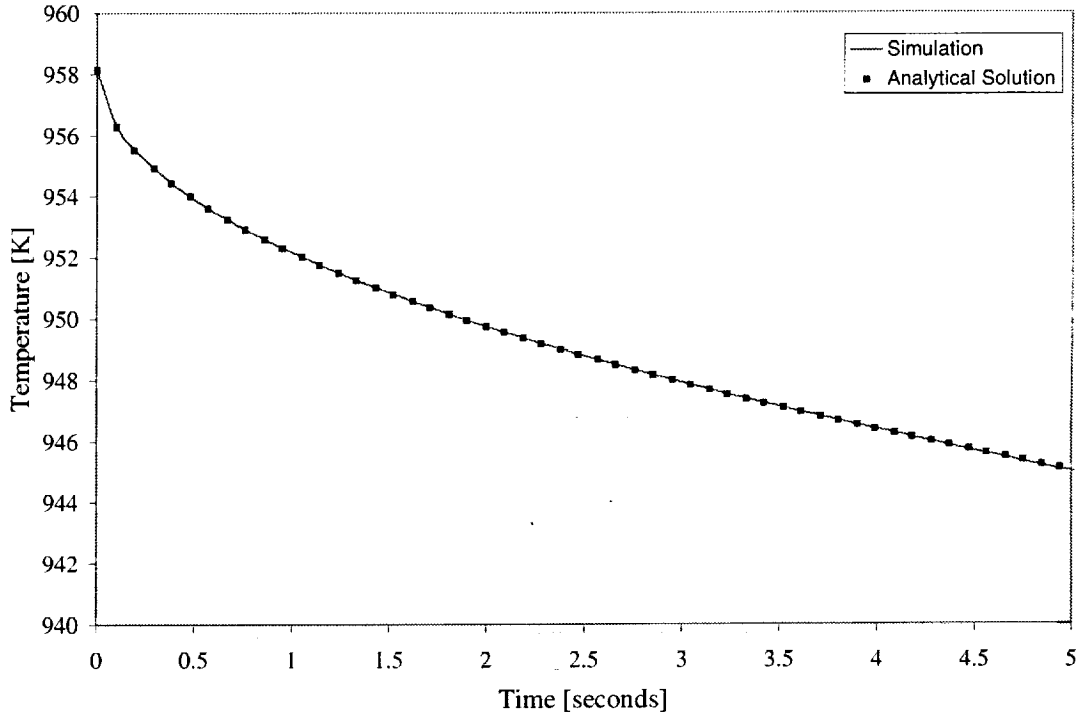

Figure 7.1 Validation of one-dimensional simulation code by comparison to analytical solution of transient conduction in a semi-infinite medium. Results are compared at the bottom interior surface of the ingot (x = 0).

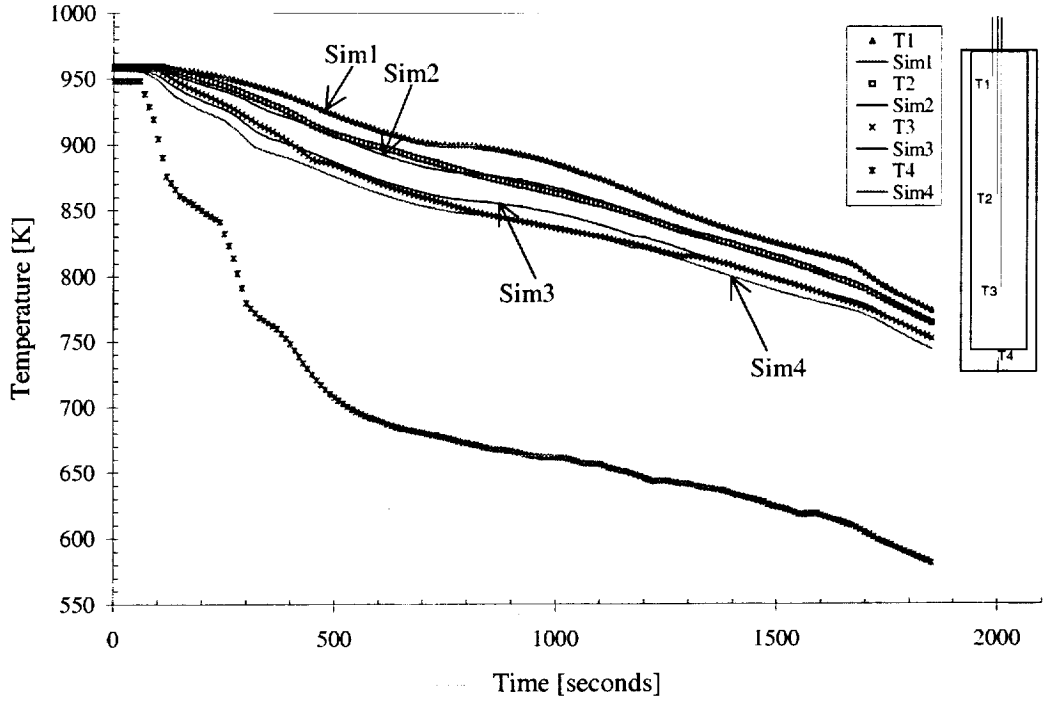

Figure 7.2 Plot of Thermocouple readings versus simulation for Experiment E1, bottom cooled Al-10 wt. pct. Cu. Sim1is an input boundary condition equal to T1, Sim2 and Sim3 are simulated temperatures at T2 and T3 locations, Sim4 is a calculated input boundary condition based on T4.

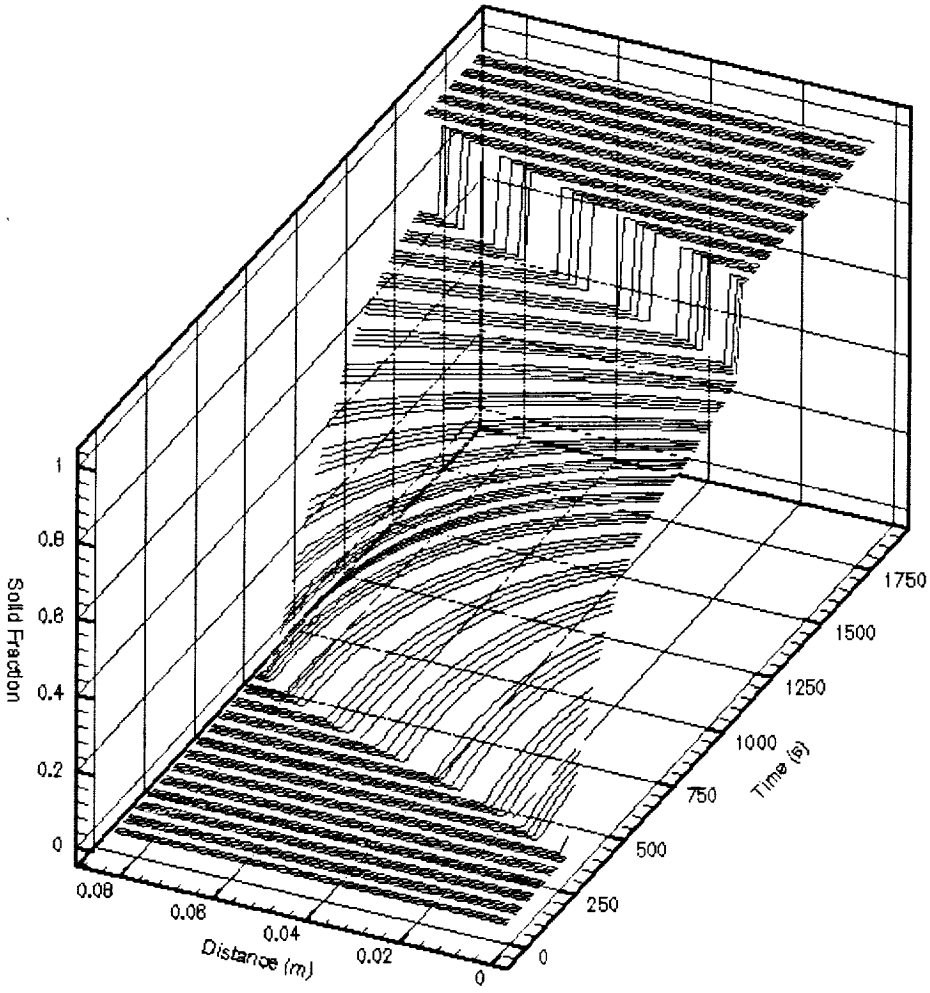

Figure 7.3 Simulation predicted solid fraction evolution for experiment E1, bottom cooled Al- 10 wt. pct. Cu.

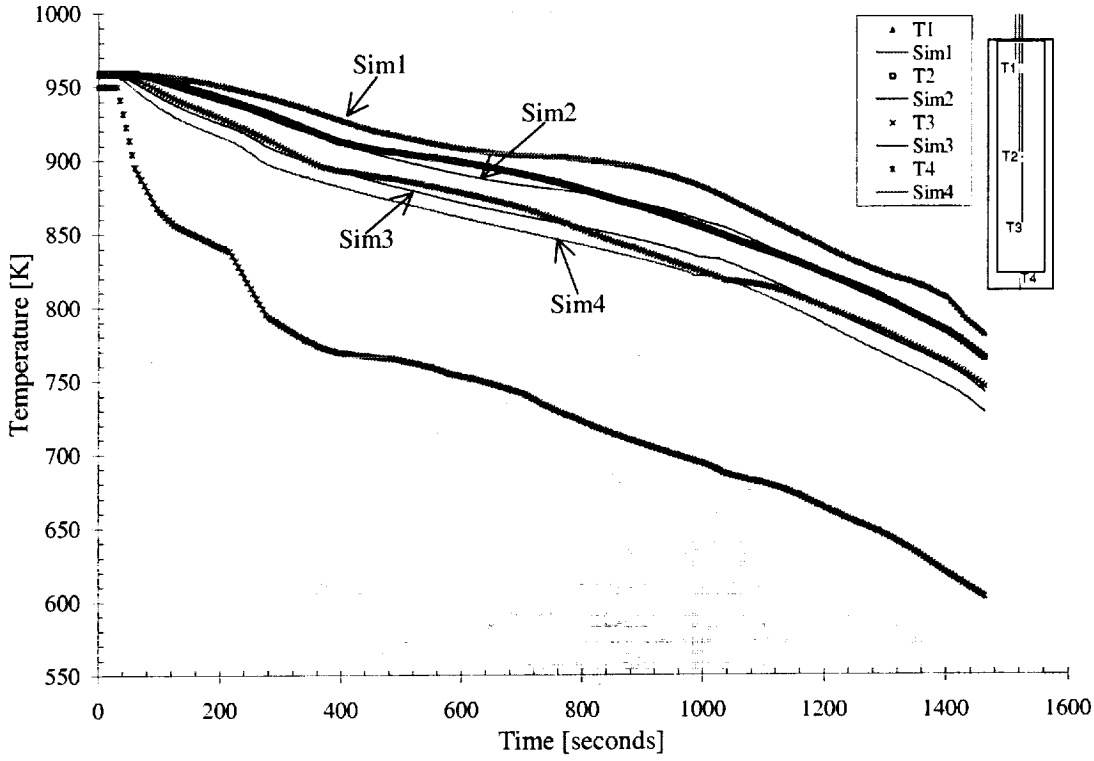

Figure 7.4 Plot of Thermocouple readings versus simulation for experiment E2, bottom cooled Al-10 wt. pct. Cu with 0.045 wt pct. TiB_2. Sim1 is an input boundary condition equal to T1, Sim2 and Sim3 are simulated temperatures at T2 and T3 locations, Sim4 is a calculated input boundary condition based on T4.

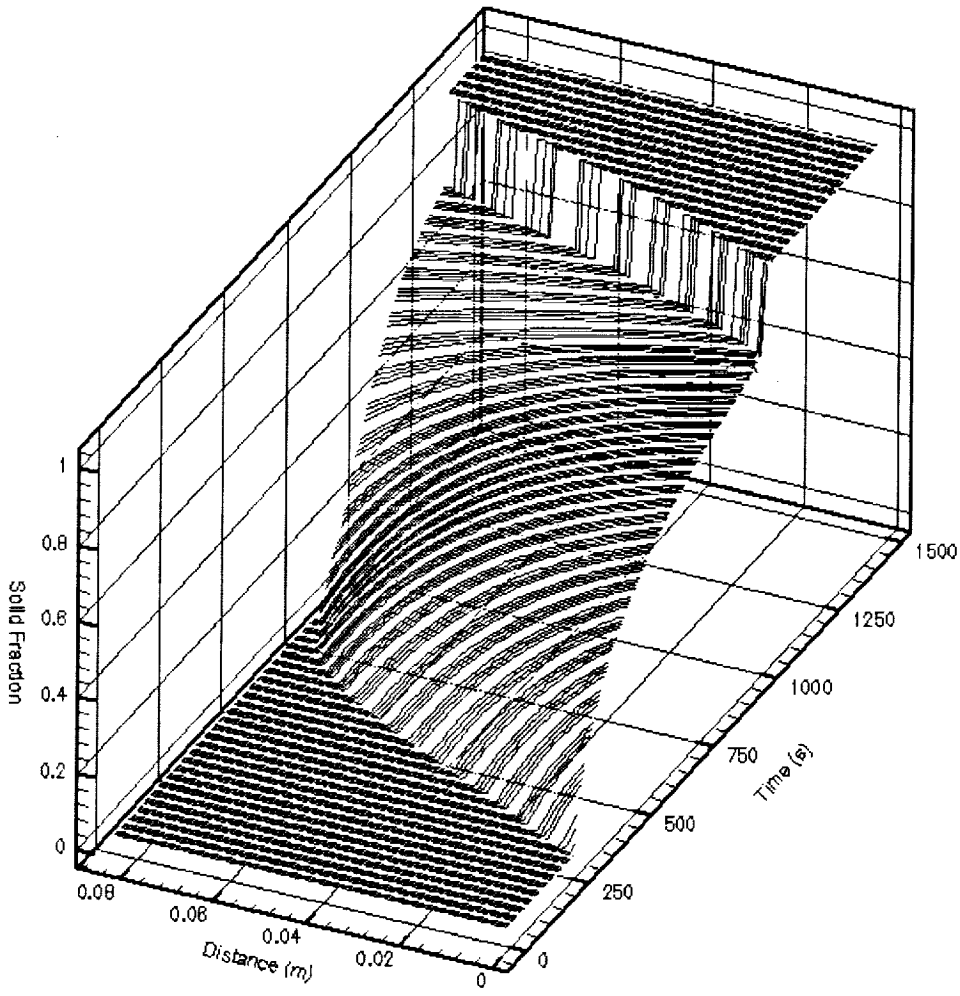

Figure 7.5 Simulation predicted solid fraction evolution for experiment E2, bottom cooled Al-10 wt. pct. Cu with 0.045 wt. pct. TiB_2.

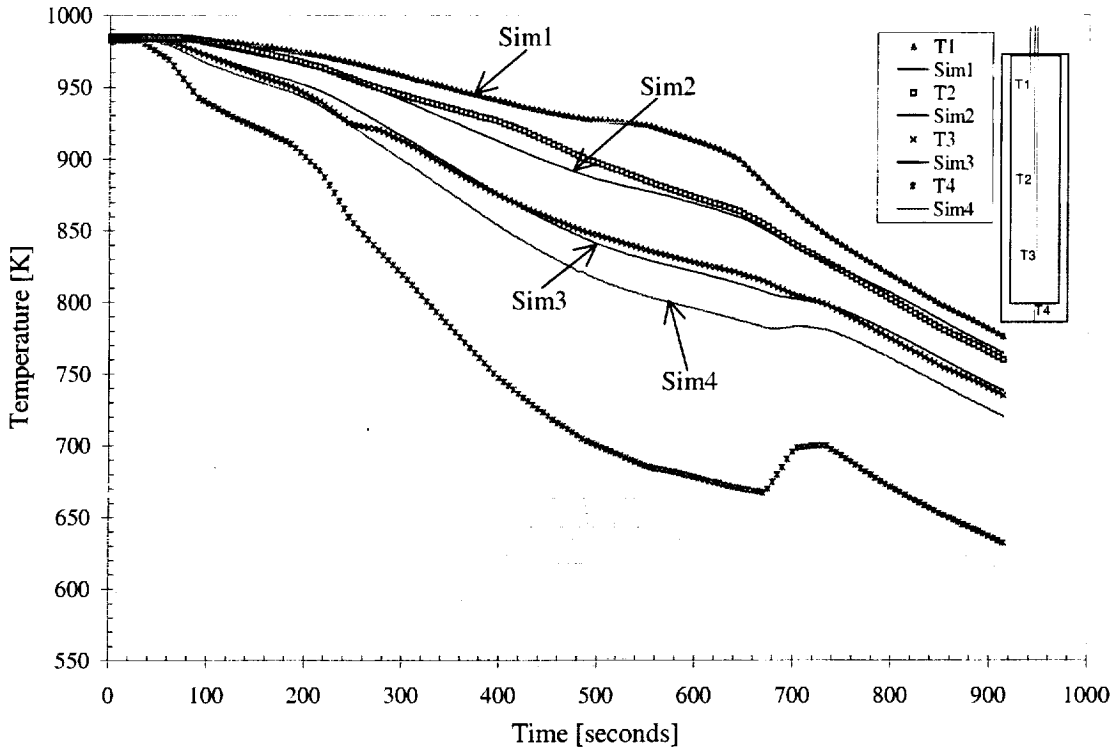

Figure 7.6 Plot of Thermocouple readings versus simulation for experiment E3, bottom cooled Al-1 wt. pct. Cu with 0.45 wt. pct. TiB_2. Sim1is an input boundary condition equal to T1, Sim2 and Sim3 are simulated temperatures at T2 and T3 locations, Sim4 is a calculated input boundary condition based on T4.

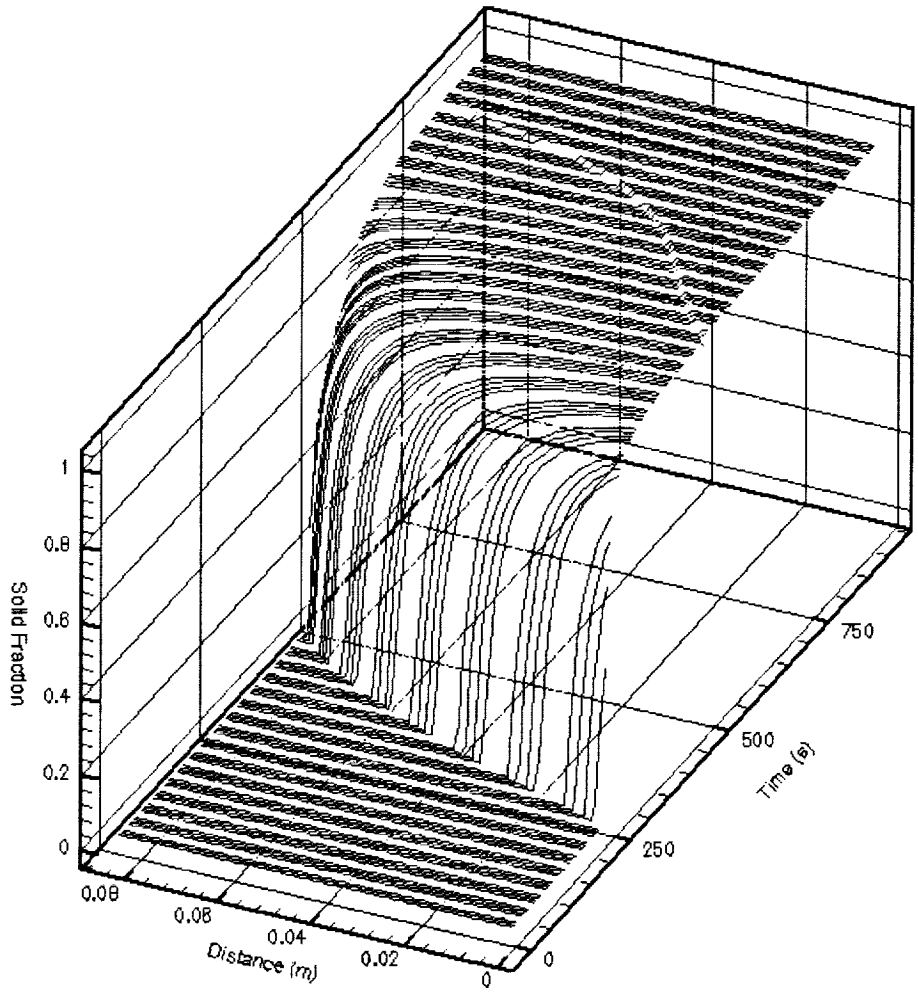

Figure 7.7 Simulation predicted solid fraction evolution for experiment E3, bottom cooled Al-1 wt. pct. Cu with 0.45 wt. pct. TiB_2.

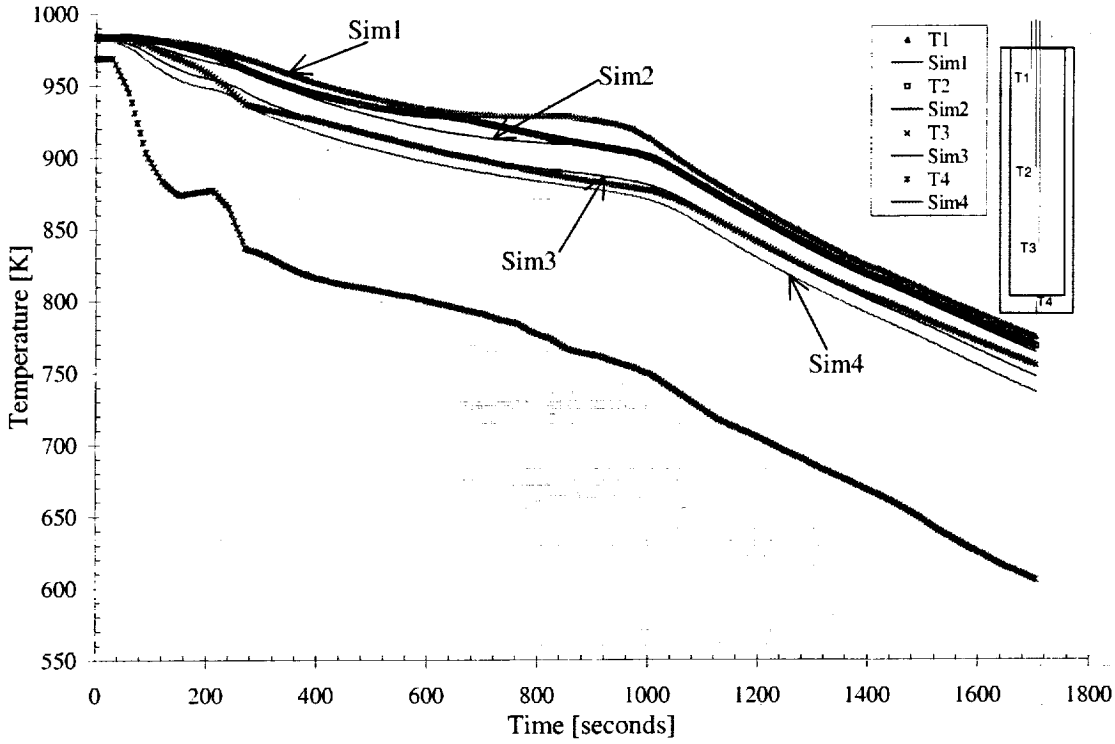

Figure 7.8 Plot of thermocouple readings versus simulation for experiment E4, bottom cooled Al-1 wt. pct. Cu. Sim1is an input boundary condition equal to T1, Sim2 and Sim3 are simulated temperatures at T2 and T3 locations, Sim4 is a calculated input boundary condition based on T4.

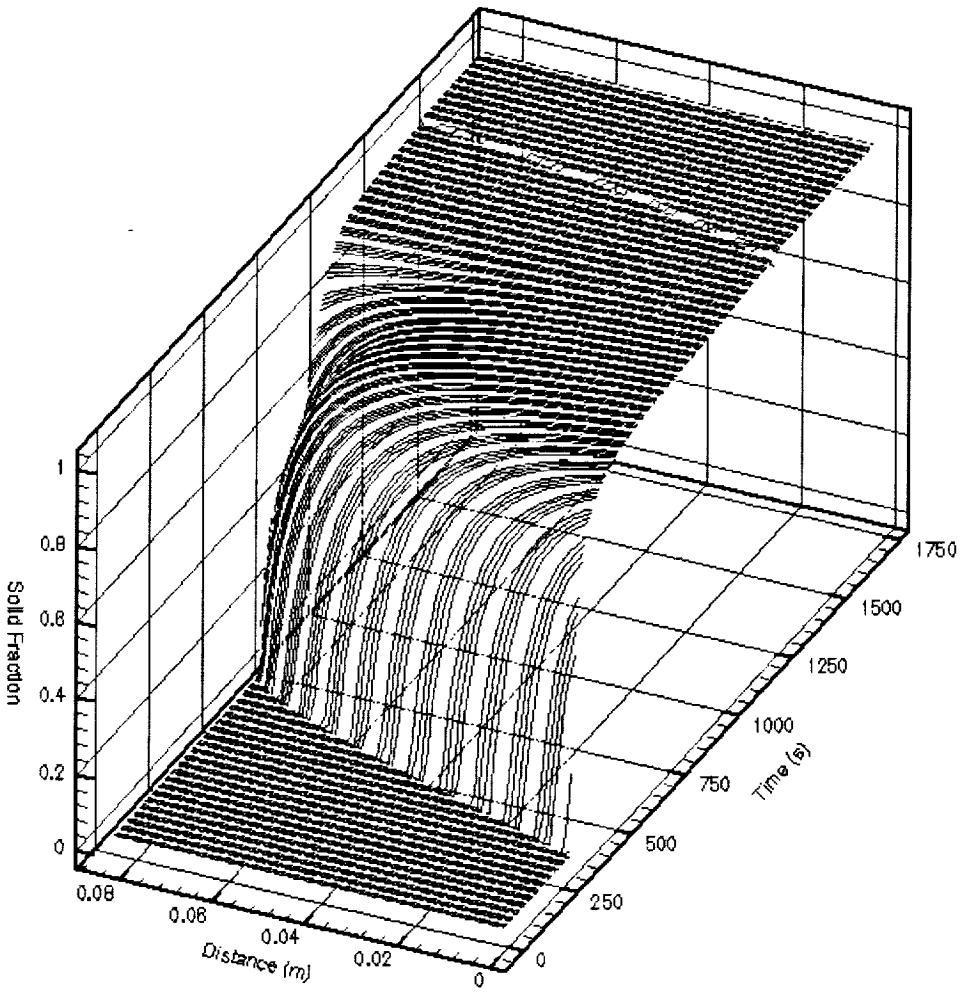

Figure 7.9 Simulation predicted solid fraction evolution for experiment E4, bottom cooled Al-1 wt. pct. Cu.

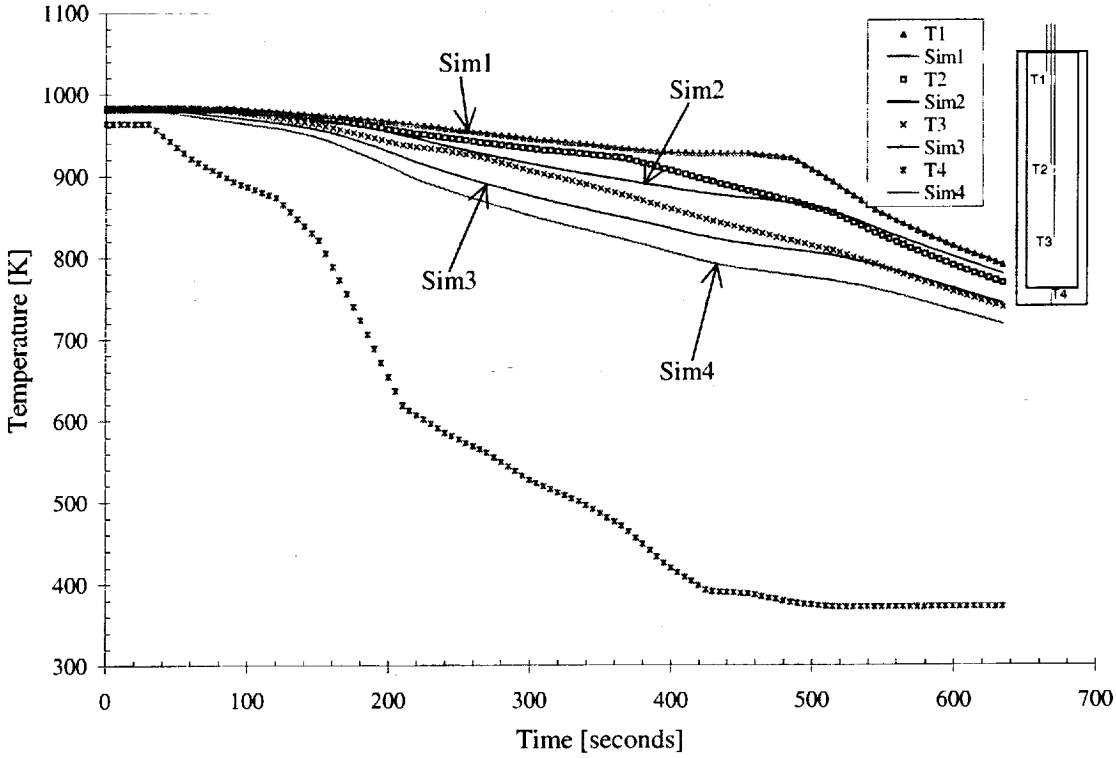

Figure 7.10 Plot of thermocouple readings versus simulation for experiment E5, bottom cooled Al-1 wt. pct. Cu with 0.67 wt. pct. TiB_2. Sim1is an input boundary condition equal to T1, Sim2 and Sim3 are simulated temperatures at T2 and T3 locations, Sim4 is a calculated input boundary condition based on T4.

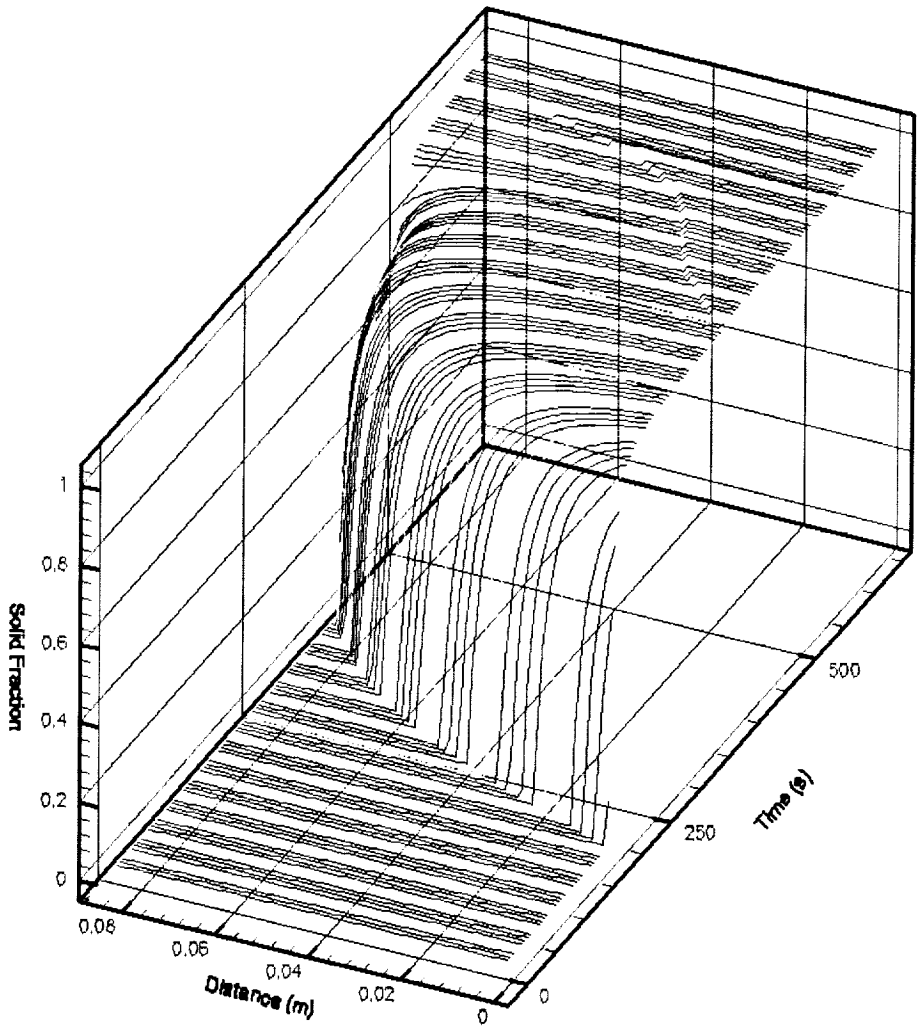

Figure 7.11 Simulation predicted solid fraction evolution for experiment E5, bottom cooled Al-1 wt. pct. Cu with 0.67 wt. pct. TiB_2.

CHAPTER 8

CONCLUSIONS

The objectives of this research were to: 1) Experimentally study the effects of solid transport and thermosolutal convection on macrosegregation and grain size distribution patterns; 2) Provide a complete set of experimental data, controlled thermal boundary conditions, temperature data, and segregation and grain size data, to validate numerical models such as the one developed by Beckermann and Wang (1995).

These objectives were met by performing nine directional solidification experiments using Al-Cu alloys. The resulting macrosegregation and grain size variations were studied. Concentration profiles along the center-line were determined for two top cooled experiments, one for Al-1wt. pct. Cu and one for Al-10 wt. pct. Cu. A progression from solute poor at the top to solute rich at the bottom, or end of solidification, was observed for the top cooled Al-10 wt. pct. Cu alloy and is believed to be due to more aggressive sinking of the more dense interdendritic liquid with some tempering of the segregation due to advection of solid grains. For the top cooled Al-1 wt. pct. Cu alloy, a relatively flat concentration profile was observed and is believed to be due to the contributions of thermosolutal convection transporting solute rich liquid downwards and the solute poor solid grains sinking more extensively as compared to the 10wt. pct. Cu ingot.

Of the nine solidification experiments performed a variety of grain size distributions were obtained and analyzed. It was evident that alloys with a higher copper content were more inclined to have equiaxed grains. This is in agreement with work done by Griffiths, Xiao, and McCartney (1996) during their study of the influence of bulk liquid natural convection on the formation of the equiaxed regions in Al-Cu and Al-Si alloys. This effect was apparent due to the difficulty of obtaining equiaxed grains in the Al-1 wt. pct. Cu. Alloy. Even with the additions of grain refiner none of the solutally and thermally stable bottom cooled experiments exhibited an equiaxed grain structure. Only in the top cooled experiments, which were thermally and solutally unstable, were equiaxed grain structure achievable. Equiaxed growth in the 1wt. pct. Cu top cooled experiments may have been assisted by the lower cooling rate imposed (as compared to the bottom cooled 1wt. pct. Cu experiments) and in particular, by exacerbation of settling, advection, and fragmentation of dendrites caused by the more aggressive thermosolutal convection.

The grain size in the top cooled 10wt. pct. Cu ingots was about 3 times larger than in the bottom cooled 10wt. pct. Cu ingots. We believe this difference is due to advection of nucleated grains from cooler regions nearer the top of the top cooled ingots to warmer areas nearer the bottom of the ingots where some melt.

In addition to the observation on macrosegregation and grain size distribution a complete set of experimental data was obtained for use in numerical simulation work. Preliminary simulation work was performed to refine boundary conditions and assess property values for the Al-Cu alloy. The preliminary simulation work successfully narrowed down the property data of the two alloy compositions and provided a starting point for the thermal boundary conditions to be used in future modeling.

APPENDIX A

ALUMINUM-COPPER DENSITY CALCULATIONS

A.1 Introduction

It was intended to have two case studies for the Aluminum-copper experiments. One case study was to have dendrites that would sink at the start of solidification, the initial solid having a higher density than the surrounding liquid. The other case study was to have nearly equal buoyancy of the solid and liquid states at the start of solidification.

A.2 Calculations for Al-10 wt pct. Cu

From Ganesan and Poirier, 1987, the densities of the liquid and solid for Al-10 wt. pct. Cu were calculated as follows:
The density of the solid,

$$\rho_s = 2.5581 + 2.1743\text{E}-3 C_L + 6.0443\text{E}-5 C_L^2$$

The density of the bulk liquid,

$$\rho_L = 2.3585 + 2.1685\text{E}-2 C_L + 7.2914\text{E}-5 C_L^2 - 7.2351\text{E}-7 C_L^3$$

where C_L = Composition of the interdendritic liquid, wt % Cu, equation valid for $C_L \leq$ 32.7 wt % Cu.
For Al-10 wt % Cu Alloy,

$$\rho_s = 2.5581 + 2.1743\text{E}-3(10) + 6.0443\text{E}-5(10)^2 = 2.58 \frac{g}{cm^3}$$

$$\rho_L = 2.3585 + 2.1685\text{E}-2(10) + 7.2914\text{E}-5(10)^2 - 7.2351\text{E}-7(10)^3 = 2.58 \frac{g}{cm^3}$$

Since $\rho_S \cong \rho_L$ Al-10 wt % Cu has a nearly equal buoyancy of the liquid and solid states at the start of solidification.

A.3 Calculations for Al-1 wt. pct. Cu

The densities of the liquid and solid for Al-1 wt. pct. Cu were calculated as follows:
The density of the solid,

$$\rho_s = 2.5581 + 2.1743\text{E}-3 C_L + 6.0443\text{E}-5 C_L^2$$

The density of the bulk liquid,

$$\rho_L = 2.3585 + 2.1685\text{E}-2 C_L + 7.2914\text{E}-5 C_L^2 - 7.2351\text{E}-7 C_L^3$$

where C_L = Composition of the interdendritic liquid, wt % Cu, equation valid for $C_L \leq$ 32.7 wt % Cu.
For Al-1 wt % Cu Alloy,

$$\rho_s = 2.5581 + 2.1743\text{E}-3(1) + 6.0443\text{E}-5(1)^2 = 2.56 \frac{g}{cm^3}$$

$$\rho_L = 2.3585 + 2.1685\text{E}-2(1) + 7.2914\text{E}-5(1)^2 - 7.2351\text{E}-7(1)^3 = 2.38 \frac{g}{cm^3}$$

since $\rho_S > \rho_L$ Al- 1 wt % Cu will form grains that will tend to sink.

APPENDIX B

GRAIN REFINER ADDITIONS

B.1 Introduction

The refined samples of Al-1 wt. pct. Cu and Al-10 wt. pct. Cu consisted of 0.45 and 0.045 wt. pct. TiB_2, respectively. The amount of TiB_2 added is based on the study by McCartney and Ahmady (1994) according to the phase diagram parameter β. Later, additional experiments were performed with additional refiner, 0.67 wt. pct. for the 1 wt. pct. Cu alloy and 0.067 wt. pct. for the 10 wt. pct. aluminum alloy. The additional refiner was needed to further reduce the grain size in the resulting casting.

B.2 Calculations

If solute interactions are neglected, β can be interpreted as being a term which determines dendrite tip undercooling in a multicomponent alloy (McCartney et al., 1980; Desnain et al., 1990) because it is defined as Equation B.1.

$$\beta = \sum_{i=1}^{n} -m_i(1-k_i)C_{oi} \qquad \text{(B.1)}$$

C_{oi} = the weight percent of element i in the base alloy.
k_i = the equilibrium partition coefficient of the Al-Cu phase diagram containing solute i.
m_i = the liquidus slope of the Al-Cu phase diagram.

For the Al-Cu Alloy: $k = 0.14$, m_i = -2.6 K/wt. pct. (Source: Mondolfo, 1976).

The amount of grain refiner addition correlates well to β^{-1}. Table B1 shows the computed values and the corresponding wt. pct. and grams of grain refiner added to the experiments.

Table 7. Values of β and amount of TiB_2 added for the experiments.

Alloy	β (in K) for Base Alloy	wt. pct. TiB_2 (β^{-1})	TiB_2 added (grams)
Al-10 wt % Cu	22.360	.045	.0311
Al -1 wt % Cu	2.236	.45	.2916

APPENDIX C

TEMPERATURE MEASUREMENTS

This appendix includes the temperature measurements taken during Experiments 1 through 9, see Table 4. In all tables the first column is time in the units of minutes, the second column, TP, is the percent of 300 watts of power sent to the upper heater, the third column, BP, is the percent of 300 watts of power sent to the bottom heater. Columns 4, 5 and 6 (labeled T1, T2, and T3) are temperature readings in °C inside the ingot along its centerline near the top, middle and bottom, location details as indicated in Figures 2.3 and 2.4. Columns 7, 8, 9, and 10 (labeled T4, T5, T6, and T7) provide the temperature measurements in °C taken in the crucible wall at the bottom, and near the top, middle and lower portion of the ingot container as shown in Figures 2.2, and 2.3. The last two columns, T8 and T9, list temperatures measured in the furnace near the top and bottom respectively, see Figure 2.3. In order to shorten the data tables, the initial heating and much of the soak period have been omitted by deleting the first 100 min. to 150 min. of each batch of data. Thus the later portion of the soak and all of the solidification period are in the tables.

Table C1 Experiment 1, Al-10%Cu, no refiner, cooled from the bottom.

TIME	TP	BP	T1	T2	T3	T4	T5	T6	T7	T8	T9
100.40	22.00	25.90	685.07	685.94	685.04	674.76	690.13	690.20	694.65	705.39	714.75
100.90	22.00	26.00	685.02	685.87	685.02	674.71	690.06	690.13	694.58	705.41	714.84
101.40	22.00	26.10	684.97	685.87	684.92	674.74	690.08	690.13	694.60	705.65	714.96
101.90	22.10	26.10	684.95	685.85	684.90	674.71	690.01	690.06	694.58	705.77	715.13
102.40	22.10	26.10	684.95	685.83	684.95	674.74	689.99	690.03	694.58	705.92	715.32
102.90	22.20	26.20	684.92	685.85	684.92	674.71	690.01	690.10	694.62	706.03	715.49
103.40	22.20	26.20	684.90	685.92	684.92	674.69	690.10	690.08	694.70	706.18	715.58
103.90	22.20	26.10	684.90	685.83	684.90	674.76	690.18	690.15	694.67	706.23	715.65
104.40	22.10	26.10	684.92	685.87	684.99	674.79	690.08	690.08	694.70	706.39	715.80
105.00	22.20	26.10	684.92	685.90	684.95	674.86	690.20	690.15	694.74	706.58	715.89
105.50	22.10	26.00	684.97	685.90	684.97	674.81	690.22	690.18	694.86	706.73	716.06
106.00	22.10	26.00	685.02	685.92	685.02	674.95	690.22	690.22	694.89	706.77	716.18
106.50	1.50	3.50	685.07	685.97	684.90	645.65	690.20	690.25	694.84	706.65	715.03
107.00	25.60	52.80	684.85	685.04	679.58	602.58	689.84	690.13	691.56	700.96	701.08
107.50	29.70	65.10	684.02	682.07	673.32	588.09	688.77	688.65	686.44	698.91	693.36
108.00	0.00	42.10	682.57	678.84	668.50	581.47	688.49	686.63	683.31	702.94	694.05
108.50	16.20	58.70	680.81	675.81	664.05	574.61	687.18	684.64	679.39	698.77	686.28
109.00	29.80	62.20	678.68	672.58	659.17	568.17	684.73	682.24	675.19	693.67	681.12
109.50	4.00	51.30	676.26	669.07	654.06	540.55	682.95	679.51	671.37	695.48	678.99
110.00	6.30	59.70	673.70	665.23	648.01	506.83	680.98	676.64	666.47	692.98	671.96
110.50	25.30	59.20	670.71	660.99	641.58	495.35	677.99	673.29	660.88	686.28	666.20
111.10	11.50	58.60	667.37	656.38	635.56	487.85	675.26	669.52	655.67	685.09	660.69
111.60	0.20	62.30	663.88	651.58	628.98	477.33	672.41	665.54	649.90	684.09	653.87
112.10	15.60	62.20	660.07	646.35	621.37	462.30	668.81	661.35	643.50	677.28	647.42
112.60	16.30	63.60	655.81	640.59	614.32	449.19	664.83	656.52	636.77	672.94	640.05
113.10	1.20	76.30	651.44	636.18	612.96	437.90	661.09	651.79	632.50	671.51	633.16

113.60	6.40	76.20	647.49	633.16	609.24	430.40	656.99	648.01	629.83	666.02	630.49
114.10	14.20	68.60	643.83	630.23	605.07	424.00	652.86	644.58	626.91	660.14	629.05
114.60	3.30	70.80	640.43	627.43	600.84	419.30	649.31	641.42	623.30	657.99	624.79
115.10	2.70	74.30	637.26	624.83	596.98	416.13	646.12	638.44	619.48	654.79	620.31
115.60	10.60	67.80	634.29	622.19	593.45	411.97	642.72	635.71	616.04	649.45	618.00
116.10	9.40	69.60	631.53	619.04	590.16	409.46	639.58	633.16	612.61	646.31	614.14
116.60	0.90	70.40	629.12	615.86	586.97	407.52	637.05	630.92	609.19	644.70	610.49
117.20	6.10	66.60	627.21	612.70	583.91	405.10	634.53	628.82	606.06	640.85	607.99
117.70	14.30	67.90	626.39	609.69	580.93	402.50	632.47	626.51	602.86	637.14	604.41
118.20	11.30	68.60	626.53	606.67	578.01	399.89	632.24	624.17	599.76	637.10	601.19
118.70	4.40	66.20	625.59	603.85	575.31	397.57	632.38	621.91	596.98	638.23	598.72
119.20	6.20	64.60	624.01	601.24	573.01	395.15	631.93	619.77	594.32	636.96	596.25
119.70	11.60	64.30	622.24	598.75	570.97	394.13	630.56	617.46	591.88	634.45	593.74
120.20	5.50	64.00	620.19	596.39	568.90	392.52	628.82	615.24	589.67	633.49	591.43
120.70	0.50	63.10	617.81	594.14	566.88	389.51	626.74	612.98	587.41	631.93	589.29
121.20	8.10	63.00	615.08	591.81	564.84	388.75	623.98	610.53	585.23	627.78	587.06
121.70	9.50	62.30	612.04	589.43	562.85	388.46	620.99	607.87	583.02	624.38	584.83
122.20	0.90	62.00	608.67	586.90	560.90	387.04	618.23	605.14	580.76	622.85	582.55
122.70	2.10	61.30	604.98	584.22	558.88	383.93	615.34	602.34	578.44	619.77	580.25
123.30	6.90	61.10	601.05	581.30	556.81	383.26	611.85	599.36	575.97	615.31	577.80
123.80	3.60	60.20	597.03	578.32	554.63	379.39	608.51	596.30	573.51	612.18	575.31
124.30	1.10	59.30	592.84	575.17	552.35	377.51	605.00	592.94	570.52	609.43	572.45
124.80	2.40	60.40	588.56	571.96	549.89	373.97	601.31	589.55	567.47	605.31	569.07
125.30	2.90	57.10	584.31	568.60	547.21	370.00	597.52	586.07	564.44	601.10	566.53
125.80	0.00	56.60	580.06	565.19	544.47	370.28	593.76	582.64	561.27	597.64	563.22
126.30	0.30	58.30	575.88	561.74	542.15	368.45	590.00	579.14	557.92	593.95	559.51
126.80	1.20	58.30	571.88	558.74	541.82	367.28	586.31	575.81	555.47	589.79	556.93
127.30	1.40	57.50	568.22	556.13	539.99	364.71	582.55	572.61	553.25	585.91	554.89
127.80	0.20	56.30	564.77	553.39	537.38	363.59	579.05	569.54	550.69	582.43	552.42
128.30	0.90	56.90	561.58	550.55	534.57	360.63	575.74	566.58	547.75	578.81	549.26
128.80	1.00	55.70	558.43	547.61	531.45	357.79	572.50	563.67	544.56	575.34	546.20
129.30	0.00	54.40	555.45	544.68	528.40	355.43	569.28	560.62	541.39	572.12	543.20
129.80	0.00	53.30	552.38	541.89	525.27	351.25	566.23	557.66	538.04	568.97	539.94
130.40	0.80	53.10	549.33	538.27	522.06	348.46	563.15	554.63	534.64	565.76	536.49
130.90	0.70	53.70	546.60	534.71	518.80	344.08	560.22	551.70	531.07	562.70	532.71
131.40	0.10	51.60	544.16	531.12	515.54	345.56	557.31	548.60	527.39	559.84	529.31
131.90	0.60	53.20	541.89	527.50	512.20	342.55	554.58	545.41	523.66	556.95	525.25
132.40	0.40	52.30	539.09	524.03	508.82	339.25	551.91	542.12	520.06	554.18	521.71
132.90	0.00	50.20	535.46	520.46	505.56	335.77	549.33	538.91	516.43	551.44	518.30
133.40	0.00	47.70	527.83	516.24	502.11	330.14	546.16	535.48	512.93	548.74	515.14
133.90	0.30	44.50	520.93	510.70	497.51	324.95	541.93	530.86	508.56	545.81	511.33
134.40	0.00	44.00	515.32	505.42	492.67	320.56	537.48	525.88	503.40	542.73	506.12
134.90	0.00	44.00	510.09	500.28	487.74	316.08	533.16	521.10	498.02	539.49	500.44
135.40	0.00	43.50	505.07	495.21	482.90	311.87	528.82	516.24	492.62	536.26	495.18
135.90	0.00	41.50	500.07	490.27	478.03	307.46	524.64	511.55	487.46	532.92	490.11

Table C2, Experiment 2, Al-10%Cu, 0.045% refiner, cooled from the bottom.

TIME	TP	BP	T1	T2	T3	T4	T5	T6	T7	T8	T9
100.40	21.60	29.30	684.83	686.06	684.97	678.99	689.06	689.63	694.55	699.84	717.54
100.90	21.60	29.30	684.83	686.02	684.90	679.06	689.06	689.65	694.58	699.96	717.66
101.40	21.80	29.30	684.76	685.99	684.90	678.99	689.03	689.61	694.53	700.08	717.66
101.90	21.70	29.40	684.80	686.04	684.95	679.01	689.11	689.65	694.55	700.17	717.71
102.40	21.70	29.40	684.80	686.06	684.92	679.06	689.15	689.68	694.58	700.24	717.68
102.90	21.70	29.30	684.83	686.04	684.95	679.03	689.11	689.65	694.55	700.29	717.73
103.40	21.70	29.40	684.88	686.02	684.92	679.15	689.18	689.70	694.62	700.34	717.73
103.90	21.70	29.30	684.88	686.04	684.92	679.13	689.13	689.68	694.58	700.36	717.76
104.40	21.70	29.30	684.88	686.06	684.99	679.18	689.15	689.70	694.58	700.41	717.76
104.90	21.70	29.20	684.92	686.09	684.99	679.29	689.25	689.75	694.67	700.48	717.83
105.40	21.60	29.30	684.95	686.11	685.04	679.27	689.30	689.80	694.70	700.53	717.90
105.90	21.60	29.20	684.92	686.16	685.04	679.25	689.27	689.80	694.67	700.53	717.87
106.50	21.50	29.20	684.99	686.16	685.02	679.20	689.30	689.80	694.70	700.53	717.85
107.00	21.50	29.20	685.02	686.21	685.11	679.22	689.32	689.84	694.72	700.53	717.78
107.50	21.50	29.20	685.02	686.21	685.11	679.34	689.34	689.87	694.72	700.48	717.76
108.00	21.50	29.10	685.04	686.25	685.14	679.29	689.32	689.84	694.70	700.43	717.76
108.50	21.40	29.00	685.07	686.23	685.11	679.44	689.37	689.89	694.77	700.39	717.71
109.00	21.50	29.00	685.04	686.28	685.16	679.41	689.34	689.87	694.70	700.34	717.68
109.50	21.40	29.10	685.07	686.25	685.18	679.56	689.39	689.91	694.79	700.29	717.71
110.00	2.50	8.80	685.07	686.21	683.64	643.33	689.39	689.91	694.46	699.36	714.84
110.50	22.50	56.90	684.61	683.31	672.96	607.31	688.46	689.08	688.08	692.93	697.89
111.00	28.30	63.00	682.64	677.97	663.53	593.52	686.94	686.21	680.17	689.94	688.63
111.50	9.60	40.40	680.17	672.60	656.17	584.57	685.52	682.62	674.45	692.86	686.49
112.00	5.00	68.00	677.04	667.46	648.10	577.08	683.33	678.87	667.65	691.25	673.51
112.50	16.50	79.30	673.48	660.73	633.79	542.59	680.08	674.60	658.34	684.73	659.93
113.00	16.40	64.10	668.69	651.29	618.45	501.69	676.00	668.62	646.12	680.51	650.59
113.60	4.90	80.00	662.94	643.02	609.43	474.34	671.54	661.75	636.58	678.54	636.65
114.10	2.00	79.60	657.14	636.65	598.16	452.44	666.35	655.60	627.71	673.62	626.13
114.60	7.70	71.10	651.41	630.18	585.51	431.55	660.73	649.69	617.60	666.11	617.69
115.10	8.70	65.90	645.50	622.76	572.78	413.60	654.96	643.64	606.30	659.88	607.40
115.60	3.50	65.00	639.91	612.68	560.66	398.90	649.50	637.85	594.70	655.41	595.90
116.10	1.90	62.00	634.57	602.11	549.56	388.63	644.23	631.84	583.47	650.11	585.18
116.60	6.30	61.40	630.30	591.95	542.40	381.55	639.25	624.48	573.51	643.69	575.17
117.10	11.30	66.30	627.57	584.10	537.97	376.09	635.47	616.80	566.23	638.47	566.88
117.60	13.50	58.30	622.31	577.08	531.40	370.88	633.70	609.76	559.44	636.04	561.70
118.10	5.10	53.20	616.35	569.68	524.80	364.76	631.08	602.98	552.05	635.35	555.08
118.60	0.00	57.70	609.64	562.61	518.80	359.51	626.36	596.37	544.42	632.54	546.44
119.10	0.20	58.20	600.79	555.73	513.31	354.31	619.95	589.39	537.43	625.94	539.21
119.70	0.00	52.40	589.51	548.60	507.95	348.74	612.13	581.70	530.81	618.00	533.60
120.20	0.00	50.80	576.98	540.78	502.02	341.16	603.14	573.04	523.54	609.64	526.52
120.70	0.00	50.20	564.58	531.96	495.51	334.31	593.83	564.07	515.30	600.96	518.21
121.20	0.50	50.90	553.48	522.90	488.61	329.06	584.33	554.96	506.59	591.24	509.20
121.70	0.50	52.50	545.15	513.52	481.21	323.30	575.48	545.64	498.17	581.96	500.28
122.20	1.90	50.60	536.68	503.94	473.21	318.30	567.54	536.04	489.85	573.32	492.22
122.70	0.60	45.00	523.30	494.60	465.31	311.39	559.79	526.64	481.35	565.64	484.64
123.20	0.00	38.40	506.52	482.50	456.02	303.09	549.51	514.95	471.66	558.03	476.08

Table C3, Experiment 3, Al-1%Cu, 0.045% refiner, bottom cooled.

TIME	TP	BP	T1	T2	T3	T4	T5	T6	T7	T8	T9
145.40	23.80	29.80	710.23	711.78	710.16	709.78	715.41	715.77	719.55	730.65	744.91
145.90	23.90	29.90	710.23	711.86	710.11	709.78	715.44	715.87	719.64	730.68	744.86
146.40	23.80	29.80	710.19	711.86	710.21	709.78	715.44	715.82	719.62	730.61	744.81
146.90	23.80	29.80	710.23	711.78	710.16	709.83	715.44	715.80	719.57	730.56	744.74
147.40	23.70	29.80	710.19	711.86	710.19	709.85	715.44	715.84	719.67	730.56	744.74
147.90	23.80	29.80	710.21	711.81	710.16	709.76	715.44	715.84	719.62	730.51	744.76
148.40	23.70	29.70	710.16	711.83	710.14	709.78	715.39	715.75	719.50	730.49	744.71
149.00	23.70	29.70	710.23	711.86	710.14	709.80	715.41	715.82	719.57	730.49	744.79
149.50	23.70	29.90	710.23	711.81	710.19	709.76	715.41	715.84	719.64	730.44	744.76
150.00	23.80	29.70	710.21	711.88	710.14	709.71	715.39	715.75	719.52	730.41	744.69
150.50	23.70	29.60	710.19	711.86	710.14	709.73	715.37	715.70	719.48	730.37	744.64
151.00	23.70	29.70	710.23	711.78	710.16	709.73	715.37	715.77	719.55	730.37	744.57
151.50	23.70	29.70	710.19	711.76	710.19	709.66	715.37	715.80	719.60	730.29	744.57
152.00	23.70	29.70	710.14	711.78	710.19	709.76	715.32	715.70	719.48	730.20	744.52
152.50	23.70	29.70	710.16	711.78	710.19	709.71	715.27	715.65	719.40	730.13	744.45
153.00	23.70	29.70	710.16	711.76	710.09	709.68	715.32	715.75	719.52	730.13	744.47
153.50	23.70	29.80	710.09	711.76	710.11	709.68	715.27	715.68	719.48	730.10	744.45
154.00	0.40	2.10	710.07	711.64	709.85	696.10	715.22	715.61	719.36	729.74	743.61
154.50	20.90	47.70	709.78	710.28	701.43	669.29	714.39	715.03	714.43	722.97	728.14
155.10	31.50	68.40	708.09	705.92	691.77	655.67	712.81	712.57	706.27	718.52	715.58
155.60	13.30	37.00	705.56	700.91	683.97	646.64	711.33	708.75	699.89	721.15	714.55
156.10	7.90	59.90	702.53	696.05	677.02	636.86	709.49	705.30	694.84	719.88	704.01
156.60	18.00	75.30	698.91	690.75	666.49	618.07	706.23	701.08	686.92	713.53	692.77
157.10	17.60	67.00	694.55	682.93	651.39	585.02	702.41	695.62	675.05	709.49	682.12
157.60	7.90	80.00	689.13	675.64	646.52	562.05	698.10	689.01	665.87	707.11	667.93
158.10	6.40	80.00	683.78	669.95	636.89	541.49	693.22	683.43	658.72	701.96	657.78
158.60	10.40	77.00	678.51	664.33	625.19	519.15	687.89	678.06	649.81	695.20	649.36
159.10	9.30	70.20	673.24	658.70	613.24	497.98	682.69	672.63	639.10	689.84	639.98
159.60	5.80	68.00	667.96	653.30	602.49	476.04	677.63	667.22	627.64	685.26	628.86
160.10	5.50	69.20	662.94	645.81	593.01	459.41	672.58	662.06	616.35	679.77	617.32
160.60	7.40	64.80	658.39	636.20	584.26	444.24	667.65	656.59	605.99	673.93	607.73
161.10	8.60	61.90	654.72	627.02	576.25	431.17	663.24	649.73	596.39	668.91	598.56
161.70	9.50	63.40	652.55	618.52	569.04	420.83	659.81	642.29	587.55	664.83	589.34
162.20	17.30	63.90	650.02	610.79	562.70	412.25	657.85	634.74	579.61	660.76	581.16
162.70	18.30	65.10	643.26	603.66	557.40	408.32	656.36	627.38	572.59	658.91	573.81
163.20	7.10	64.30	636.46	597.24	552.31	402.97	652.90	620.66	566.27	658.01	567.59
163.70	0.00	62.80	627.71	590.94	547.28	397.88	645.95	614.25	560.26	653.26	561.79
164.20	0.00	58.40	608.42	580.43	540.62	393.94	632.40	604.63	553.36	643.07	555.69
164.70	0.10	60.00	589.88	566.37	531.38	424.97	617.95	589.74	542.69	629.64	544.33
165.20	3.90	79.20	574.40	555.08	525.58	427.35	603.24	575.74	534.33	613.34	530.72
165.70	2.40	51.70	561.18	543.27	515.23	414.52	590.23	563.15	524.12	600.11	526.07
166.20	0.00	42.50	548.76	531.33	503.99	400.94	578.25	551.25	512.37	588.94	515.86
166.70	0.00	57.60	536.65	519.50	492.65	389.60	566.91	539.92	499.27	577.92	499.60
167.20	2.00	60.80	524.69	507.72	481.51	378.94	555.99	528.54	486.40	565.97	486.21
167.80	0.00	45.20	512.86	496.15	470.72	367.69	544.98	517.06	474.81	555.29	477.68
168.30	0.00	40.30	501.43	485.01	460.32	357.48	534.54	506.12	463.62	545.34	467.17

Table C4, Experiment 4, Al-1%Cu, no refiner, bottom cooled.

TIME	TP	BP	T1	T2	T3	T4	T5	T6	T7	T8	T9
128.10	29.00	27.30	710.16	710.52	709.85	695.29	717.04	714.03	715.77	739.89	728.40
128.60	28.90	27.40	710.26	710.50	709.88	695.36	717.09	714.08	715.80	739.86	728.40
129.10	28.90	27.30	710.33	710.54	709.97	695.72	717.13	714.15	715.92	739.86	728.45
129.60	28.70	27.30	710.38	710.54	709.95	695.70	717.16	714.17	715.89	739.79	728.26
130.10	28.60	27.10	710.33	710.73	710.07	695.62	717.18	714.17	715.87	739.67	728.14
130.70	28.60	27.20	710.40	710.66	710.02	695.67	717.13	714.17	715.87	739.50	728.11
131.20	28.50	27.10	710.52	710.66	709.95	695.98	717.16	714.22	715.94	739.38	728.07
131.70	28.50	27.10	710.45	710.66	710.04	695.48	717.11	714.17	715.87	739.24	728.04
132.20	28.50	27.20	710.33	710.76	710.09	695.58	717.09	714.17	715.84	739.09	727.92
132.70	28.40	27.20	710.42	710.71	709.99	695.74	717.11	714.17	715.84	738.95	727.87
133.20	28.40	27.30	710.47	710.69	710.09	695.72	717.06	714.12	715.82	738.78	727.85
133.70	28.40	27.10	710.42	710.59	709.95	695.74	716.99	714.10	715.75	738.66	727.73
134.20	28.40	26.90	710.54	710.69	710.16	695.81	716.97	714.08	715.77	738.54	727.68
134.70	28.40	27.30	710.26	710.69	709.95	695.77	716.94	714.03	715.72	738.49	727.61
135.20	28.60	27.20	710.28	710.57	709.71	696.03	716.92	714.05	715.75	738.49	727.61
135.70	28.30	27.20	710.33	710.59	709.78	695.74	716.90	713.96	715.65	738.47	727.59
136.20	28.40	27.30	710.35	710.50	709.92	695.98	716.90	714.00	715.72	738.49	727.54
136.70	28.40	27.30	710.28	710.57	709.88	695.67	716.87	713.91	715.61	738.47	727.61
137.30	28.30	27.40	710.21	710.52	709.85	695.98	716.87	713.96	715.68	738.54	727.66
137.80	28.40	27.40	710.21	710.50	709.76	695.84	716.85	713.93	715.65	738.57	727.71
138.30	28.50	27.40	710.23	710.66	709.83	695.60	716.82	713.89	715.58	738.64	727.78
138.80	28.50	27.30	710.28	710.45	709.85	695.89	716.85	713.93	715.72	738.71	727.83
139.30	4.50	9.00	710.14	710.71	709.54	672.15	716.73	713.91	715.39	736.67	725.34
139.80	33.00	60.90	709.78	709.76	705.77	630.26	715.46	713.31	711.78	727.37	711.12
140.30	32.30	63.30	708.59	707.58	700.10	610.49	714.08	711.45	707.08	725.62	706.32
140.80	10.50	32.30	707.06	704.79	695.36	600.49	713.22	709.09	704.01	729.34	709.11
141.30	14.70	56.10	705.15	701.93	690.46	602.34	711.62	706.85	699.46	725.65	699.43
141.80	26.40	68.70	702.60	698.39	683.59	604.16	708.90	703.65	693.13	719.31	690.94
142.30	19.30	69.20	699.53	693.79	674.71	592.04	706.13	699.60	686.16	717.76	683.85
142.80	10.80	80.00	695.86	688.13	664.12	563.83	703.10	694.79	676.90	716.01	670.14
143.40	13.80	80.00	691.53	682.52	660.38	559.18	699.00	689.49	670.14	710.42	658.82
143.90	15.50	80.00	686.90	678.18	657.99	552.92	694.43	684.90	666.04	704.75	651.67
144.40	12.70	80.00	682.86	674.53	655.74	547.35	690.22	681.00	662.91	700.62	646.80
144.90	11.10	80.00	679.10	671.23	653.04	543.27	686.32	677.56	660.21	696.48	642.95
145.40	12.20	80.00	675.66	668.36	650.02	540.34	682.64	674.41	657.61	691.96	639.67
145.90	12.20	80.00	672.46	665.64	647.02	537.55	679.20	671.49	654.87	687.96	636.79
146.40	11.10	80.00	669.52	663.22	643.95	535.95	676.07	668.81	652.07	684.61	634.17
146.90	10.50	80.00	666.77	660.97	640.97	533.46	673.13	666.37	649.26	681.27	631.88
147.40	10.70	79.80	664.24	659.03	638.02	531.05	670.40	664.21	646.50	677.99	629.88
147.90	11.00	80.00	662.01	657.54	635.19	529.33	667.93	662.32	643.73	675.02	627.94
148.40	11.00	79.80	660.10	656.38	632.43	526.31	665.71	660.73	641.06	672.37	626.18
148.90	11.00	79.80	658.39	655.50	629.62	523.84	663.79	659.43	638.47	670.02	624.50
149.50	11.60	78.80	657.07	653.26	626.95	520.25	662.15	658.11	635.92	667.93	622.90
150.00	11.70	79.60	656.12	650.61	624.48	517.60	660.88	656.45	633.44	666.30	621.06
150.50	11.70	78.60	655.46	648.08	621.91	513.59	659.93	654.39	631.08	665.00	619.60
151.00	12.50	79.60	655.20	645.48	619.69	511.31	659.41	652.19	628.79	664.03	617.79
151.50	13.70	78.10	655.27	643.09	617.27	504.55	659.38	649.95	626.58	663.39	616.56

152.00	12.80	79.80	655.34	640.59	615.08	500.96	659.36	647.75	624.36	663.36	614.51
152.50	12.20	78.00	655.20	638.25	612.89	493.56	659.20	645.58	622.22	663.10	613.26
153.00	12.20	77.60	653.66	636.20	610.86	490.49	658.72	643.52	620.33	662.39	611.90
153.50	12.10	79.50	651.79	634.03	608.86	488.25	657.92	641.49	618.30	661.40	609.97
154.00	10.60	75.70	649.71	631.95	607.10	484.05	656.59	639.48	616.54	660.24	609.45
154.50	6.00	77.80	646.24	629.83	605.19	480.64	653.73	637.36	614.68	658.32	607.62
155.10	0.00	77.70	638.66	625.94	602.81	474.91	647.42	633.84	612.44	654.04	605.83
155.60	0.30	71.80	629.95	619.93	599.10	467.19	639.62	628.25	609.00	646.40	603.94
156.10	1.70	69.20	621.96	613.38	594.11	459.74	632.02	621.89	604.16	638.07	599.87
156.60	1.60	69.70	614.63	606.63	588.28	452.04	624.97	615.41	598.39	630.70	594.25
157.10	0.10	68.00	607.59	599.97	582.22	444.55	618.42	608.91	592.35	624.27	588.80
157.60	0.10	66.70	600.70	593.31	576.11	439.24	612.25	602.53	586.24	618.02	583.11
158.10	0.00	66.70	593.97	586.85	570.03	434.31	606.32	596.23	580.06	611.85	577.17
158.60	0.00	64.40	587.34	580.41	564.02	428.63	600.58	590.05	574.00	606.04	571.72
159.10	0.00	61.80	581.07	574.26	558.22	422.72	594.96	583.98	568.06	600.53	566.37
159.60	0.00	62.10	574.84	568.06	552.28	417.67	589.48	578.09	562.07	595.31	560.43
160.10	0.10	61.30	568.81	562.07	546.56	411.42	584.10	572.31	556.16	590.33	554.77
160.60	0.00	59.70	562.87	556.32	541.00	406.41	578.81	566.63	550.43	585.51	549.49
161.10	0.00	59.50	557.12	550.66	535.97	401.24	573.65	561.13	544.73	580.88	543.81
161.60	0.00	59.50	551.65	545.27	530.81	395.56	568.62	555.85	539.02	576.39	538.20
162.20	0.00	56.20	546.32	539.96	525.70	389.18	563.74	550.66	533.60	572.07	533.44
162.70	0.00	56.70	540.95	534.78	520.70	382.84	558.90	545.52	528.18	567.82	528.04
163.20	0.00	56.90	535.81	529.57	515.65	376.06	554.16	540.46	522.79	563.71	522.51
163.70	0.00	54.60	530.67	524.45	510.56	368.28	549.49	535.43	517.55	559.63	517.77
164.20	0.00	52.70	525.53	519.34	505.65	361.59	544.87	530.46	512.39	555.66	512.95
164.70	0.00	53.90	520.56	514.39	500.89	355.19	540.32	525.56	507.18	551.72	507.46
165.20	0.00	52.50	515.65	509.53	496.12	349.32	535.79	520.75	502.04	547.85	502.58
165.70	0.00	50.40	510.82	504.62	491.50	342.69	531.33	516.00	496.99	544.05	497.91
166.20	0.00	50.50	506.03	499.90	486.75	338.10	526.96	511.33	491.89	540.29	492.76
166.70	0.00	49.50	501.24	495.09	481.91	332.49	522.65	506.64	486.87	536.63	487.85

Table C5, Experiment 5, Al-1%Cu, 0.670% refiner, cooled from the bottom.

TIME	TP	BP	T1	T2	T3	T4	T5	T6	T7	T8	T9
146.40	30.10	23.30	710.33	708.56	709.97	690.37	728.66	712.81	710.21	733.94	711.14
146.90	30.10	23.30	710.28	708.59	709.99	690.65	728.71	712.81	710.21	734.03	711.14
147.40	30.20	23.30	710.28	708.56	709.99	690.44	728.66	712.79	710.21	733.96	711.14
147.90	30.10	23.40	710.28	708.59	709.99	690.46	728.64	712.76	710.16	733.94	711.14
148.40	30.20	23.40	710.26	708.61	709.99	690.27	728.66	712.74	710.19	733.91	711.16
148.90	30.00	23.40	710.35	708.59	709.95	690.46	728.69	712.76	710.19	733.94	711.21
149.40	30.10	23.40	710.28	708.61	710.04	690.46	728.71	712.76	710.19	733.96	711.21
150.00	30.00	23.40	710.38	708.63	710.04	690.63	728.74	712.79	710.21	734.08	711.16
150.50	30.00	23.30	710.30	708.59	710.02	690.58	728.71	712.79	710.19	733.91	711.24
151.00	30.00	23.30	710.30	708.61	710.02	690.48	728.66	712.79	710.21	733.98	711.24
151.50	29.90	23.40	710.40	708.61	710.02	690.82	728.69	712.79	710.26	733.94	711.31
152.00	29.90	23.30	710.35	708.71	710.07	690.39	728.64	712.81	710.28	733.89	711.28
152.50	29.80	23.30	710.40	708.61	710.07	690.72	728.64	712.81	710.26	733.94	711.28
153.00	29.80	23.40	710.35	708.63	710.04	690.22	728.55	712.76	710.19	733.77	711.21
153.50	29.70	23.30	710.28	708.66	709.99	690.60	728.62	712.79	710.21	733.96	711.19
154.00	29.70	23.40	710.40	708.59	710.04	690.79	728.62	712.76	710.21	733.98	711.21

154.50	29.80	23.30	710.35	708.59	710.04	690.51	728.57	712.76	710.19	733.79	711.24
155.00	29.80	23.30	710.30	708.61	710.02	690.53	728.55	712.76	710.21	733.87	711.19
155.50	29.70	23.30	710.38	708.59	710.07	690.84	728.59	712.76	710.23	733.94	711.26
156.00	29.80	23.30	710.30	708.61	710.02	690.51	728.57	712.74	710.21	733.79	711.28
156.60	29.60	23.30	710.38	708.68	710.07	690.53	728.59	712.74	710.23	733.89	711.26
157.10	29.70	23.30	710.35	708.63	710.04	690.68	728.57	712.79	710.23	733.94	711.19
157.60	29.70	23.30	710.35	708.68	709.99	690.25	728.43	712.74	710.19	733.63	711.12
158.10	3.90	9.50	710.21	708.56	709.76	647.84	727.40	712.64	709.40	731.49	708.35
158.60	14.10	33.30	708.75	706.87	705.56	619.62	719.62	710.93	700.67	720.96	695.05
159.10	19.40	55.20	705.41	702.46	697.84	599.71	712.69	706.25	689.01	712.72	679.51
159.60	18.10	61.20	701.12	696.41	689.18	546.98	708.71	700.15	679.08	709.11	669.07
160.10	14.00	53.80	696.39	689.72	676.95	449.40	705.46	693.41	665.59	706.82	657.66
160.60	12.10	59.80	690.87	680.79	664.24	344.39	700.89	684.33	649.55	702.60	635.37
161.10	11.30	64.90	684.42	673.27	657.66	311.89	694.86	676.64	639.32	696.67	623.21
161.60	10.50	53.70	678.04	666.35	647.51	287.28	688.58	669.62	625.56	690.46	612.63
162.10	9.90	43.80	671.68	659.69	632.66	253.62	682.21	662.77	609.85	684.19	599.57
162.70	9.50	44.20	665.40	653.61	617.60	227.11	675.69	655.98	592.02	677.63	582.27
163.20	10.10	30.10	659.50	647.96	602.70	196.18	669.38	647.04	573.34	671.11	566.86
163.70	11.00	25.10	654.61	634.10	587.06	150.43	663.36	634.48	549.72	664.76	544.68
164.20	13.50	20.00	652.78	620.10	572.26	118.27	658.51	621.06	529.36	659.12	525.51
164.70	14.50	14.40	652.50	606.81	558.69	115.40	654.35	607.99	510.18	654.65	507.67
165.20	11.40	6.60	647.25	594.30	545.90	103.59	649.10	595.59	491.14	650.23	490.25
165.70	0.00	9.70	616.07	578.91	533.51	98.57	638.40	582.15	474.39	642.53	473.00
166.20	0.00	7.50	582.13	554.47	516.54	98.50	619.13	561.41	457.15	627.92	456.28
166.70	0.00	0.00	556.58	531.84	498.02	98.62	597.45	540.39	438.72	611.22	440.85
167.20	0.00	1.30	535.01	511.80	480.81	98.77	578.39	521.21	422.34	595.24	424.71
167.70	0.00	0.00	515.96	493.84	464.82	98.86	561.34	503.66	405.39	580.39	408.63

Table C6, Experiment 6, Al-10%Cu, 0.045% refiner, cooled from the top.

TIME	TP	BP	T1	T2	T3	T4	T5	T6	T7	T8	T9
129.70	25.40	29.80	685.18	690.82	685.04	683.66	697.81	690.89	694.03	724.62	715.15
130.20	25.40	29.90	685.16	690.77	684.97	684.07	697.84	690.87	694.03	724.64	715.32
130.70	25.40	30.00	685.09	690.75	684.95	683.59	697.79	690.82	693.98	724.76	715.25
131.20	25.40	30.00	685.09	690.72	684.97	683.71	697.81	690.77	693.98	724.88	715.41
131.70	25.40	30.00	685.11	690.68	684.90	684.09	697.86	690.77	694.01	725.15	715.63
132.20	25.40	30.00	685.11	690.70	684.92	683.76	697.91	690.77	694.03	725.27	715.72
132.70	25.40	30.00	685.09	690.70	684.95	683.74	697.96	690.79	694.05	725.50	715.87
133.20	25.30	29.90	685.18	690.72	684.97	684.14	698.05	690.84	694.12	725.55	716.11
133.70	25.20	29.90	685.23	690.75	684.99	683.85	698.05	690.87	694.12	725.65	716.15
134.20	25.20	29.80	685.26	690.82	685.04	683.88	698.12	690.89	694.17	725.62	716.23
134.70	25.10	29.80	685.30	690.84	685.11	684.14	698.15	690.94	694.22	725.67	716.25
135.20	25.00	29.70	685.28	690.91	685.09	683.74	698.15	690.98	694.22	725.50	716.08
135.80	0.00	0.00	685.37	690.89	685.18	684.33	698.17	691.01	694.27	725.43	716.20
136.30	13.00	15.30	679.77	690.63	685.18	683.40	695.00	690.63	693.43	717.66	711.21
136.80	21.70	35.80	676.21	689.13	683.83	682.45	689.91	688.96	691.32	709.28	704.22
137.30	12.70	22.80	672.22	687.04	682.24	681.05	685.87	686.49	690.06	706.25	704.84
137.80	14.20	17.10	668.43	684.71	680.32	679.86	681.84	683.69	688.63	700.62	703.48
138.30	16.40	28.30	666.18	681.74	677.80	677.63	676.92	680.67	685.64	694.12	697.46

138.80	15.10	32.90	662.94	678.87	675.14	674.69	673.32	677.56	682.78	689.77	693.08
139.30	13.10	26.40	659.76	676.00	672.56	672.79	669.52	674.45	680.65	685.52	691.58
139.80	13.60	24.40	656.40	673.20	670.11	670.40	665.64	671.44	678.27	680.55	688.94
140.30	13.10	27.80	653.30	670.45	667.56	667.93	662.08	668.53	675.59	676.23	684.92
140.80	12.50	26.80	650.14	667.53	664.85	665.28	658.67	665.52	672.84	672.11	681.88
141.30	12.20	24.30	646.92	664.59	662.13	662.34	655.29	662.46	670.14	668.01	679.10
141.90	11.50	23.80	643.97	661.68	659.34	660.10	652.05	659.48	667.29	664.21	675.83
142.40	11.30	24.60	641.04	658.77	656.55	657.07	648.81	656.50	664.33	660.28	672.25
142.90	11.40	24.60	638.44	655.81	653.68	654.09	645.74	653.54	661.40	656.50	668.79
143.40	12.10	23.40	636.74	653.02	650.96	651.67	643.26	650.82	658.53	653.23	665.75
143.90	11.60	23.60	635.49	650.44	648.20	648.62	641.30	648.32	655.67	650.77	662.42
144.40	12.50	24.00	634.71	648.10	645.60	646.21	639.74	646.09	652.95	648.46	659.24
144.90	12.60	23.20	633.82	645.95	643.14	643.50	638.35	644.06	650.49	646.52	656.55
145.40	12.80	23.90	632.97	643.97	640.83	641.32	637.05	642.27	648.17	644.70	653.71
145.90	12.50	23.50	631.72	642.24	638.75	638.89	635.78	640.66	646.09	643.02	651.41
146.40	12.20	23.40	630.68	640.62	636.96	637.00	634.43	639.22	644.16	641.32	649.19
146.90	11.90	23.80	629.64	639.20	635.28	635.54	632.92	637.97	642.41	639.53	647.06
147.40	11.60	23.30	628.42	637.90	633.77	633.51	631.51	636.86	640.80	637.73	645.27
148.00	11.90	24.00	627.26	636.86	632.33	632.07	630.09	635.87	639.41	635.85	643.47
148.50	11.40	23.60	626.20	635.89	631.10	630.99	628.68	635.00	638.16	634.22	642.03
149.00	11.50	24.00	624.88	635.04	630.07	629.43	627.24	634.19	637.03	632.40	640.62
149.50	11.70	24.70	623.82	634.34	629.12	628.77	625.87	633.44	636.04	630.80	639.25
150.00	11.80	25.60	622.43	633.58	628.13	627.50	624.48	632.61	635.12	629.01	638.02
150.50	10.70	24.60	621.11	632.85	627.35	626.74	623.09	631.76	634.31	627.61	637.22
151.00	12.00	24.20	619.91	631.95	626.48	625.85	621.72	630.68	633.49	625.70	636.27
151.50	10.70	24.00	618.54	631.08	625.70	624.83	620.33	629.45	632.59	624.31	635.28
152.00	11.10	24.00	617.24	630.16	624.81	624.13	618.94	628.11	631.69	622.66	634.22
152.50	11.10	23.90	615.88	629.19	624.01	623.09	617.50	626.81	630.77	621.01	633.18
153.00	11.00	24.20	614.56	628.46	623.14	622.50	616.07	625.54	629.97	619.46	632.17
153.50	10.20	25.20	613.12	627.59	622.43	621.39	614.63	624.29	629.17	617.88	631.03
154.10	10.30	25.80	611.76	626.65	621.74	620.76	613.17	623.04	628.42	616.30	630.04
154.60	10.10	25.00	610.30	625.61	621.01	619.93	611.73	621.84	627.68	614.68	629.36
155.10	10.00	25.40	609.03	624.43	620.19	619.32	610.32	620.57	626.91	613.12	628.39
155.60	10.10	25.50	607.57	623.30	619.46	618.30	608.91	619.32	626.06	611.55	627.50
156.10	9.70	25.30	606.23	622.00	618.54	617.41	607.45	618.00	625.19	609.95	626.55
156.60	10.00	25.20	605.05	620.85	617.90	616.82	606.04	616.75	624.31	608.37	625.59
157.10	9.50	25.40	603.59	619.60	617.01	615.88	604.67	615.43	623.35	606.84	624.50
157.60	9.40	25.30	602.11	618.28	616.11	614.94	603.29	614.11	622.38	605.38	623.51
158.10	9.50	24.70	600.84	616.99	615.13	614.37	601.90	612.77	621.34	604.01	622.50
158.60	9.50	25.40	599.45	615.64	614.18	613.10	600.56	611.48	620.24	602.39	621.23
159.10	9.10	25.00	597.99	614.30	613.15	612.39	599.12	610.09	619.11	601.12	620.07
159.70	9.30	24.90	596.61	612.94	612.32	611.45	597.71	608.70	618.00	599.43	618.94
160.20	8.70	25.50	595.29	611.69	611.29	610.49	596.35	607.38	616.87	598.02	617.67
160.70	9.20	24.10	593.90	610.20	609.87	609.66	594.91	606.01	615.62	596.65	616.61
161.20	9.30	22.90	592.47	608.77	608.46	608.23	593.50	604.65	614.28	595.01	615.48
161.70	8.40	23.80	591.03	607.26	606.93	606.98	592.07	603.19	612.77	593.50	613.71
162.20	8.70	23.90	589.72	605.69	605.38	605.43	590.59	601.73	611.22	592.14	612.11
162.70	8.30	22.80	588.17	604.13	603.69	603.73	589.06	600.30	609.66	590.54	610.72
163.20	8.10	23.20	586.52	602.44	602.01	601.71	587.51	598.70	607.92	588.82	608.86

163.70	8.20	23.10	585.06	600.74	600.23	600.23	585.91	597.10	606.13	587.27	606.98
164.20	8.10	23.00	583.37	598.96	598.35	598.06	584.31	595.45	604.30	585.56	605.12
164.70	8.00	22.10	581.75	597.15	596.49	596.44	582.69	593.76	602.46	583.84	603.38
165.20	7.80	21.70	580.06	595.22	594.54	594.54	580.97	592.02	600.51	582.10	601.50
165.80	7.30	21.20	578.18	593.27	592.51	592.44	579.24	590.23	598.51	580.46	599.50
166.30	6.70	21.40	576.39	591.32	590.52	590.49	577.50	588.33	596.44	578.88	597.36
166.80	6.70	21.50	574.59	589.22	588.42	588.33	575.67	586.40	594.32	577.03	595.17
167.30	7.00	20.80	572.64	587.15	586.29	586.10	573.83	584.48	592.21	575.08	593.13
167.80	8.20	20.40	570.64	585.13	584.15	583.72	572.00	582.57	590.07	572.73	591.03
168.30	8.10	20.60	568.81	583.02	582.06	581.61	570.17	580.60	587.88	570.92	588.73
168.80	6.70	20.60	566.81	580.81	579.73	579.40	568.25	578.48	585.63	569.37	586.45
169.30	5.70	20.50	564.72	578.58	577.43	576.89	566.25	576.32	583.37	567.24	584.17
169.80	6.80	19.40	562.56	576.28	575.03	574.59	564.16	574.14	581.09	564.86	582.03
170.30	5.80	19.30	560.47	573.93	572.68	572.40	561.98	571.91	578.79	563.15	579.68
170.80	6.20	19.00	558.20	571.58	570.29	569.94	559.77	569.70	576.46	560.52	577.40
171.30	6.60	18.20	556.04	569.18	567.85	567.85	557.61	567.47	574.16	558.57	575.17
171.80	4.80	17.80	553.76	566.81	565.43	565.38	555.38	565.24	571.81	556.44	572.85
172.40	6.10	18.40	551.46	564.39	562.99	562.99	553.17	562.92	569.40	553.79	570.26
172.90	5.50	17.70	549.30	561.98	560.52	560.83	550.92	560.57	567.05	551.86	567.99
173.40	4.40	17.60	546.91	559.51	558.03	558.41	548.67	558.24	564.68	549.72	565.57
173.90	5.80	18.20	544.91	557.07	555.55	556.09	546.42	555.90	562.24	547.28	562.96
174.40	5.90	17.30	543.58	554.77	553.10	553.41	544.47	553.60	559.79	544.89	560.66
174.90	6.10	17.10	542.73	552.80	550.80	551.18	542.90	551.49	557.45	543.58	558.27
175.40	7.90	17.90	541.82	551.04	548.79	548.79	541.56	549.63	555.15	542.00	555.76
175.90	7.00	17.90	540.43	549.58	547.07	546.35	540.29	548.01	553.10	540.39	553.69
176.40	4.70	17.20	539.05	548.46	545.57	544.44	538.84	546.56	551.30	539.66	552.02
176.90	6.80	18.40	537.62	547.71	544.37	542.66	537.34	545.38	549.70	537.57	550.12
177.40	5.60	18.70	536.02	547.17	543.95	541.37	535.81	544.16	548.41	536.49	548.74
177.90	5.60	19.30	534.43	547.14	544.23	540.20	534.17	542.94	547.61	534.31	547.82
178.50	4.70	19.80	533.11	546.93	544.28	539.63	532.52	541.72	547.05	533.35	547.14
179.00	7.30	20.90	531.89	546.58	544.35	539.05	531.02	540.64	546.56	531.02	546.42
179.50	5.80	20.40	530.76	545.71	544.42	538.51	529.66	539.61	546.09	529.73	546.09
180.00	4.90	20.40	529.76	544.68	544.37	538.25	528.42	538.70	545.71	529.10	545.67
180.50	6.20	20.80	528.63	543.27	544.19	537.76	527.25	537.78	545.24	527.25	545.13
181.00	3.60	20.40	527.53	542.05	544.00	537.31	526.03	536.75	544.66	526.68	544.68
181.50	5.60	19.90	526.38	540.85	543.51	536.70	524.76	535.67	543.95	524.62	544.05
182.00	5.10	17.80	525.11	537.95	537.12	535.60	523.47	534.59	542.59	524.38	543.11
182.50	1.80	13.00	522.39	533.44	531.75	532.97	521.73	532.71	539.87	522.79	541.30
183.00	3.60	13.50	519.48	529.85	528.00	529.99	519.29	530.11	536.65	520.23	537.85
183.50	2.80	15.50	516.52	526.78	524.73	526.64	516.45	527.27	533.28	517.27	533.98
184.00	4.10	15.90	513.78	523.75	521.68	523.56	513.49	524.36	530.08	514.01	530.69
184.60	2.80	15.00	511.08	520.84	518.75	520.65	510.58	521.43	527.10	511.64	527.86
185.10	3.60	14.10	508.33	517.93	515.82	517.77	507.63	518.49	524.22	508.35	525.13
185.60	2.80	14.30	505.54	515.09	513.05	514.93	504.74	515.68	521.36	505.42	522.15

Table C7, Experiment 7, Al-10%Cu, 0.067% refiner, cooled from the top.

TIME	TP	BP	T1	T2	T3	T4	T5	T6	T7	T8	T9
142.40	25.60	27.00	685.49	685.26	685.02	676.00	695.72	689.22	691.44	704.79	694.17
142.90	25.60	27.00	685.52	685.26	684.97	676.30	695.39	689.22	691.82	704.56	694.22
143.40	25.60	27.00	685.49	685.26	685.02	676.45	695.12	689.20	691.75	704.53	694.20
143.90	25.50	27.00	685.42	685.28	684.99	676.38	694.98	689.13	691.67	704.39	694.15
144.40	25.60	27.10	685.37	685.18	684.92	676.21	694.84	689.03	691.60	704.15	694.08
144.90	25.70	27.20	685.30	685.14	684.83	676.23	694.81	688.96	691.56	704.20	694.03
145.40	25.70	27.30	685.23	685.09	684.80	676.19	694.79	688.92	691.51	704.20	694.01
145.90	25.80	27.30	685.21	685.02	684.78	676.02	694.77	688.84	691.53	704.06	694.01
146.40	25.80	27.30	685.21	684.99	684.73	676.02	694.74	688.82	691.51	704.13	694.05
146.90	25.70	27.30	685.16	685.02	684.76	676.04	694.77	688.80	691.51	704.25	694.15
147.40	25.70	27.40	685.21	685.02	684.83	676.16	694.86	688.82	691.60	704.44	694.22
147.90	25.70	27.30	685.21	685.04	684.88	676.04	694.86	688.84	691.67	704.32	694.34
148.40	25.60	27.30	685.28	685.16	684.90	676.14	694.93	688.92	691.77	704.46	694.46
149.00	25.50	27.20	685.37	685.14	684.99	676.38	695.03	689.01	691.82	704.70	694.51
149.50	25.50	27.10	685.42	685.23	685.02	676.28	694.96	689.03	691.84	704.46	694.51
150.00	25.40	27.10	685.42	685.26	685.07	676.23	694.93	689.06	691.84	704.32	694.48
150.50	25.20	27.10	685.49	685.26	685.07	676.38	694.96	689.11	691.82	704.44	694.48
151.00	25.30	27.10	685.42	685.30	685.02	676.23	694.86	689.06	691.79	704.15	694.43
151.50	25.20	27.10	685.40	685.26	685.04	676.33	694.86	689.06	691.77	704.25	694.36
152.00	25.30	27.10	685.40	685.23	685.04	676.19	694.81	689.03	691.75	704.01	694.31
152.50	25.30	27.20	685.37	685.16	684.99	676.09	694.74	688.99	691.70	703.91	694.27
153.00	25.30	27.20	685.35	685.14	684.99	676.26	694.79	688.96	691.70	704.13	694.24
153.50	25.30	27.20	685.28	685.14	684.97	676.04	694.62	688.92	691.63	703.84	694.24
154.00	25.30	27.20	685.23	685.09	684.88	676.07	694.60	688.87	691.60	703.84	694.20
154.50	25.30	27.30	685.23	685.09	684.90	676.16	694.60	688.87	691.56	704.01	694.17
155.10	25.30	27.30	685.23	685.02	684.88	676.00	694.51	688.82	691.53	703.84	694.20
155.60	25.40	27.30	685.23	685.07	684.88	676.11	694.58	688.82	691.58	703.98	694.24
156.10	25.30	27.30	685.23	685.04	684.85	676.16	694.60	688.82	691.60	704.03	694.29
156.60	0.00	0.10	685.07	685.07	684.90	676.14	694.60	688.82	691.63	704.01	694.31
157.10	6.60	5.90	682.57	684.19	684.26	675.57	691.25	688.18	689.82	698.67	691.20
157.60	19.50	19.10	678.84	681.48	681.79	672.68	684.64	685.61	685.30	688.42	684.00
158.10	19.60	24.50	674.57	677.70	678.30	669.43	679.56	681.76	681.36	683.09	679.15
158.60	14.30	22.20	670.71	674.03	675.12	666.65	676.14	677.99	678.91	680.74	677.35
159.10	11.40	17.80	667.25	670.64	672.46	664.95	672.51	674.83	677.02	677.61	676.38
159.60	13.80	16.50	663.84	667.56	669.74	662.79	668.31	671.68	674.50	672.39	674.12
160.10	12.70	17.90	659.81	664.24	666.77	660.24	663.72	668.38	671.37	667.82	670.78
160.60	8.80	18.20	655.50	660.83	663.98	657.11	659.12	664.90	668.38	663.98	667.72
161.20	4.90	17.20	648.58	655.84	660.26	654.68	653.04	660.54	665.42	658.60	665.00
161.70	3.70	16.20	642.34	650.51	656.19	651.84	646.19	655.48	661.92	651.74	661.70
162.20	6.50	16.30	636.44	645.39	651.89	647.84	639.60	650.21	657.85	644.09	657.63
162.70	9.80	16.20	631.98	640.05	647.44	643.14	634.29	645.34	653.61	637.69	653.49
163.20	13.50	15.70	630.94	636.25	642.86	639.15	631.53	640.99	649.19	633.86	649.14
163.70	12.00	15.90	630.28	634.41	639.32	635.07	629.97	638.66	645.27	632.59	645.17
164.20	6.10	16.20	629.22	632.68	636.39	631.62	627.78	636.58	641.98	631.65	641.84
164.70	5.30	17.00	627.64	630.77	633.91	628.72	625.07	634.55	639.25	628.89	638.96
165.20	8.00	17.30	625.33	628.89	631.58	626.15	621.77	632.45	636.70	624.71	636.39
165.70	8.40	17.50	622.97	627.66	629.57	623.89	618.38	630.77	634.53	621.09	634.15

166.20	6.20	17.70	620.59	626.77	628.18	622.00	615.13	629.48	632.87	618.16	632.50
166.70	4.80	18.10	618.33	625.70	627.40	620.73	612.04	628.11	631.88	615.22	631.41
167.30	5.40	19.20	615.97	624.34	626.91	619.81	608.82	626.67	631.20	611.71	630.63
167.80	5.80	20.40	613.64	622.71	626.34	619.15	605.66	624.90	630.61	608.30	629.81
168.30	5.40	21.10	611.38	621.01	625.63	618.56	602.79	623.02	629.93	605.33	629.03
168.80	5.00	21.10	609.14	619.04	624.83	617.98	600.20	620.92	629.29	602.72	628.46
169.30	4.50	21.30	606.89	616.94	624.01	617.36	597.69	618.80	628.68	600.18	627.87
169.80	4.40	21.00	604.63	614.89	622.97	616.68	595.19	616.77	627.94	597.57	627.21
170.30	4.20	21.00	602.39	612.84	621.79	615.90	592.70	614.80	626.98	594.94	626.29
170.80	4.10	21.00	600.18	610.79	620.35	615.03	590.30	612.82	625.89	592.44	625.21
171.30	3.90	21.20	597.99	608.72	618.78	614.14	587.98	610.79	624.64	590.02	624.03
171.80	3.70	20.70	595.90	606.63	617.13	613.19	585.70	608.72	623.32	587.72	622.78
172.30	3.50	20.80	593.78	604.58	615.48	612.13	583.47	606.74	621.93	585.42	621.49
172.80	3.20	20.10	591.71	602.51	613.67	610.77	581.26	604.72	620.33	583.11	620.02
173.30	3.30	19.40	589.62	600.42	611.57	609.07	579.07	602.70	618.45	580.86	618.26
173.90	3.00	19.30	587.55	598.27	609.31	607.12	576.91	600.56	616.37	578.63	616.28
174.40	2.90	18.50	585.39	596.04	606.86	605.03	574.73	598.35	614.16	576.37	614.18
174.90	2.50	17.50	583.25	593.69	604.30	602.77	572.57	596.06	611.85	574.16	612.09
175.40	2.40	16.60	580.95	591.24	601.54	600.37	570.31	593.74	609.38	571.91	609.76
175.90	2.30	16.30	578.58	588.68	598.67	597.69	568.01	591.29	606.51	569.49	606.93
176.40	2.10	16.20	576.16	586.03	595.62	594.82	565.64	588.68	603.40	567.09	603.78
176.90	1.80	16.20	573.55	583.18	592.44	591.74	563.17	585.96	600.25	564.58	600.63
177.40	1.60	15.70	570.83	580.22	589.18	588.68	560.62	583.11	597.10	562.02	597.57
177.90	1.30	15.00	567.94	577.15	585.82	585.56	557.94	580.20	594.02	559.35	594.58
178.40	1.00	14.00	564.93	573.93	582.34	582.50	555.15	577.19	590.96	556.51	591.69
178.90	0.90	13.00	561.86	570.64	578.74	579.40	552.26	574.12	587.74	553.55	588.61
179.40	0.70	12.60	558.69	567.26	575.13	576.21	549.28	570.95	584.29	550.57	585.20
180.00	0.60	12.50	555.40	563.81	571.44	572.82	546.28	567.68	580.81	547.50	581.68
180.50	0.30	12.00	552.02	560.24	567.68	569.49	543.11	564.32	577.36	544.40	578.25
181.00	0.20	11.30	548.58	556.65	563.88	566.16	539.87	560.90	573.88	541.16	574.87
181.50	1.50	11.30	547.26	553.76	560.17	562.75	537.08	557.61	570.31	537.95	571.30
182.00	2.80	11.20	545.74	551.32	556.88	559.42	534.80	554.65	566.79	535.32	567.71
182.50	1.40	9.80	544.21	549.26	554.37	556.20	532.85	552.28	563.24	533.72	564.39
183.00	0.00	9.90	542.26	547.12	551.77	553.03	530.84	549.80	560.12	532.03	561.13
183.50	0.20	10.70	539.63	545.15	549.21	549.87	528.44	547.24	557.00	529.64	557.80
184.00	0.90	11.30	536.91	543.60	547.03	546.91	525.84	544.75	554.09	526.78	554.72
184.50	1.20	12.10	534.00	542.03	545.15	544.16	523.21	542.33	551.46	524.10	551.93
185.00	0.60	12.40	531.23	539.75	543.95	541.72	520.60	539.87	549.19	521.57	549.58
185.50	0.10	12.80	528.79	537.17	543.86	539.80	518.07	537.55	547.45	519.08	547.71
186.00	0.30	13.80	526.33	534.61	543.62	538.34	515.58	535.25	546.04	516.43	546.09
186.60	0.60	14.70	523.82	532.08	542.38	537.03	513.09	532.99	544.73	513.87	544.61
187.10	0.30	14.40	521.45	529.78	539.92	535.95	510.68	530.84	543.58	511.45	543.48
187.60	0.10	12.60	519.03	526.92	534.82	534.80	508.35	528.70	542.22	509.15	542.52
188.10	0.10	7.60	514.67	521.05	526.54	532.08	505.80	525.77	539.33	506.87	540.60
188.60	0.00	4.60	509.88	515.93	521.05	528.47	502.65	522.11	535.39	504.36	537.15
189.10	0.00	4.70	505.47	511.38	516.26	524.15	499.29	518.16	530.62	501.62	532.27
189.60	0.00	6.00	501.24	507.02	511.71	519.43	495.86	514.06	525.46	498.78	526.73

Table C8, Experiment 8, Al-1%Cu, 0.45% refiner, cooled from the top.

Time	BP	TP	T1	T2	T3	T4	T5	T6	T7	T8	T9
149.6	24.7	28.6	710.52	710.85	710.35	707.25	717.78	714.77	716.56	732.33	732.59
150.1	24.7	28.5	710.52	710.85	710.4	707.42	717.64	714.77	716.49	731.66	731.83
150.6	24.7	28.5	710.5	710.78	710.38	707.54	717.49	714.75	716.42	731.11	731.08
151.1	24.8	28.7	710.35	710.66	710.26	707.04	717.3	714.6	716.25	730.65	730.51
151.6	24.9	28.8	710.28	710.57	710.09	707.35	717.16	714.48	716.18	730.29	730.05
152.1	25.1	29.1	710.09	710.42	709.92	706.99	716.94	714.29	715.96	730.08	729.69
152.6	25.2	29.2	709.97	710.21	709.76	706.75	716.8	714.12	715.82	729.96	729.48
153.2	25.4	29.4	709.83	710.09	709.64	706.87	716.68	713.96	715.65	729.98	729.38
153.7	25.7	29.6	709.64	709.92	709.47	706.27	716.56	713.81	715.51	730.08	729.46
154.2	25.8	29.9	709.52	709.78	709.35	706.34	716.51	713.67	715.39	730.27	729.55
154.7	26	30	709.45	709.66	709.21	706.44	716.47	713.57	715.34	730.53	729.79
155.2	26.1	30.2	709.35	709.56	709.18	705.94	716.47	713.5	715.27	730.82	730.15
155.7	26.2	30.3	709.35	709.52	709.14	706.03	716.51	713.48	715.27	731.16	730.53
156.2	26.2	30.3	709.4	709.54	709.18	706.49	716.61	713.48	715.34	731.49	730.92
156.7	26.2	30.3	709.35	709.56	709.16	706.15	716.68	713.5	715.37	731.78	731.3
157.2	26.2	30.3	709.52	709.64	709.21	706.44	716.78	713.6	715.51	732.04	731.71
157.7	26.1	30.4	709.56	709.71	709.33	706.65	716.9	713.67	715.61	732.26	732.04
158.2	26.1	30.2	709.59	709.83	709.47	706.3	716.99	713.77	715.7	732.47	732.31
158.7	26	30.1	709.73	709.92	709.54	706.44	717.09	713.86	715.8	732.59	732.55
159.2	25.8	30	709.9	710.07	709.68	706.96	717.23	714.03	715.94	732.69	732.67
159.8	25.7	29.9	709.99	710.19	709.78	707.11	717.33	714.12	716.06	732.69	732.69
160.3	25.6	29.7	710.07	710.28	709.88	706.92	717.4	714.24	716.15	732.67	732.71
160.8	25.4	29.7	710.16	710.35	709.97	706.85	717.44	714.32	716.2	732.59	732.67
161.3	25.3	29.6	710.28	710.5	710.04	707.2	717.49	714.41	716.3	732.45	732.59
161.8	25.2	29.4	710.28	710.54	710.09	707.37	717.54	714.48	716.35	732.31	732.52
162.3	25.1	29.3	710.38	710.57	710.21	707.3	717.52	714.55	716.42	732.09	732.43
162.8	25.1	29.3	710.38	710.61	710.21	707.08	717.52	714.55	716.42	731.92	732.26
163.3	25.1	29.3	710.38	710.64	710.23	707.08	717.44	714.58	716.39	731.71	732.09
163.8	25	29.3	710.38	710.66	710.21	707.58	717.42	714.58	716.42	731.52	731.88
164.3	25	29.3	710.38	710.64	710.21	707.54	717.4	714.55	716.39	731.35	731.71
164.8	25	29.3	710.33	710.59	710.16	707.11	717.33	714.51	716.35	731.23	731.52
165.3	25.1	29.3	710.21	710.57	710.16	707.13	717.25	714.46	716.25	731.08	731.3
165.9	25.1	29.4	710.21	710.54	710.09	707.32	717.23	714.43	716.25	730.99	731.13
166.4	25.2	29.5	710.14	710.42	710.07	706.85	717.11	714.34	716.13	730.92	731.01
166.9	25.2	29.6	710.14	710.38	709.97	707.18	717.09	714.29	716.13	730.89	730.99
167.4	25.4	29.6	710.02	710.3	709.95	706.8	717.04	714.22	716.06	730.94	731.01
167.9	25.3	29.7	710.02	710.28	709.85	707.23	717.04	714.2	716.01	731.01	731.11
168.4	25.4	29.7	709.97	710.21	709.85	706.92	717.01	714.15	715.99	731.16	731.25
168.9	25.5	29.8	709.92	710.21	709.78	706.94	717.04	714.1	715.96	731.3	731.44
169.4	25.5	29.8	709.92	710.19	709.8	706.8	717.06	714.12	715.99	731.52	731.68
169.9	25.4	29.8	709.95	710.21	709.8	706.8	717.11	714.12	716.04	731.76	731.95
170.4	25.4	29.7	709.97	710.26	709.88	706.85	717.16	714.17	716.06	731.92	732.09
170.9	25.4	29.7	710.07	710.3	709.92	706.8	717.23	714.22	716.08	732.09	732.14
171.4	25.3	29.6	710.09	710.35	709.97	707.11	717.33	714.27	716.13	732.16	732.12
172	25.2	29.6	710.14	710.4	710.02	706.82	717.37	714.29	716.18	732.19	732.09
172.5	25	29.6	710.21	710.42	710.02	707.42	717.42	714.39	716.23	732.19	732.09
173	25.1	29.5	710.21	710.5	710.04	706.92	717.42	714.39	716.2	732.14	731.97
173.5	25	29.4	710.28	710.5	710.11	706.94	717.42	714.41	716.23	732.02	731.88
174	25	29.4	710.3	710.47	710.14	707.44	717.44	714.46	716.27	731.9	731.78
174.5	24.9	29.4	710.33	710.52	710.11	707.44	717.44	714.46	716.25	731.78	731.68

175	24.9	29.4	710.3	710.52	710.11	707.13	717.4	714.43	716.25	731.66	731.64
175.5	24.8	29.4	710.3	710.47	710.07	707.18	717.37	714.43	716.2	731.52	731.49
176	24.9	29.4	710.26	710.45	710.07	707.11	717.3	714.39	716.18	731.35	731.32
176.5	25	29.5	710.21	710.47	710.02	707.35	717.25	714.39	716.15	731.23	731.16
177	25	29.6	710.16	710.42	709.99	706.85	717.18	714.29	716.06	731.16	731.08
177.5	25	29.7	710.14	710.35	709.95	707.23	717.16	714.29	716.06	731.13	731.01
178	25.1	29.7	710.07	710.33	709.92	706.7	717.09	714.22	715.96	731.08	731.04
178.6	25.1	29.7	710.07	710.23	709.88	707.13	717.06	714.17	715.99	731.11	731.08
179.1	25.2	29.8	709.99	710.23	709.85	706.63	717.04	714.12	715.92	731.18	731.16
179.6	25.2	29.9	709.95	710.26	709.73	706.63	717.04	714.1	715.89	731.25	731.28
180.1	25.2	30	709.92	710.21	709.76	706.92	717.04	714.1	715.89	731.3	731.37
180.6	25.2	29.9	709.92	710.21	709.73	706.92	717.04	714.08	715.92	731.35	731.49
181.1	25.2	29.9	709.95	710.16	709.78	707.16	717.06	714.12	715.94	731.4	731.56
181.6	25.2	30	709.9	710.23	709.73	706.77	717.04	714.08	715.92	731.42	731.64
182.1	25.2	30	709.95	710.23	709.76	706.94	717.04	714.1	715.94	731.42	731.66
182.6	25.2	30	709.97	710.19	709.76	706.89	717.06	714.1	715.92	731.47	731.73
183.1	25.2	30	709.99	710.23	709.78	707.25	717.09	714.15	715.99	731.47	731.8
183.6	25.2	30	709.99	710.26	709.78	707.27	717.11	714.12	716.01	731.49	731.85
184.1	25.2	29.9	709.97	710.21	709.8	706.8	717.09	714.15	716.01	731.52	731.88
184.7	25.2	30	709.97	710.28	709.83	707.23	717.13	714.17	716.04	731.52	731.88
185.2	25.2	29.9	710.02	710.28	709.83	707.18	717.13	714.2	716.04	731.54	731.9
185.7	0.4	0.6	709.33	710.3	709.88	707.23	717.01	714.22	716.06	731.16	731.61
186.2	0.7	24.4	700.89	707.47	709.25	706.27	706.37	711.9	714.96	721.29	724.88
186.7	15	32.9	692.01	703.15	706.94	704.65	697.79	707.68	712.48	708.37	720.39
187.2	11.5	18.8	685.02	698.24	703.91	702.24	689.44	702.72	709.71	700.34	719.91
187.7	7.1	15.8	680.58	691.53	700.2	699.67	683.28	696.29	706.27	694.53	716.39
188.2	8.7	19.6	676.87	685.9	695.08	695.74	678.32	691.2	701.32	688.58	710.07
188.7	7.6	21.4	670.02	681.67	690.32	690.87	672.68	686.68	696.41	682.59	704.37
189.2	8.1	18.4	663.98	677.63	685.78	686.56	667.96	681.38	691.84	677.18	699.84
189.7	4	16.2	658.7	672.56	681.27	682.07	662.15	676.85	687.37	671.82	695.29
190.2	3.9	18	657.09	668.34	676.71	677.87	656.55	672.89	682.78	665.61	689.96
190.7	10	18.8	655.69	664.5	672.51	673.53	652.71	669.52	678.54	659.74	685.11
191.3	9.9	16.2	654.39	661.89	668.62	669.31	649.55	665.71	674.55	656.19	681.24
191.8	7.7	17.7	653.42	659.76	665.28	665.78	647.28	663.43	671.06	654.11	677.06
192.3	7.6	19.8	652.74	657.99	662.39	662.6	645.36	661.54	668.03	651.79	673.34
192.8	7.4	18.7	651.6	656.4	659.95	659.83	643.14	659.81	665.52	649.24	670.68
193.3	7.5	17.6	650.23	654.98	657.89	657.82	640.92	658.32	663.43	646.61	668.5
193.8	7.3	18.5	648.62	653.82	656.07	655.58	638.66	656.99	661.47	644.06	666.02
194.3	7.4	19.8	647.04	652.9	654.49	653.97	636.51	655.95	659.81	641.58	663.81
194.8	7.6	20.5	645.46	652.41	653.16	652.22	634.5	655.13	658.37	639.25	662.06
195.3	7.3	21.6	643.83	652.29	652.38	651.08	632.61	654.65	657.44	637.14	660.66
195.8	7.2	23.3	642.2	652.31	652.24	650.96	630.87	654.32	657.23	635.14	659.98
196.3	7.4	23.2	640.5	652.29	652.45	650.75	629.1	653.82	657.3	633.09	659.91
196.8	7.2	21.9	638.89	652.05	652.5	650.94	627.45	653.21	657.42	631.25	660.07
197.4	6.8	22.3	637.24	651.32	652.48	650.87	625.75	652.26	657.4	629.43	659.83
197.9	6.5	23.6	635.54	650.28	652.45	650.59	624.1	651.2	657.28	627.64	659.31
198.4	6.5	23	633.89	648.93	652.38	650.56	622.45	649.95	657.26	625.8	659.29
198.9	6.3	22.5	632.31	647.44	652.34	650.56	620.85	648.53	657.23	624.01	659.2
199.4	6	23.5	630.66	645.86	652.26	650.25	619.2	647.11	657.02	622.29	658.67
199.9	5.8	23.9	629.05	644.37	652.22	650.16	617.57	645.72	656.85	620.5	658.34
200.4	5.7	23	627.45	642.86	652.07	650.11	615.97	644.35	656.71	618.75	658.34
200.9	5.8	23.1	625.89	641.32	651.91	649.95	614.37	642.95	656.38	616.96	657.82

201.4	5.6	24.3	624.43	639.79	651.67	649.76	612.77	641.54	655.93	615.24	657.11
201.9	5.4	22.7	622.99	638.25	651.22	649.47	611.24	640.12	655.32	613.59	656.73
202.4	5.2	23	621.53	636.72	650.35	649.43	609.76	638.7	654.63	612.04	655.93
202.9	5	23.3	620.02	635.19	649.19	648.81	608.23	637.29	653.61	610.42	654.75
203.4	4.9	23	618.56	633.65	647.77	648.13	606.72	635.85	652.52	608.79	653.71
204	5	21.2	617.15	632	646.21	646.64	605.19	634.34	651.13	607.14	652.57
204.5	4.9	20.3	615.5	630.47	644.13	644.65	603.66	632.76	649.31	605.54	650.85
205	4.4	19.2	613.83	628.44	641.3	642.17	602.04	630.96	646.9	603.92	648.53
205.5	4.1	16.3	611.9	625.92	637.38	638.68	600.32	628.77	643.69	602.13	645.76
206	3.7	14.1	609.47	622.71	632.64	634.53	598.35	625.99	639.74	600.2	642.15
206.5	2.9	14.5	606.53	618.96	627.38	630.04	596.02	622.69	635.4	597.92	637.55
207	2.3	15	602.96	614.72	622.17	625.28	593.31	618.99	630.92	595.22	632.87
207.5	1.6	13.3	599.17	610.39	618.28	620.92	590.12	615.03	626.6	592.11	628.75
208	1.2	12.7	595.24	605.8	612.58	616.99	586.59	611	622.29	588.59	624.43
208.5	0.6	10.8	590.89	600.86	607.07	612.37	582.71	606.7	617.48	584.71	619.88
209	0.1	10.2	586.36	595.92	601.69	607.47	578.51	602.2	612.51	580.53	614.89
209.5	0.1	10.8	581.7	590.99	596.68	602.77	574.09	597.57	607.54	576.14	609.62
210.1	0	10.4	577	586.05	591.81	597.92	569.56	592.82	602.6	571.63	604.7
210.6	0	8.8	572.24	580.88	586.38	593.34	564.93	588.02	597.78	567.19	600.02
211.1	0	8	567.49	575.74	580.93	588.66	560.12	583.16	592.84	562.77	595.1
211.6	0	8.5	562.87	570.71	575.69	583.65	555.05	578.25	587.77	558.24	589.83
212.1	0	8.5	558.08	565.76	570.55	578.86	550.26	573.34	582.76	553.95	584.69
212.6	0	7.6	553.32	560.8	565.5	574.09	545.64	568.46	577.8	549.8	579.82
213.1	0.1	6.6	548.58	555.92	560.57	569.33	541.14	563.62	572.92	545.78	574.98
213.6	0	6.7	543.93	551.16	555.69	564.61	536.75	558.85	568.03	541.89	569.98
214.1	0	6.8	539.33	546.46	550.87	560.05	532.48	554.18	563.24	538.09	565.01
214.6	0	6.2	534.78	541.75	546.16	555.4	528.25	549.51	558.48	534.33	560.24
215.1	0	5.6	530.3	537.12	541.44	550.78	524.05	544.94	553.76	530.62	555.57
215.6	0	5.3	525.84	532.57	536.84	546.28	519.97	540.41	549.14	527.01	550.9
216.1	0	5.5	521.45	528.09	532.29	541.72	515.91	535.95	544.52	523.42	546.16
216.6	0	5.3	517.13	523.66	527.76	537.31	511.9	531.54	539.96	519.88	541.54
217.1	0	4.9	512.91	519.29	523.35	532.88	508	527.15	535.43	516.36	537.05
217.7	0	4.4	508.64	514.97	518.99	528.56	504.13	522.88	531.02	512.95	532.6
218.2	0	4.3	504.46	510.7	514.67	524.29	500.25	518.63	526.66	509.55	528.09
218.7	0	4.4	500.37	506.5	510.37	520.04	496.5	514.43	522.32	506.17	523.68

Table C9, Experiment 9, Al-1%Cu, 0.67 refiner, cooled from the top.

TIME	TP	BP	T1	T2	T3	T4	T5	T6	T7	T8	T9
148.90	27.00	27.50	710.38	715.27	709.95	702.03	725.41	714.91	717.11	728.76	718.35
149.40	27.00	27.50	710.35	715.25	709.99	701.98	725.36	714.94	717.13	728.71	718.35
149.90	27.00	27.60	710.33	715.25	709.99	701.77	725.31	714.89	717.09	728.57	718.33
150.40	27.00	27.60	710.30	715.25	709.97	701.62	725.29	714.89	717.11	728.55	718.31
150.90	27.00	27.60	710.30	715.22	709.97	702.03	725.29	714.89	717.11	728.62	718.33
151.40	27.00	27.50	710.33	715.20	709.97	701.62	725.22	714.86	717.06	728.50	718.33
151.90	27.00	27.50	710.30	715.22	709.97	701.65	725.19	714.84	717.09	728.45	718.31
152.50	27.00	27.60	710.30	715.22	709.97	701.96	725.19	714.84	717.09	728.47	718.31
153.00	27.00	27.50	710.26	715.20	709.92	701.82	725.17	714.82	717.09	728.43	718.33
153.50	27.00	27.60	710.26	715.18	709.95	701.62	725.17	714.82	717.11	728.47	718.35
154.00	26.90	27.50	710.26	715.20	709.97	701.82	725.19	714.86	717.13	728.55	718.38
154.50	26.90	27.60	710.26	715.20	709.97	701.74	725.19	714.84	717.13	728.52	718.40
155.00	26.90	27.60	710.26	715.22	709.95	701.93	725.19	714.86	717.13	728.55	718.38
155.50	26.90	27.60	710.28	715.25	710.02	701.70	725.17	714.84	717.13	728.43	718.38
156.00	26.90	27.60	710.26	715.22	709.99	702.08	725.19	714.86	717.13	728.47	718.40
156.50	26.90	27.60	710.26	715.25	710.02	702.05	725.17	714.86	717.13	728.43	718.40
157.00	26.80	27.50	710.28	715.20	709.99	702.13	725.12	714.86	717.11	728.40	718.38
157.50	26.90	27.60	710.21	715.20	709.99	701.72	725.00	714.82	717.09	728.21	718.33
158.00	26.90	27.60	710.16	715.18	709.95	701.91	724.98	714.79	717.06	728.23	718.28
158.50	0.50	0.10	700.15	714.43	709.83	701.65	724.62	714.58	716.92	727.90	718.50
159.00	8.80	8.80	684.52	711.35	708.04	700.15	717.16	712.29	714.00	718.19	713.79
159.60	12.00	20.10	675.00	704.77	703.87	696.12	706.44	706.54	708.49	706.70	706.08
160.10	11.40	21.90	675.28	697.50	698.36	691.94	697.60	699.46	703.17	698.00	700.58
160.60	10.20	18.30	667.37	691.27	693.01	687.82	690.37	693.05	698.58	691.01	696.86
161.10	8.70	15.20	664.78	685.85	688.37	683.76	683.55	687.63	694.29	684.52	693.22
161.60	8.60	14.30	657.30	680.77	683.62	680.13	677.44	682.40	689.70	678.37	688.89
162.10	8.50	14.10	655.29	675.55	678.91	675.95	671.63	677.23	684.99	672.53	684.28
162.60	8.20	13.70	652.43	670.83	674.29	671.61	666.39	672.46	680.34	667.37	679.72
163.10	7.70	13.60	651.18	666.61	669.62	667.44	661.40	667.48	675.62	662.39	675.07
163.60	7.90	14.40	650.47	663.76	665.54	663.22	656.50	664.36	671.18	657.37	670.54
164.10	8.60	14.70	649.88	661.42	661.87	659.74	652.67	661.37	667.41	653.33	666.73
164.60	9.60	15.00	649.12	659.76	658.94	656.36	649.66	659.22	664.24	650.02	663.53
165.10	10.00	15.60	648.39	658.23	656.45	653.73	647.28	657.33	661.59	647.54	660.81
165.60	10.10	16.30	647.42	657.09	654.32	651.37	645.15	655.76	659.29	645.39	658.39
166.20	10.00	17.50	646.35	656.50	652.64	649.47	643.33	654.70	657.42	643.59	656.38
166.70	10.10	17.90	645.27	656.38	651.53	647.99	641.61	654.13	656.17	641.82	655.10
167.20	10.10	17.90	644.04	656.29	650.89	646.85	640.02	653.73	655.48	640.19	654.51
167.70	10.10	18.50	642.86	656.12	650.77	646.50	638.77	653.35	655.29	638.96	654.23
168.20	10.20	19.80	641.56	656.05	650.89	646.33	637.45	652.97	655.27	637.62	654.01
168.70	10.20	20.80	640.17	655.79	650.94	646.19	636.13	652.48	655.24	636.27	653.90
169.20	10.00	21.10	638.73	655.08	650.99	646.24	634.88	651.84	655.36	635.02	653.99
169.70	10.00	20.90	637.26	654.06	651.01	646.40	633.63	651.03	655.50	633.79	654.30
170.20	10.00	20.80	635.78	652.90	651.01	646.45	632.31	650.11	655.55	632.47	654.44
170.70	10.00	21.10	634.29	651.58	650.99	646.33	630.96	649.00	655.48	631.10	654.35
171.20	10.00	21.90	632.85	650.21	650.94	646.24	629.67	647.87	655.39	629.78	654.20
171.70	9.50	22.50	631.43	648.86	650.89	646.31	628.39	646.78	655.34	628.60	654.11
172.30	9.80	22.50	630.00	647.49	650.85	646.14	627.07	645.67	655.27	627.24	654.09

172.80	9.70	22.60	628.70	646.24	650.70	646.19	625.85	644.63	655.20	626.06	654.09
173.30	9.50	22.50	627.45	644.96	650.51	646.17	624.67	643.59	655.03	624.88	654.01
173.80	9.20	22.70	626.25	643.69	650.21	646.19	623.58	642.58	654.75	623.87	653.75
174.30	9.20	22.60	625.02	642.46	649.76	646.02	622.48	641.56	654.30	622.78	653.35
174.80	9.00	22.40	623.84	641.28	649.12	645.72	621.39	640.54	653.75	621.65	652.90
175.30	8.90	22.30	622.71	640.07	648.41	645.48	620.31	639.53	653.21	620.61	652.43
175.80	8.90	22.40	621.60	638.89	647.47	645.20	619.22	638.56	652.55	619.51	651.84
176.30	8.80	21.90	620.50	637.76	646.40	644.63	618.07	637.55	651.79	618.33	651.18
176.80	8.80	21.60	619.37	636.60	645.20	643.90	616.96	636.48	650.89	617.22	650.37
177.30	8.80	21.20	618.28	635.37	643.85	642.72	615.81	635.40	649.76	616.02	649.36
177.80	8.80	20.30	617.13	634.12	642.24	641.42	614.70	634.24	648.43	614.94	648.22
178.40	8.80	19.50	616.02	632.80	640.33	639.84	613.57	633.02	646.85	613.83	646.83
178.90	8.60	18.10	614.54	631.27	637.95	637.92	612.35	631.69	644.84	612.61	645.06
179.40	8.30	17.10	612.96	629.41	635.16	635.82	611.03	630.04	642.62	611.31	643.05
179.90	8.00	16.30	611.24	627.47	632.10	633.35	609.55	628.20	640.19	609.95	640.73
180.40	7.60	15.90	609.43	625.35	629.17	630.63	607.97	626.20	637.38	608.37	637.97
180.90	7.40	16.10	607.29	622.83	626.67	627.90	606.18	623.91	634.55	606.65	635.04
181.40	7.00	16.60	604.81	620.19	624.24	625.26	604.16	621.41	631.81	604.65	632.21
181.90	6.70	15.40	602.23	617.13	620.02	622.57	601.92	618.73	628.93	602.53	629.50
182.40	6.00	13.90	599.26	613.69	616.02	619.72	599.52	615.81	625.89	600.20	626.77
182.90	5.60	12.30	596.13	610.27	612.23	616.73	596.91	612.70	622.76	597.69	623.84
183.40	5.30	11.90	592.98	606.96	608.93	613.57	594.02	609.57	619.44	594.87	620.57
183.90	4.90	11.60	590.02	603.69	605.50	610.53	591.13	606.49	616.16	591.97	617.27
184.40	4.50	10.70	586.68	600.02	601.24	607.14	587.98	603.17	612.63	588.87	613.83
185.00	4.20	10.20	583.16	596.23	597.15	603.66	584.78	599.69	608.89	585.70	610.13
185.50	3.70	9.60	579.61	592.35	593.15	600.11	581.49	596.09	605.07	582.46	606.37
186.00	3.30	9.20	575.92	588.52	589.18	596.56	577.99	592.44	601.19	579.03	602.46
186.50	2.90	8.90	572.17	584.62	585.23	592.98	574.52	588.73	597.24	575.57	598.51
187.00	2.50	8.60	568.43	580.76	581.30	588.94	570.90	584.99	593.38	571.98	594.65
187.50	2.30	8.30	564.68	576.82	577.38	585.18	567.26	581.19	589.41	568.32	590.68
188.00	2.00	7.90	560.92	572.97	573.46	581.35	563.46	577.38	585.49	564.54	586.71
188.50	1.70	7.40	557.14	569.09	569.54	577.57	559.68	573.53	581.54	560.80	582.78
189.00	1.40	7.10	553.43	565.22	565.62	573.79	555.97	569.72	577.62	557.05	578.86
189.50	1.20	6.60	549.70	561.39	561.72	570.01	552.12	565.87	573.65	553.22	574.87
190.00	0.90	6.60	545.97	557.56	557.87	566.20	548.36	562.07	569.72	549.44	570.92
190.50	0.70	6.40	542.22	553.74	554.02	562.40	544.47	558.22	565.78	545.57	566.93
191.00	0.40	6.30	538.51	549.94	550.19	558.62	540.69	554.40	561.84	541.77	562.99
191.50	0.30	5.90	534.85	546.13	546.42	554.82	536.84	550.57	557.94	537.90	559.04
192.10	0.00	5.80	531.16	542.31	542.57	551.06	533.02	546.74	554.04	534.07	555.15
192.60	0.20	5.40	527.46	538.58	538.81	547.31	529.17	542.94	550.17	530.20	551.25
193.10	0.00	5.40	523.82	534.82	535.04	543.60	525.46	539.19	546.35	526.52	547.40
193.60	0.00	5.10	520.21	531.09	531.26	539.85	521.75	535.39	542.50	522.86	543.51
194.10	0.00	4.90	516.57	527.36	527.53	536.09	518.12	531.66	538.70	519.29	539.68
194.60	0.00	4.70	512.98	523.68	523.84	532.43	514.60	527.93	534.89	515.82	535.88
195.10	0.00	4.50	509.43	520.02	520.16	528.77	511.19	524.27	531.16	512.51	532.13
195.60	0.10	4.20	505.89	516.40	516.52	525.11	507.79	520.65	527.41	509.22	528.37
196.10	0.00	4.10	502.41	512.84	512.93	521.43	504.46	517.06	523.70	506.01	524.62

REFERENCES

Ahuja, S., 1992, "Solid/Liquid Interfacial Drag in Equiaxed Solidification," Masters Thesis, Univ. of Iowa, Dept. of Mech. Eng., Iowa City.

Ahuja, S., Beckermann, C., Zakhem, R., Weidman, P.D. and de Groh III, H.C., 1992 "Drag Coefficient of an Equiaxed Dendrite Settling in an Infinite Medium" in Micro/Macro Scale Phenomena in Solidification, edited by C. Beckermann, L.A. Bertram, S.J. Pien, and R.E. Smelser, HTD-Vol. 218/AMD- Vol. 139, 1992, pp. 85-92.

ASTM Grain Size, 1987, "Planimetric Method." Metallography, vol. 35, pp. 18-19.

Beckermann, C., 1996, "Modeling of Transport Phenomena in Mushy Zones." Annual Review of Heat Transfer, Vol. 6, pp. 181-192.

Beckermann, C.; Bertram, L. A.; Pien, S. J.; Smelser, R. E., 1992, "Micro/Macro Scale Phenomena in Solidification." ASME HTD, Vol. 218, ASME, New York.

Beckermann, C.; Viskanta, R., 1993, "Mathematical Modeling of Transport Phenomena During Alloy Solidification." Appl. Mech. Rev.,46, pp.1-27.

Beckermann, C.; Wang C.Y., 1995, "Multiphase/-Scale Modeling of Alloy Solidification." In Annual Review of Heat Transfer, Vol. 6, pp. 115-198.

Beer, S.Z. (editor) 1972, "Liquid Metals Chemistry and Physics," Marcel Dekker, Inc. pub. NY, p. 186.

de Groh III, H.C., 1988, "Macrosegregation and Nucleation in Undercooled Pb-Sn Alloys," Masters Thesis, Case Western Reserve University, Cleveland, OH, NASA TM 102023.

de Groh III, H.C., 1994, "Undercooling Induced Macrosegregation in Directional Solidification," Metall. and Mat. Trans. A, vol. 25A, pp. 2507-2516.

de Groh III, H.C., 1998, unpublished work.

de Groh III, H.C.; Laxmanan, V., 1988, "Macrosegregation in Undercooled Pb-Sn Eutectic Alloys," Solidification Processing of Eutectic Alloys, Stefanescu, D.M. Abbaschian. G.J., and Bayuzick, R.J. (ed), The Metallurgical Society, Inc., Warrendale, Pennsylvania, pp. 229-242.

de Groh III, H.C., Weidman, P.D., Zakhem, R., Ahuja, S., and Beckermann, C., 1993, "Calculation of Dendrite Settling Velocities using a Porous Envelope," Metall. Trans. B, Vol. 24 B, pp. 749-753.

de Groh III, H.C., Weidman, P.D., Zakhem, R., Ahuja, S., and Beckermann C., 1993b"Calculation of Dendrite Settling Velocities 1.0, User's Manual", LEW-15751, COSMIC, Software Technology Transfer News Letter, vol. 1, No. 4, p. 12.

de Groh III, H.C. and Lindstrom, L. 1994, "Interface Shape and Convection during Melting and Solidification of Succinonitrile," NASA Technical Memorandum 106487.

DeHoff; Rhines, 1968, "Quantitative Microscopy." Material Science and Engineering Series, McGraw-Hill.

Desnain, P.; Fautrelle, Y.; Meyer, J.P.; Riquet; Durand, F., 1990, Acta Metall. Mater., vol. 38, pp. 1513-23.

Doherty, R.D. et al., 1977 ,"On the Columnar to Equiaxed Transition in Small Ingots." Metall. Trans. A, Vol. 8A, pp. 397-401.

Ganesan, S.; Poirier, D.R., 1987, "Densities of Aluminum-Rich Aluminum-Copper Alloys during Solidification." Metall. Trans. A, Vol. 18A, no. 4, pp. 721-723.

Griffiths, W.D.; McCartney, D.G., 1993, "Macrostructural Development in Aluminum Alloys Solidified Vertically Downwards." Materials Science and Engineering, A173, pp. 123-127.

Griffiths, W.D.; Xiao, L.; McCartney, D.G., 1996, "The Influence of Bulk Liquid Natural Convection of the Formation of the Equiaxed regions in Al-Cu and Al-Si alloys," Materials Science and Engineering, vol. 205A, pp. 31-39.

Kurz, W.; Fisher, D.J., 1989, Fundamentals of Solidification, 3rd ed., Trans Tech Publications, Aedermannsdorf, Switzerland.

Hansen, G.; Hellawell, A.; Lu, S.Z.; Steube, R.S., 1996, "Some Consequences of Thermosolutal Convection: The Grain Structure of Castings," Metall. Trans. A, vol. 27A, pp. 569-581.

Jackson, K.A., Hunt, J.D., Uhlmann, D.R., and Seward III, T.P., 1966, "On the Origin of the Equiaxed Zone in Castings," Transactions of the Metallurgical Soc. Of AIME, vol. 236, pp. 149-157.

McCartney, D.G.; Ahmady, S.M., 1994, "Solidification Macrostructures and Macrosegregation in Aluminum Alloys Cooled Above," Metall. Trans. A, Vol. 25A, pp. 1097-1102.

McCartney, D.G.; Hunt, J.D.; Jordan, R.M., 1980, Metall. Trans. A, vol. 11A, pp. 1243-1249.

Metals Handbook, 1985, Desk Edition, ASM, OH, p. 1-44.

Mondolfo, L.F., 1976, Aluminum Alloys: Structures and Properties, Butterworth and Co. Ltd. London.

Muller, G., Neumann, G. and Weber, W., 1984, "Natural Convection in Vertical Bridgman Configurations," J. of Crystal Growth, vol. 70, pp. 78-93.

Ni, J.; Beckermann C., 1995 "A Volume Averaged Two-Phase Model for Transport Phenomena during Solidification." Metall. Trans. B, Vol. 22B, pp. 349-361.

Nielsen, O., Arnberg, L., Mo, A., and Thevik, H., 1999, Metall. and Mat. Trans, A, Vol. 30A, pp. 2455-2462.

Ohno, A., 1987, Solidification. Springer-Verlag, Berlin.

Paradies, C.J., Glicksman, M.E., and Smith, R.N., 1993, "Convective Effects on Dendrite Remelting in Mushing Zones," First International Conference on Transport Phenomena in Processing," Ed., by Guceri, S.I., Technomic Pub. Lancaster PA, pp. 266-273.

Pehlke; Jeyarajan; Wada, 1982, "Summary of Thermal Properties for Casting Alloys and Mold Materials." National Science Foundation, MEA-82028.

Piwonka, T.S.; Voller, V.R.; Kategerman, L., 1993, "Modeling of Casting, Welding and Advanced Solidification Processes." Publication of TMS, Warrendale, PA.

Plaskett, T.S. and Winegard, W.C., 1950, Trans. AIME, vol. 51, p. 222.

Ramani, A., and Beckermann, C., 1997, "Dendrite Tip Growth Velocities of Settling NH4Cl Equiaxed Crystals," Scripta Materialia, Vol. 36, pp. 633-638.

Rappaz, M.; Voller, V.R., 1990, "Modeling of Micro-Macrosegregation in Solidification Process," Metall. Trans. A, Vol. 21A, pp. 749-753.

Rhines, F.N., Patterson, B.R., Ho, H.H., and Lasky, P.J., 1983, "Influence of Freezing Rate on the Grain Volume Distribution in Cast Aluminum-Zink Alloys," in Grain Refinement in Castings and Welds, Ed. by Abbaschian and David, AIME, pp. 117-137.

Sato, T.; Sato, Y., 1982, "Structure of Al-Cu Alloy Ingots Solidified Unidirectionally from the Bottom." Transactions Of the Japan Institute of Metals, Vol. 23, No. 7, pp. 388-397.

Scheidegger, A.E., 1974, in The Physics of Flow through a Porous Media, Third Edition, pp. 141.

Song, H., Tewari, S.N. and de Groh III, H.C., 1996, "Convection during Thermally Unstable Solidification of Pb-Sn in a Magnetic Field," Met. and Mat. Trans. A, Vol. 27A, pp. 1095-1110.

Suri, V.K.; El-Kaddah, N.; Berry, J.T., 1997, "Control of Macrostructure in Aluminum Castings, Part I: Determination of Columnar/Equiaxed Transition for Al-4.5% Cu Alloy." AFS Transactions, pp. 187-191.

Tiller, W.A., 1965, Physical Metallurgy, Ed. R.W. Cahn, North Holland, Amsterdam.

Touloukian, Y.S., Powell, R.W., Ho, C.Y., and Klemens, P.G., 1970, Thermophysical Properties of Matter, Vol. 1, Thermal Conductivity Metallic Elements and Alloys, Plenum Pub. Corp., NY, p. 470.

Van Vlack, L.H., 1973, "A Textbook of Materials Technology," Addison-Wesley pub., p. 18.

Voller, V.R.; Stachowicz, M.S.; Thomas, B.G., 1993, "Materials Processing in the computer age," Publication of TMS, Warrendale, PA, pp. 337-348.

Wang, C.Y., 1994, "Multi-Scale/-Phase Modeling of Dendritic Alloy Solidification." Ph.D. Dissertation, University of Iowa.

Wang, C.Y., Ahuja, S., Beckermann, C., and de Groh III, H.C., 1995, "Multiparticle Interfacial Drag in Equiaxed Solidification," Metall. and Mat. Trans. B, vol. 26B, pp.111-119.

Zakhem, R., Weidman, P.D. and de Groh III, H.C., 1993, "On the Drag of Model Dendrite Fragments at Low Reynolds Number,", Feb., NASA TM 105916, this TM is a revision of the paper published in Metallurgical Transactions A, Vol. 23A, Aug. 1992, pp. 2169-2181.

Ziv; Weinberg, F., 1989, "The Columnar-to-Equiaxed Transition in Al 3 Pct Cu." Metall. Trans. A, Vol. 20B, pp. 731-734.

REPORT DOCUMENTATION PAGE

Form Approved
OMB No. 0704-0188

1. AGENCY USE ONLY (*Leave blank*)	2. REPORT DATE	3. REPORT TYPE AND DATES COVERED
	May 2000	Technical Memorandum

4. TITLE AND SUBTITLE

Effects of Melt Convection and Solid Transport on Macrosegregation and Grain Structure in Equiaxed Al-Cu Alloys

5. FUNDING NUMBERS

WU-101-13-0A-00

6. AUTHOR(S)

Rodney S. Rerko, Henry C. de Groh, III, and Christoph Beckermann

7. PERFORMING ORGANIZATION NAME(S) AND ADDRESS(ES)

National Aeronautics and Space Administration
John H. Glenn Research Center at Lewis Field
Cleveland, Ohio 44135-3191

8. PERFORMING ORGANIZATION REPORT NUMBER

E-12217

9. SPONSORING/MONITORING AGENCY NAME(S) AND ADDRESS(ES)

National Aeronautics and Space Administration
Washington, DC 20546-0001

10. SPONSORING/MONITORING AGENCY REPORT NUMBER

NASA TM—2000-210020

11. SUPPLEMENTARY NOTES

Rodney S. Rerko and Christoph Beckermann, The University of Iowa, Department of Mechanical Engineering, 2412 Seawaus Center, Iowa City, Iowa 52242-1000 and Henry C. de Groh, III, NASA Glenn Research Center. Responsible person, Henry C. de Groh, III, organization code 6712, (216) 433-5025, Mail Stop 105-1, E-mail: henry.degroh@grc.nasa.gov, and URL: http://cml.grc.nasa.gov/degroh.

12a. DISTRIBUTION/AVAILABILITY STATEMENT

Unclassified - Unlimited
Subject Categories: 26, 34, and 64 Distribution: Nonstandard

This publication is available from the NASA Center for AeroSpace Information, (301) 621-0390.

12b. DISTRIBUTION CODE

13. ABSTRACT ***(Maximum 200 words)***

Macrosegregation in metal casting can be caused by thermal and solutal melt convection, and the transport of unattached solid crystals resulting from nucleation in the bulk liquid or dendrite fragmentation. To develop a comprehensive numerical model for the casting of alloys, an experimental study has been conducted to generate benchmark data with which such a solidification model could be tested. The objectives were: (1) experimentally study the effects of solid transport and thermosolutal convection on macrosegregation and grain size; and (2) provide a complete set of boundary conditions - temperature data, segregation data, and grain size data - to validate numerical models. Through the control of end cooling and side wall heating, radial temperature gradients in the sample and furnace were minimized. Thus the vertical crucible wall was adiabatic. Samples at room temperature were 24 cm^3 and 95 mm long. The alloys used were Al-1 wt. pct. Cu, and Al-10 wt. pct. Cu; the starting point for solidification was isothermal at 710 and 685 °C respectively. To induce an equiaxed structure various amounts of the grain refiner TiB_2 were added. Samples were either cooled from the top, or the bottom. Several trends in the data stand out. In attempting to model these experiments, concentrating on these trends or differences may be beneficial.

14. SUBJECT TERMS

Grains; Advection; Settling; Segregation; Macrosegregation

15. NUMBER OF PAGES

114

16. PRICE CODE

A06

17. SECURITY CLASSIFICATION OF REPORT	18. SECURITY CLASSIFICATION OF THIS PAGE	19. SECURITY CLASSIFICATION OF ABSTRACT	20. LIMITATION OF ABSTRACT
Unclassified	Unclassified	Unclassified	